

## Supporting Information

# Novel, Selective, and Extremely Responsive Thienyl-based Dual Fluorogenic Probe for Tandem Superoxide and Hg<sup>2+</sup> Chemosensing

Atul P. Singh,<sup>a</sup> Dhiraj P. Murale,<sup>a</sup> Yonghwang Ha,<sup>a</sup> Hyunjeong Liew,<sup>b</sup> Kang Mun Lee,<sup>a</sup>  
Aviv Segev,<sup>c</sup> Yoo-Hun Suh,<sup>b</sup> and David G. Churchill<sup>\*a</sup>

*a* Molecular Logic Gate Laboratory, Department of Chemistry, Korea Advanced Institute of Science and Technology (KAIST), 373-1 Guseong-dong, Yuseong-gu, Daejeon 305-701, Republic of Korea  
E-mail: dchurchill@kaist.ac.kr. *b* Department of Pharmacology, College of Medicine, National Creative Research Initiative Center for Alzheimer's Dementia and Neuroscience Research Institute, MRC, Seoul National University, Seoul 110-799, Republic of Korea *c* "Know Lab" Department of Knowledge Service Engineering, KAIST, 373-1 Guseong-dong, Yuseong-gu, Daejeon 305-701, Republic of Korea

E-mail: dchurchill@kaist.ac.kr

## Experimental Section

**General Considerations.** All chemicals used herein were used as received from commercial suppliers (Aldrich, Acros, and Junsei companies). The synthetic details for the preparation of the dipyrromethanes and for the BODIPY systems follow literature methods.<sup>1</sup> <sup>1</sup>H and <sup>13</sup>C NMR spectra were acquired using a Bruker Avance 400 MHz spectrometer. TMS was used as an internal standard. <sup>1</sup>H and <sup>13</sup>C NMR spectral signals were calibrated internally by the respective proton impurity or carbon resonance of the CDCl<sub>3</sub> (<sup>1</sup>H: δ 7.24; <sup>13</sup>C: δ 77.0). A high resolution hybrid tandem LC–MS/MS spectrometer was used for mass data collection by the research support staff at KAIST.

**Absorption and Emission spectroscopy.** All compounds were dissolved in acetonitrile in preparing a BODIPY solution of concentration 1 × 10<sup>-6</sup> M. UV–vis absorption and emission measurements were obtained using a CARY 300 Bio UV–vis spectrometer and a Shimadzu RF–5301 PC spectrophotometer, respectively. Emission spectra are obtained through the excitation at λ<sub>max</sub> from the absorption spectrum of each compound. Fluorescein in 0.1 N NaOH (Φ<sub>F</sub> = 0.92)<sup>2</sup> is used as the standard to calibrate quantum yield values.

**Synthetic procedures. For 1 and 2.** Synthesis of **1** and **2** was performed via a typical procedure.<sup>3</sup> Firstly, CuI (0.5 mol %) and benzotriazole (1.0 mol %) were mixed in 2–3 mL DMSO. Aryl halide (1.0 g, 3.7 mmol) was then added and stirred for 10 min. Next, aryl–thiol (0.87 g, 7.77 mmol) and Cs<sub>2</sub>CO<sub>3</sub> (1.69 g, 5.18 mmol) were added and the reaction mixture was stirred for 10–12 h at 90–95 °C. The reaction was monitored by TLC. After completion of the reaction 30 mL of ethylacetate was added and this layer was washed with water (3 times with 10 mL). Solution was dried on Na<sub>2</sub>SO<sub>4</sub> and pumped off through use of a

rotoevaporator. The viscous mass was then subjected to column chromatography (dichloromethane/methanol) to afford the desired compounds, **1** and **2**.

**1:** Yield = 0.55 g, 44.9%.  $^1\text{H}$  ( $\text{CDCl}_3$ ,  $\delta$  7.24, 400 MHz):  $\delta$  10.0 (s, 1H<sub>6</sub>), 8.40 (m, 1H<sub>11</sub>), 8.36 (m, 1H<sub>16</sub>), 7.66 (s, 1H<sub>4</sub>), 7.53 (m, 1H<sub>9</sub>), 7.48 (m, 1H<sub>14</sub>), 7.19 (dd,  $^3J_{\text{H-H}} = 8.1$  Hz,  $^4J_{\text{H-H}} = 1.2$  Hz, 1H<sub>8</sub>), 7.07 (m, 1H<sub>10</sub>), 7.03 (dd,  $^3J_{\text{H-H}} = 8.0$  Hz,  $^4J_{\text{H-H}} = 1.2$  Hz, 1H<sub>13</sub>), 7.0 (m, 1H<sub>16</sub>).  $^{13}\text{C}$  ( $\text{CDCl}_3$ ,  $\delta$  77.0, 400 MHz)  $\delta$  184.0 (C<sub>6</sub>), 158.7 (C<sub>12</sub>), 156.3 (C<sub>7</sub>), 149.4 (C<sub>11</sub>), 149.3 (C<sub>16</sub>), 145.9 (C<sub>2</sub>), 141.9 (C<sub>3</sub>), 137.1 (C<sub>9</sub>), 137.9 (C<sub>14</sub>), 134.5 (C<sub>4</sub>), 132.7 (C<sub>5</sub>), 122.1 (C<sub>8</sub>), 121.5 (C<sub>10</sub>), 120.9 (C<sub>13</sub>), 120.6 (C<sub>15</sub>). ESI-MS (positive mode,  $\text{CHCl}_3 + \text{CH}_3\text{OH}$ ) =  $[\text{M} + \text{Na}]^+$  = 352.9853 (cal.), 352.9850 (exp.);  $[\text{M} + \text{Na} + \text{CH}_3\text{OH}]^+$  = 385.0115 (cal.), 385.0103 (exp.).

**2:** Yield = 0.150 g, 13.5%.  $\delta$  9.98 (s, 1H<sub>6</sub>), 8.44 (m, 1H<sub>11</sub>), 7.58 (m, 1H<sub>9</sub>), 7.51 (s, 1H<sub>4</sub>), 7.15 (dd,  $^3J_{\text{H-H}} = 8.1$  Hz,  $^4J_{\text{H-H}} = 1.0$  Hz, 1H<sub>8</sub>), 7.12 (m, 1H<sub>10</sub>).  $^{13}\text{C}$  ( $\text{CDCl}_3$ ,  $\delta$  77.0, 400 MHz) = 183.7 (C<sub>6</sub>), 157.1 (C<sub>7</sub>), 149.8 (C<sub>11</sub>), 143.8 (C<sub>2</sub>), 141.4 (C<sub>3</sub>), 137.3 (C<sub>9</sub>), 129.3 (C<sub>4</sub>), 121.7 (C<sub>5</sub>), 121.5 (C<sub>8</sub>), 116.9 (C<sub>10</sub>). ESI-MS (positive mode,  $\text{CHCl}_3 + \text{CH}_3\text{OH}$ ) =  $[\text{M} + \text{Na}]^+$  = 321.8972 (cal.), 321.8963 (exp.);  $[\text{M} + \text{H}]^+$  = 299.9152 (cal.), 299.9090 (exp.);  $[\text{M} + \text{Na} + \text{CH}_3\text{OH} + \text{CH}_3 + \text{H}]^+$  = 299.9547 (cal.), 369.9223 (exp.).

**General procedure for the one pot synthesis of BODIPY.** Aryl aldehyde and dimethylpyrrole were added to a two-neck flask in 20 mL of dichloromethane at ice-bath temperature; sparging with nitrogen for 10 min was then undertaken to remove atmospheric

oxygen. Trifluoroacetic acid (TFA) is added dropwise; this was done to keep the reaction progress slow, and under N<sub>2</sub> for ~1 h. A thin layer chromatography (TLC) revealed the formation of a new spot at R<sub>f</sub> = ~ 0.2 (for **3**) and 0.6 (for **4**) in dichloromethane indicated consumption of the starting aldehyde. It signified the formation of dipyrromethane-based species. The resultant solution was neutralized with *N,N*-di-isopropylethylamine to maintain a pH of ~7 and the solution volume was maintained to ~50 mL with dichloromethane. The solution temperature was retained at ice-cold temperature and *p*-chloranil (tetrachloro-*p*-benzoquinone) was added slowly and stirred the solution for ~3 h to complete oxidation reaction. The resultant solution was neutralized with *N,N*-di-isopropylethylamine, followed by 10 min additional stirring. Boron trifluoride dietherate is then added and reaction is kept stirring for the next 2 h at room temperature. A thin layer chromatography (TLC) assay revealed the expected orange-red spot at R<sub>f</sub> = ~ 0.2 (for **3**) and 0.6 (for **4**) in neat dichloromethane. Solvent of the reaction mixture was pumped off on rotoevaporator and crude solid material was used for silica gel column chromatography with eluent (dichloromethane/hexane = 90/10 (for **3**), 60/40 (for **4**)). Single crystals (for **4**) suitable for X-ray diffraction study were obtained from a solvent system composed of dichloromethane and hexane.

**For Compound 3.** Compound, **1** (0.250 g, 0.7565 mmol), 2,4-dimethylpyrrole (0.16 mL, 1.51 mmol), TFA (0.01 mL, 0.076 mmol), Chloranil (0.205 g, 0.832 mmol), *N,N*-di-isopropylethylamine (1.32 mL, 7.57 mmol) and BF<sub>3</sub>·2Et<sub>2</sub>O (1.03 mL, 7.57 mmol) were used in accordance with general procedure above. Yield = 0.20 g, 41.5%.

<sup>1</sup>H (CDCl<sub>3</sub>, δ 7.24, 400 MHz): δ 8.38 ("m", 2H<sub>15+20</sub>), 7.49 ("m", 2H<sub>13+18</sub>), 7.19 (d, <sup>3</sup>J<sub>H-H</sub> = 8.4

Hz, 1H<sub>12</sub>), 7.13 (s, 1H<sub>10</sub>), 7.12 (d, <sup>3</sup>J<sub>H-H</sub> = 7.6 Hz, 1H<sub>18</sub>), 7.03 ("m", 2H<sub>14+19</sub>), 6.0 (s, 2H<sub>2</sub>), 2.5 (s, 6H<sub>21</sub>), 1.7 (s, 6H<sub>22</sub>). <sup>13</sup>C (CDCl<sub>3</sub>, δ 77.0, 400 MHz) = 160.0 (C<sub>16</sub>), 156.0 (C<sub>11</sub>), 155.4 (C<sub>1</sub>), 149.5 (C<sub>15+20</sub>), 142.7 (C<sub>3</sub>), 137.7 (C<sub>5</sub>), 136.9 (C<sub>13</sub>), 136.7 (C<sub>18</sub>), 135.9 (C<sub>10</sub>), 134.4 (C<sub>9</sub>), 134.0 (C<sub>6</sub>), 133.4 (C<sub>7</sub>), 131.3 (C<sub>4</sub>), 123.4 (C<sub>2</sub>), 121.5 (C<sub>12</sub>), 121.3 (C<sub>14</sub>), 120.7 (C<sub>17</sub>), 120.6 (C<sub>19</sub>), 14.6 (C<sub>21</sub>), 13.9 (C<sub>22</sub>). <sup>11</sup>B-NMR (CDCl<sub>3</sub>, BF<sub>3</sub>·OEt<sub>2</sub>, δ 0.00): 5.41 (t, 32.86 Hz). ESI-MS (positive mode, CHCl<sub>3</sub> + CH<sub>3</sub>OH) = [M + Na]<sup>+</sup> = 571.1044 (cal.), 571.1062 (exp.).

**For 4.** Compound, **2** (0.10 g, 0.33 mmol), 2,4-dimethylpyrrole (0.07 mL, 0.67 mmol), TFA (0.003 mL, 0.033 mmol), Chloranil (0.090 g, 0.366 mmol), *N,N*-diisopropylethylamine (0.58 mL, 3.3 mmol) and BF<sub>3</sub>·2Et<sub>2</sub>O (0.45 mL, 3.3 mmol) were used in accordance with general procedure above. Yield = 0.080 g, 46.3%. <sup>1</sup>H (CDCl<sub>3</sub>, δ 7.24, 400 MHz): δ 8.38 (dd, <sup>3</sup>J<sub>H-H</sub> = 4.6 Hz, <sup>4</sup>J<sub>H-H</sub> = 1.2 Hz, 1H<sub>15</sub>), 7.46 (m, 1H<sub>13</sub>), 7.14 (d, <sup>3</sup>J<sub>H-H</sub> = 8.0 Hz, 2H<sub>12</sub>), 7.03 (m, 1H<sub>14</sub>), 6.90 (s, 1H<sub>10</sub>), 5.93 (s, 2H<sub>2</sub>), 2.51 (s, 6H<sub>16</sub>), 1.64 (s, 6H<sub>17</sub>). <sup>13</sup>C (CDCl<sub>3</sub>, δ 77.0, 400 MHz) = 156.1 (C<sub>1</sub>), 156.7 (C<sub>11</sub>), 149.5 (C<sub>15</sub>), 142.8 (C<sub>4</sub>), 138.5 (C<sub>9</sub>), 136.7 (C<sub>13</sub>), 133.6 (C<sub>7</sub>), 131.3 (C<sub>3</sub>), 129.7 (C<sub>10</sub>), 129.2 (C<sub>6</sub>), 123.0 (C<sub>12</sub>), 121.4 (C<sub>2</sub>), 121.3 (C<sub>14</sub>), 116.9 (C<sub>5</sub>), 14.6 (C<sub>16</sub>), 13.8 (C<sub>17</sub>). <sup>11</sup>B NMR (CDCl<sub>3</sub>, BF<sub>3</sub>·OEt<sub>2</sub>, δ 0.00): 5.34 (t, 32.0 Hz). ESI-MS (positive mode, CHCl<sub>3</sub> + CH<sub>3</sub>OH) = [M + Na + 2H]<sup>+</sup> = 542.0319 (cal.), 542.0147 (exp.).

**For Compounds 5 and 6:** Compound **4** (0.040 g, 0.0772 mmol) was dissolved in 20 mL of dichloromethane and solution was kept at ice-temperature. A portion of *m*-CPBA (0.033 g, 0.193 mmol) solution in dichloromethane was added slowly and resultant solution

was kept on stirring for next 2 h. TLC assay shows consumption of starting material and generation of two new spots at  $R_f \sim 0.25$  (for 5) and  $0.40$  (for 6) in dichloromethane/methanol (99/1). Both compounds were purified and separated by silica gel column chromatography.

For **5**: Yield = 0.020 g, 48.8%.  $^1\text{H}$  ( $\text{CDCl}_3$ ,  $\delta$  7.24, 400 MHz):  $\delta$  8.49 (dd,  $^3J_{\text{H-H}} = 4.36$  Hz,  $^4J_{\text{H-H}} = 1.1$  Hz, 1H<sub>19</sub>), 7.96 (d,  $^3J_{\text{H-H}} = 7.9$  Hz 1H<sub>16</sub>), 7.88 (ddd,  $^3J_{\text{H-H}} = 7.7$  Hz,  $^3J_{\text{H-H}} = 7.7$  Hz,  $^4J_{\text{H-H}} = 1.8$  Hz, 2H<sub>17</sub>), 7.33 (ddd,  $^3J_{\text{H-H}} = 7.4$  Hz,  $^3J_{\text{H-H}} = 4.6$  Hz,  $^4J_{\text{H-H}} = 1.3$  Hz, 1H<sub>18</sub>), 6.93 (s, 1H<sub>14</sub>), 6.02/5.98 (s, 1H<sub>2</sub>, 1H<sub>8</sub>), 2.54 (s, 6H<sub>20/22</sub>), 1.71/1.61 (s, 6H<sub>21/23</sub>).  $^{13}\text{C}$  ( $\text{CDCl}_3$ ,  $\delta$  77.0, 400 MHz) = 163.3, 157.2, 156.7, 149.9, 144.4, 143.2, 143.1, 140.2, 138.1, 131.4, 131.1, 130.6, 130.5, 125.5, 122.1, 121.5, 121.3, 120.0, 14.7, 13.9, 13.7.  $^{11}\text{B}$ -NMR ( $\text{CDCl}_3$ ,  $\text{BF}_3\cdot\text{OEt}_2$ ,  $\delta$  0.00): 5.40 (t, 31.3 Hz). ESI-MS (positive mode,  $\text{CHCl}_3 + \text{CH}_3\text{OH}$ ) =  $[\text{M} + \text{Na} + 2\text{H}]^+ = 558.0268$  (cal.), 542.0072 (exp.).

For **6**: Yield = 0.008 g, 18.6%.  $^1\text{H}$  ( $\text{CDCl}_3$ ,  $\delta$  7.24, 400 MHz):  $\delta$  8.54 (m, 1H<sub>15</sub>), 7.78 (d,  $^3J_{\text{H-H}} = 7.9$  Hz, 1H<sub>12</sub>), 7.64 (ddd,  $^3J_{\text{H-H}} = 7.7$  Hz,  $^3J_{\text{H-H}} = 7.7$  Hz,  $^4J_{\text{H-H}} = 1.7$  Hz, 2H<sub>13</sub>), 7.33 (ddd,  $^3J_{\text{H-H}} = 7.7$  Hz,  $^3J_{\text{H-H}} = 4.7$  Hz,  $^4J_{\text{H-H}} = 1.2$  Hz, 1H<sub>14</sub>), 6.98 (s, 1H<sub>10</sub>), 5.80 (s, 2H<sub>2</sub>), 2.50 (s, 6H<sub>16</sub>), 1.38 (s, 6H<sub>17</sub>).  $^{13}\text{C}$  ( $\text{CDCl}_3$ ,  $\delta$  77.0, 400 MHz) = 156.8, 155.9, 150.1, 142.6, 138.9, 138.5, 137.7, 132.4, 130.5, 127.4, 124.2, 122.0, 121.5, 14.6, 13.5.  $^{11}\text{B}$ -NMR ( $\text{CDCl}_3$ ,  $\text{BF}_3\cdot\text{OEt}_2$ ,  $\delta$  0.00): 5.23 (t, 33.6 Hz). ESI-MS (positive mode,  $\text{CHCl}_3 + \text{CH}_3\text{OH}$ ) =  $[\text{M} + \text{Na} + 2\text{H}]^+ = 574.0217$  (cal.), 542.0019 (exp.).

**Crystallographic Data: Compound 4 (CCDC 877969):**  $C_{22}H_{19}BBrF_2N_3S_2$ , F.W.:  
518.24. Monoclinic,  $P2(1)/n$ ,  $Z = 4$ ,  $a = 7.5410(14) \text{ \AA}$ ,  $b = 11.291(2) \text{ \AA}$ ,  $c = 27.486(5) \text{ \AA}$ ,  $\beta =$   
 $95.942(8)^\circ$ ,  $V = 2327.7(7) \text{ \AA}^3$ ,  $T = 296(2) \text{ K}$ , No. reflections = 38634, No. independent  
reflections = 6972 [ $R(\text{int}) = 0.1663$ ],  $R1 = 0.0671$ ,  $wR2 = 0.1157$ , Abs. coeff. ( $\text{mm}^{-1}$ ) = 1.976,  
Largest diff. peak and hole = 0.793 and 0.553  $e^{-}/\text{\AA}^3$ .

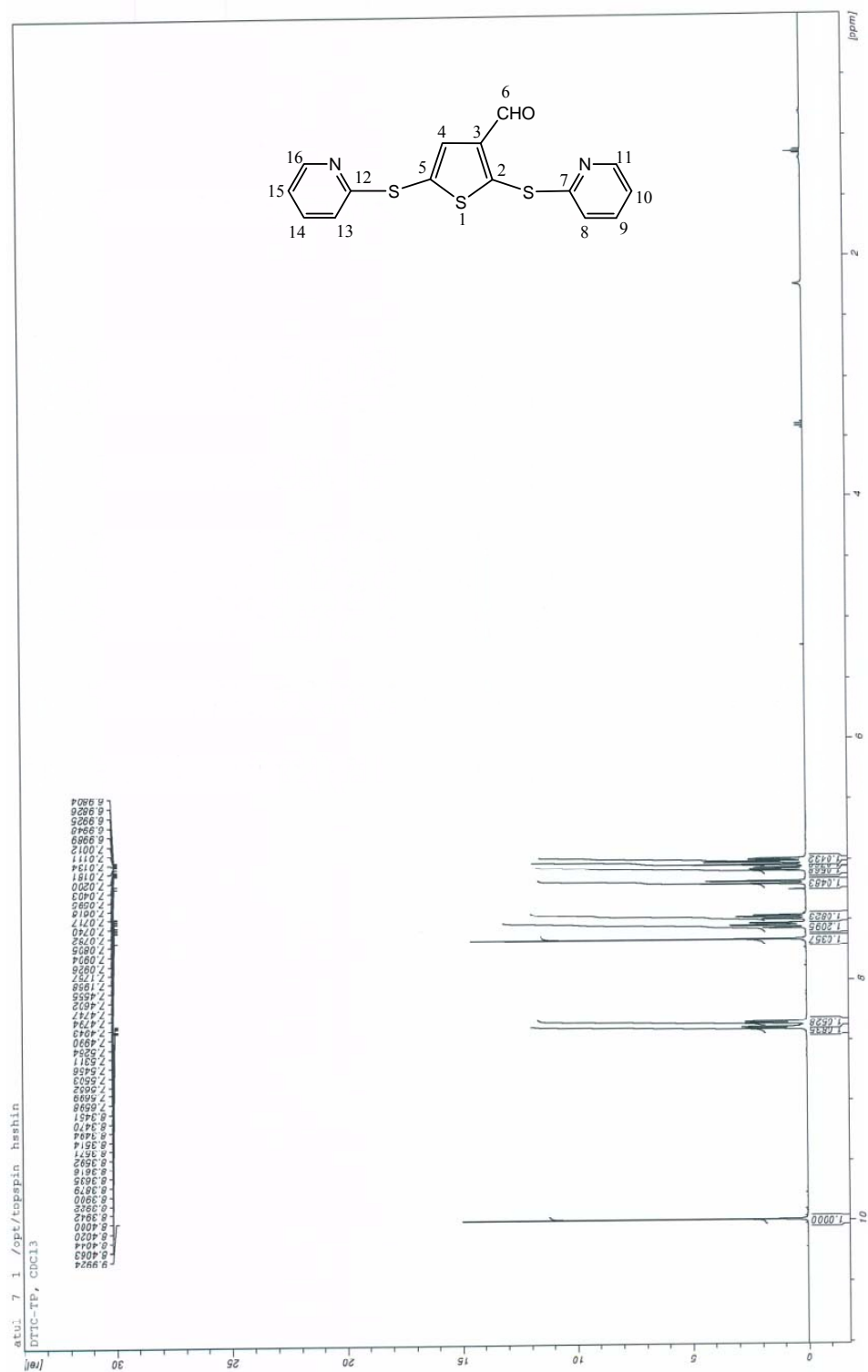
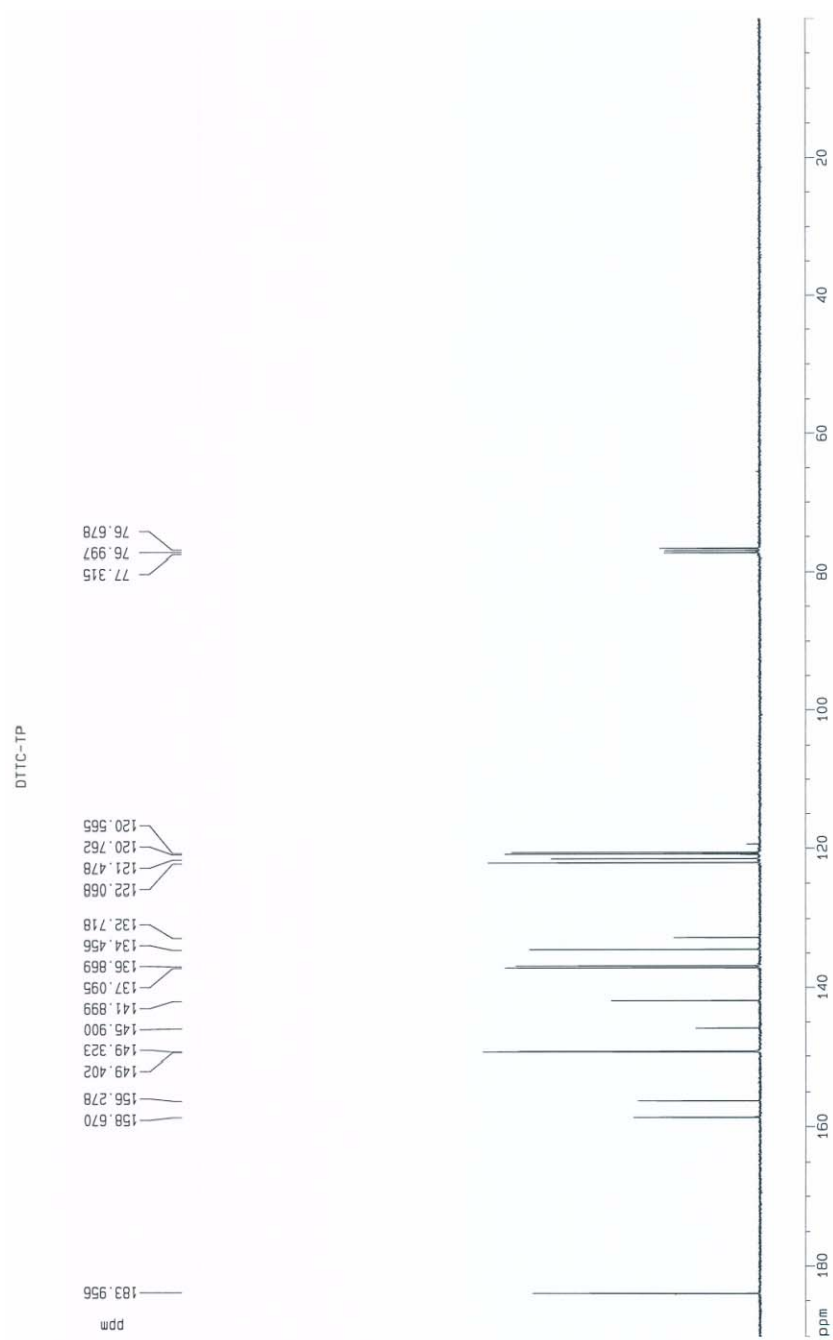


Figure S1.1: <sup>1</sup>H NMR spectrum of compound 1.



**Figure S1.2:**  $^{13}\text{C}$  NMR spectrum of compound **1**.

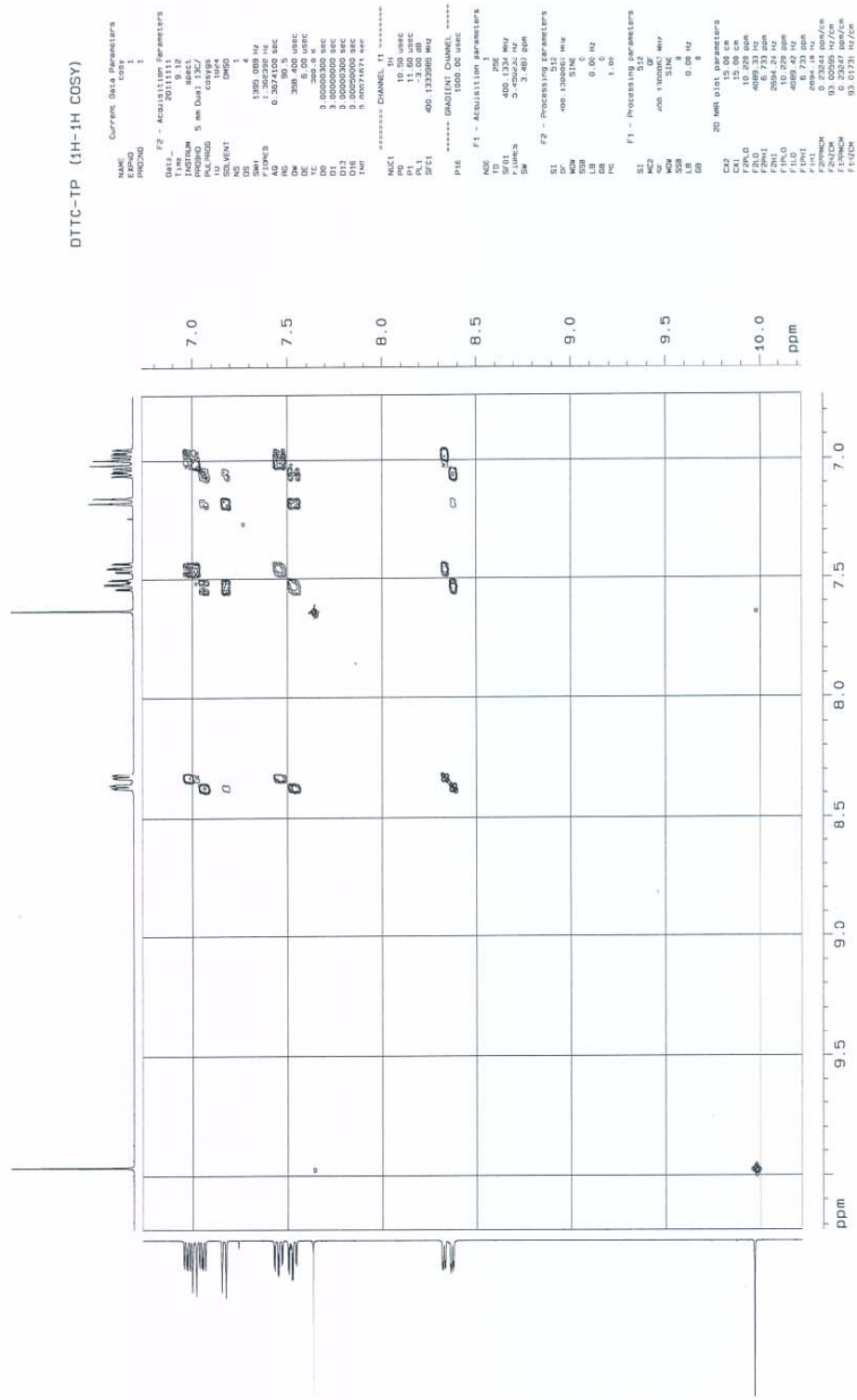
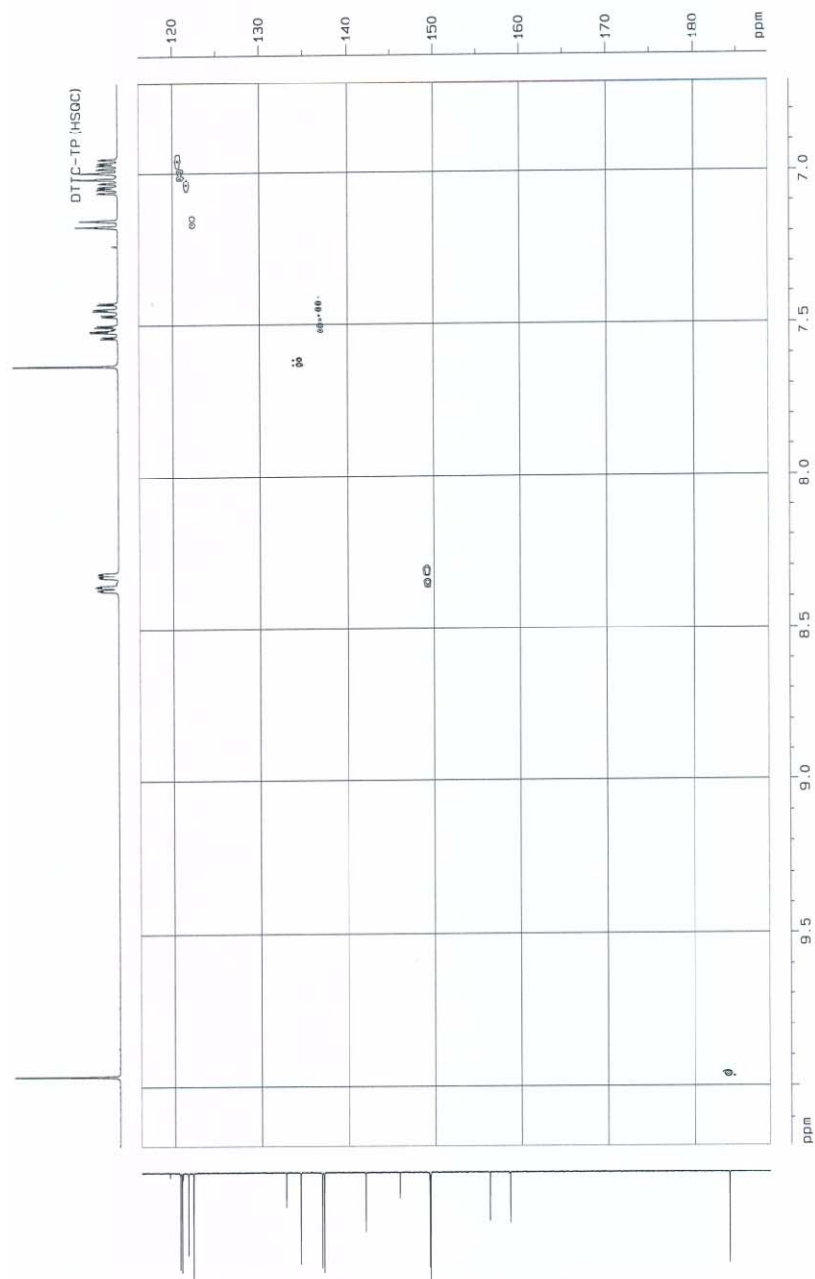


Figure S1.3:  $^1\text{H}$ - $^1\text{H}$  COSY spectrum of compound 1.



**Figure S1.4:**  $^1\text{H}$ - $^{13}\text{C}$  HSQC NMR spectrum of compound **1**.



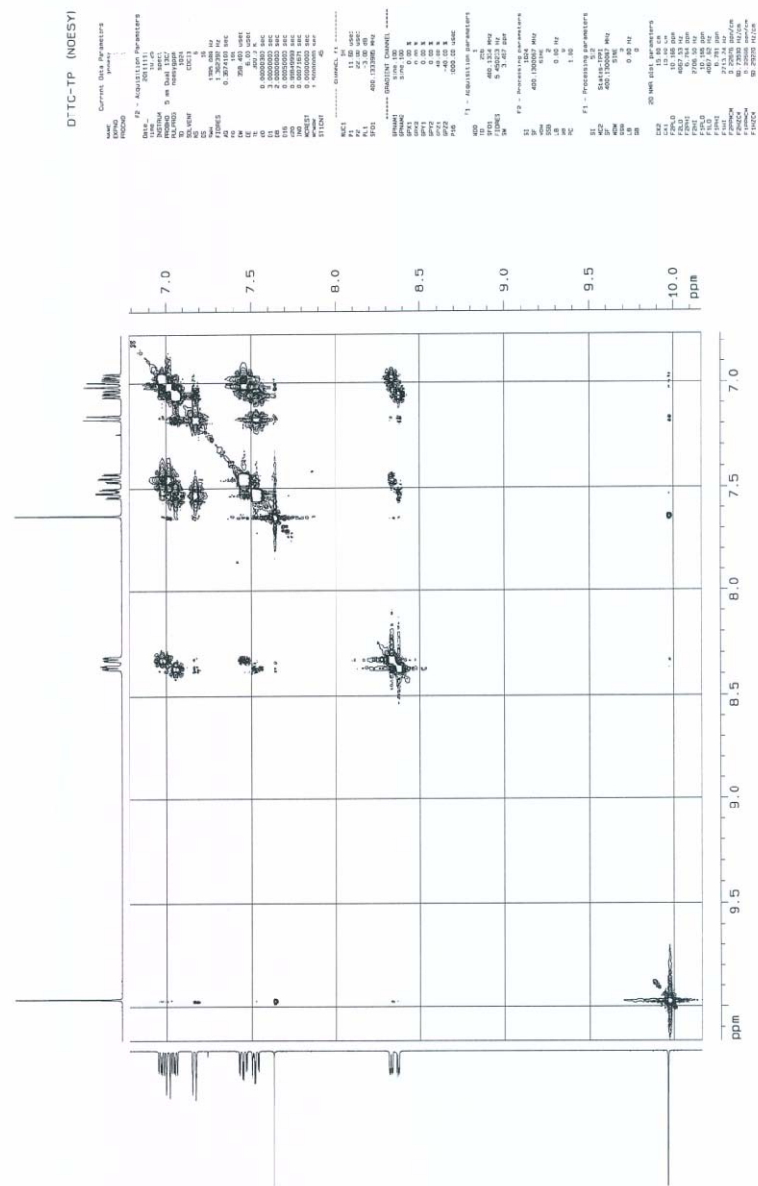


Figure S1.6: NOESY spectrum of compound 1.

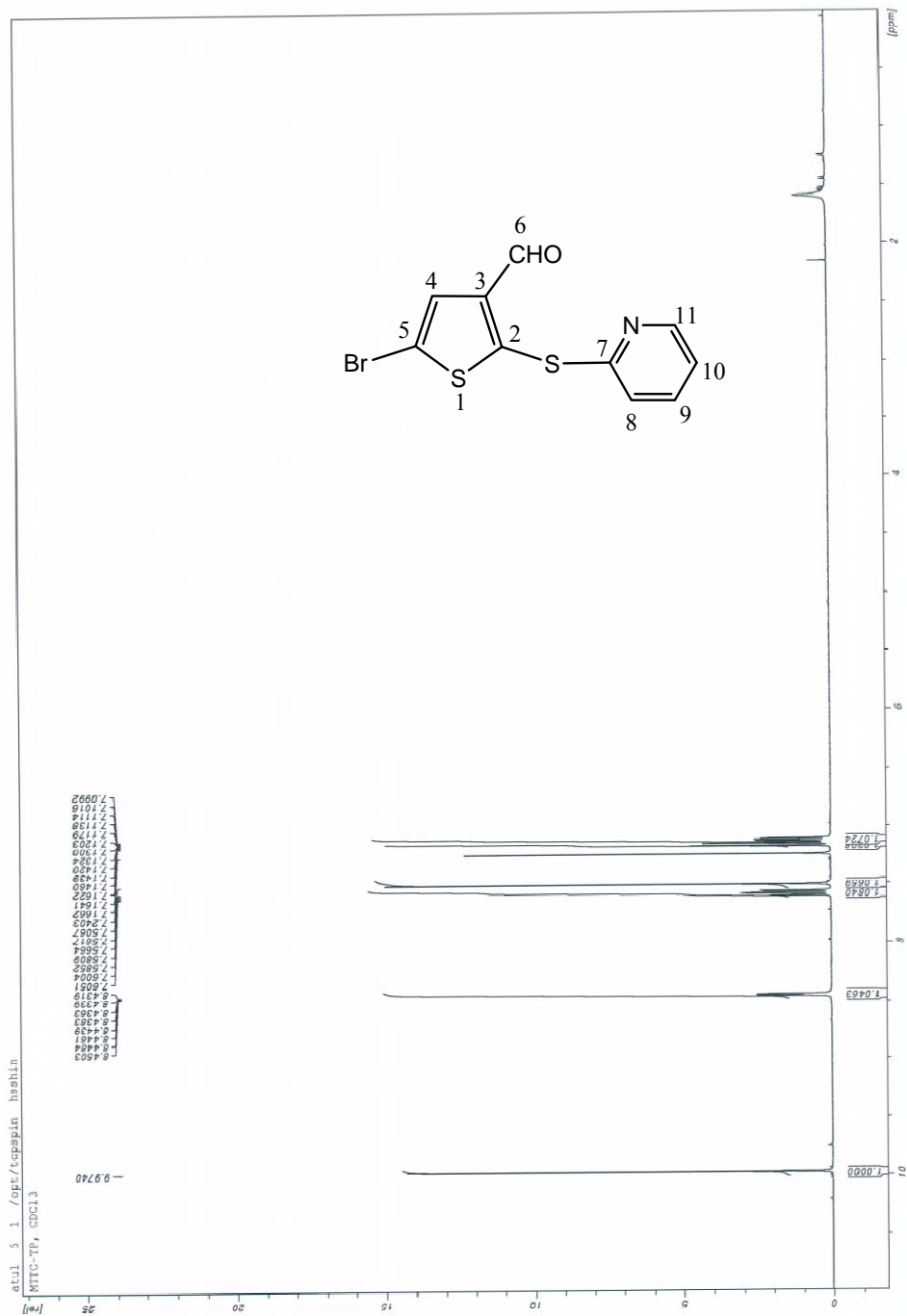
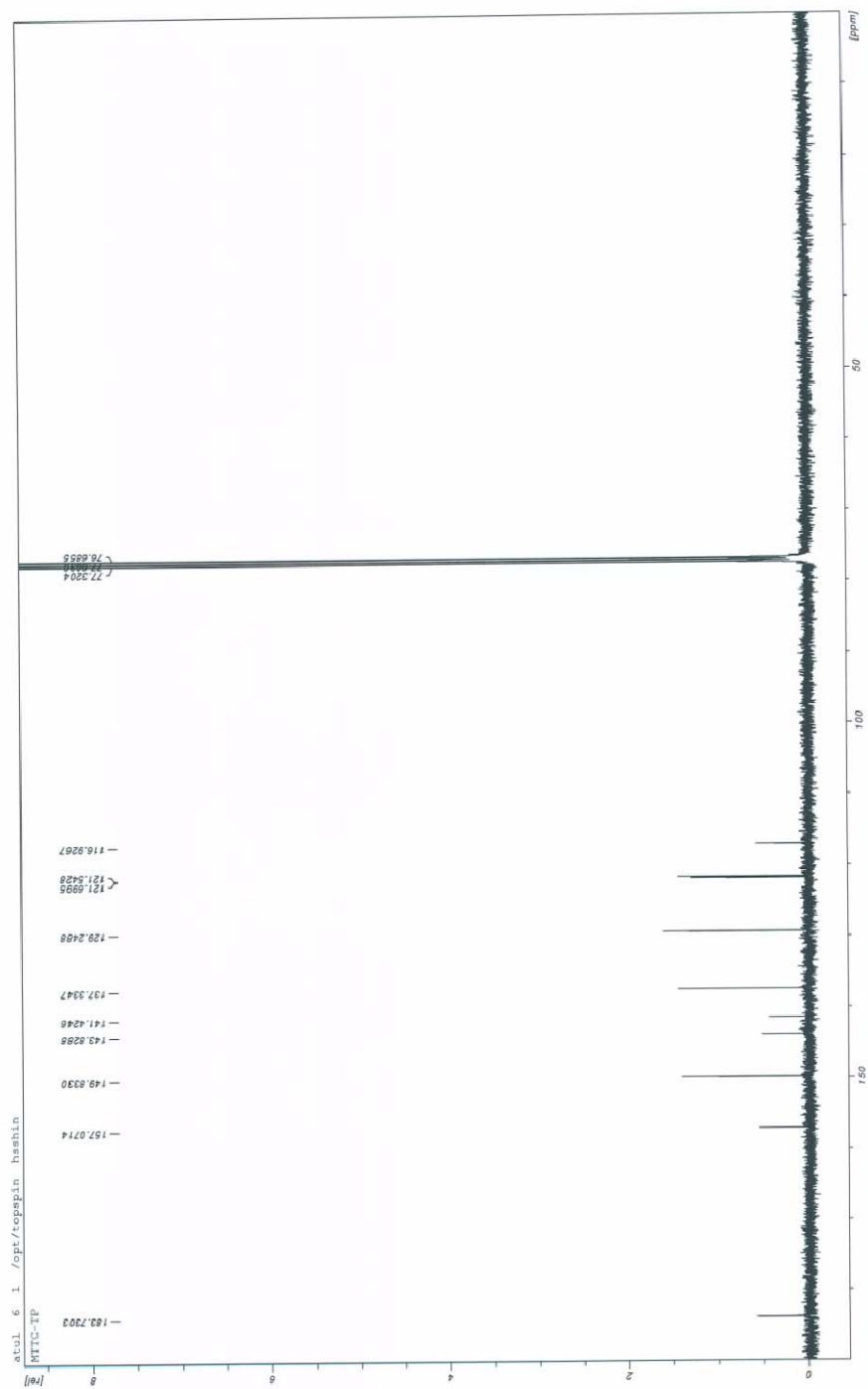
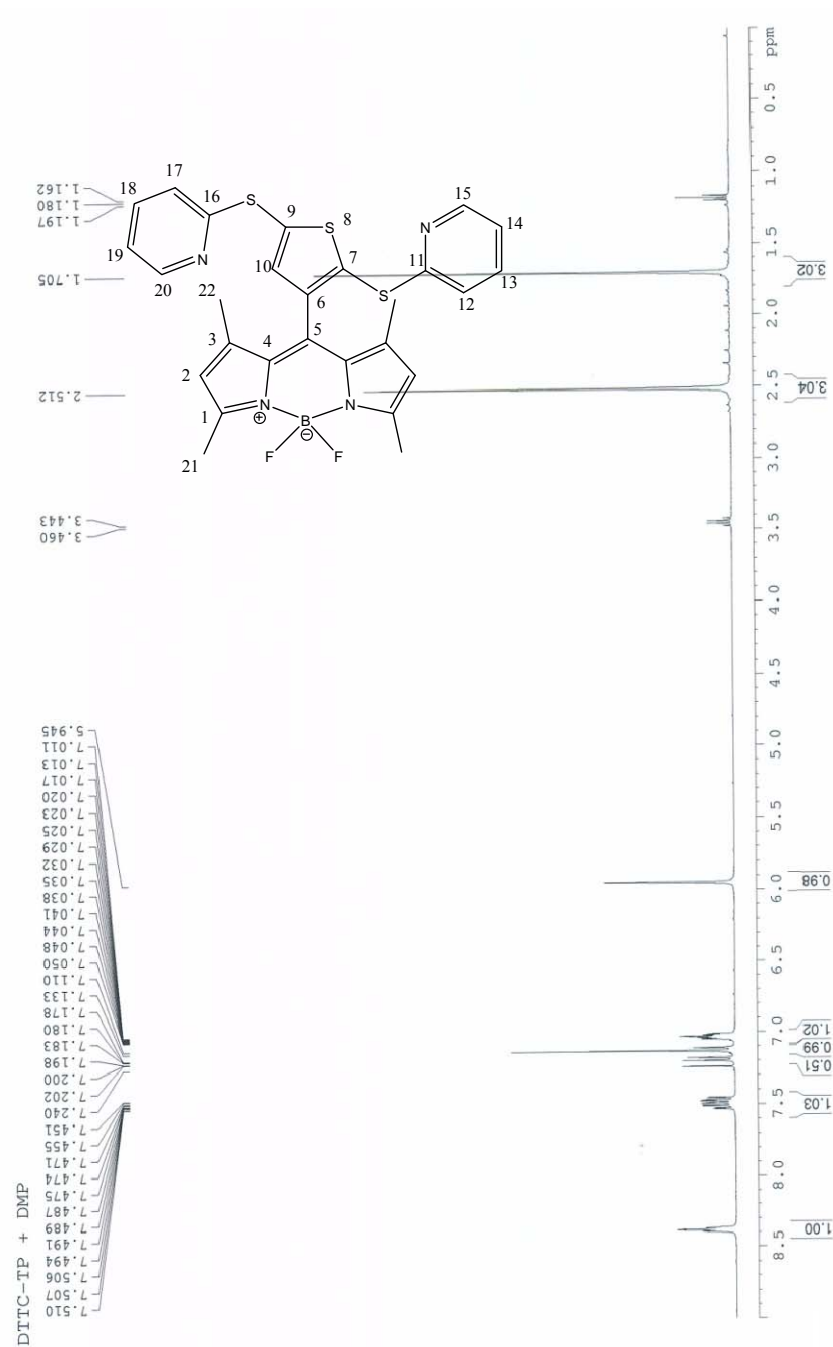


Figure S2.1: <sup>1</sup>H NMR spectrum of compound 2.



**Figure S2.2:**  $^{13}\text{C}$  NMR spectrum of compound **2**.



**Figure S3.1:** <sup>1</sup>H NMR spectrum of compound 3.

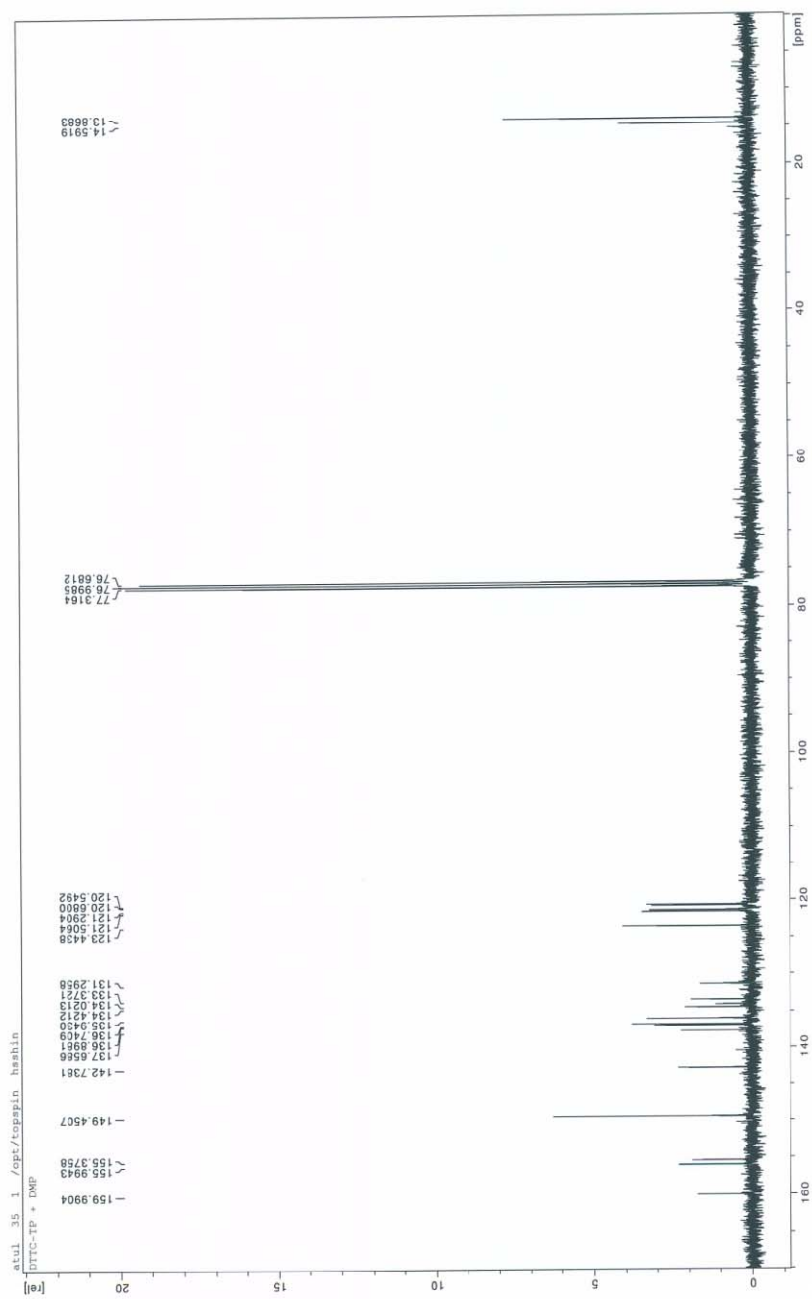


Figure S3.2:  $^{13}\text{C}$  NMR spectrum of compound 3.



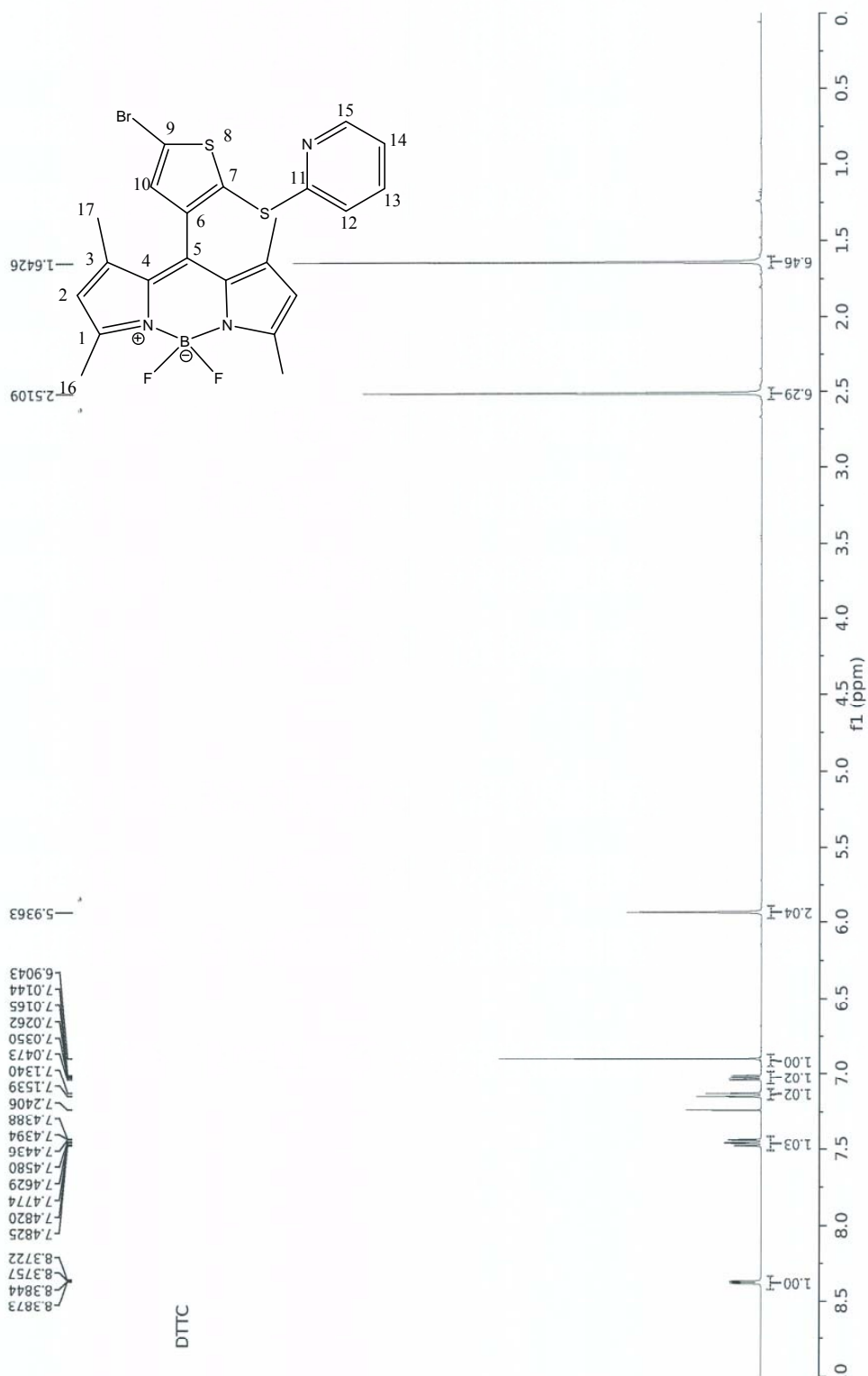


Figure S4.1:  $^1\text{H}$  NMR spectrum of compound 4.

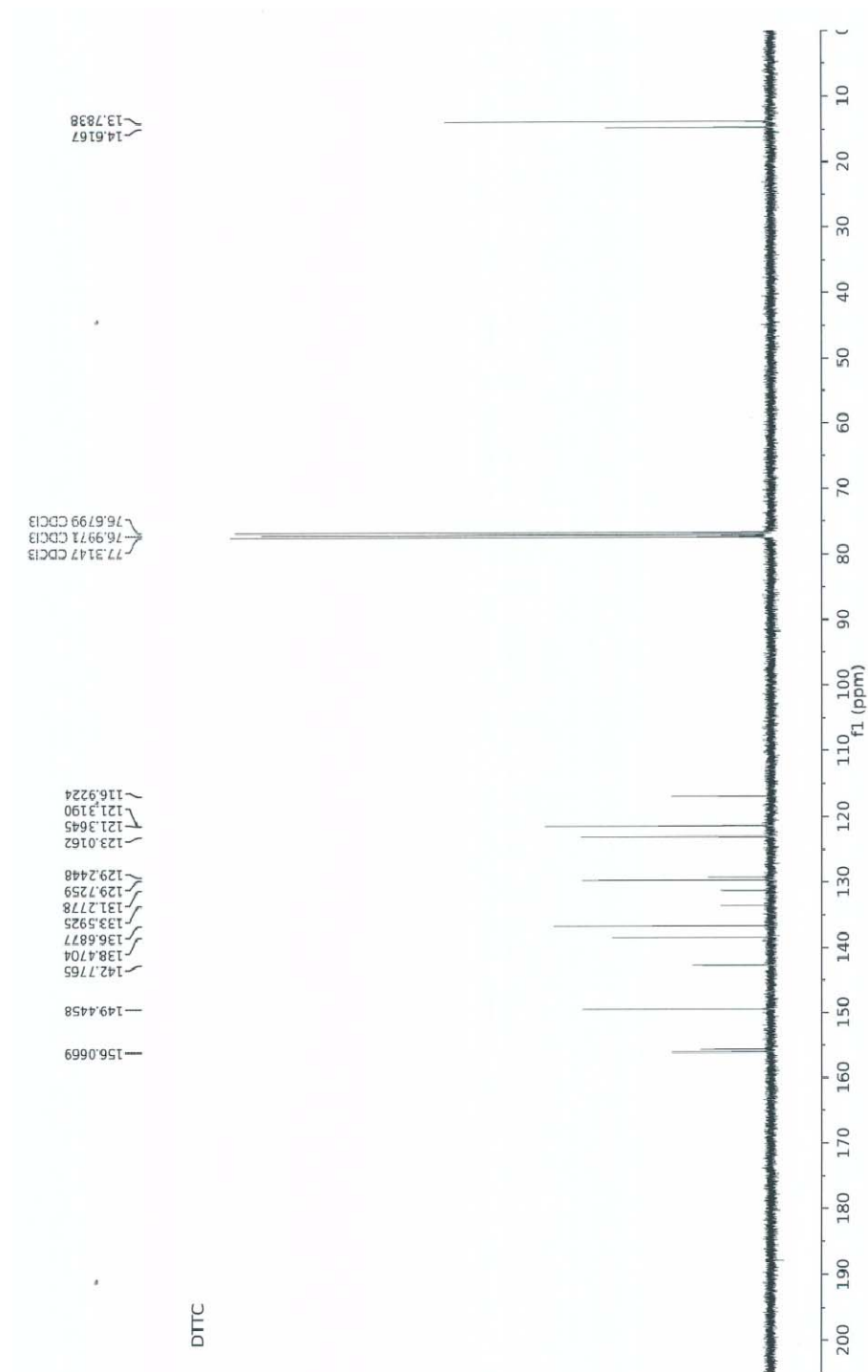


Figure S4.2:  $^{13}\text{C}$  NMR spectrum of compound 4.

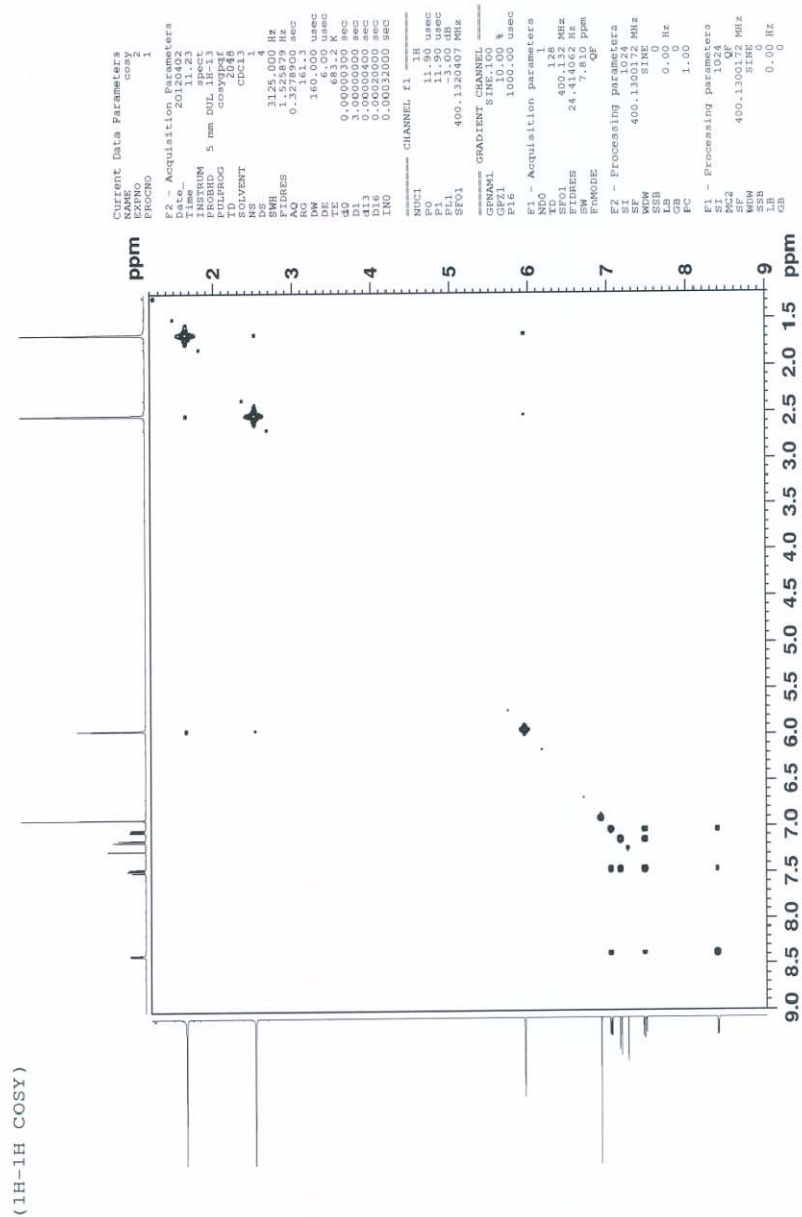


Figure S4.3: <sup>1</sup>H-<sup>1</sup>C COSY spectrum of compound 4.



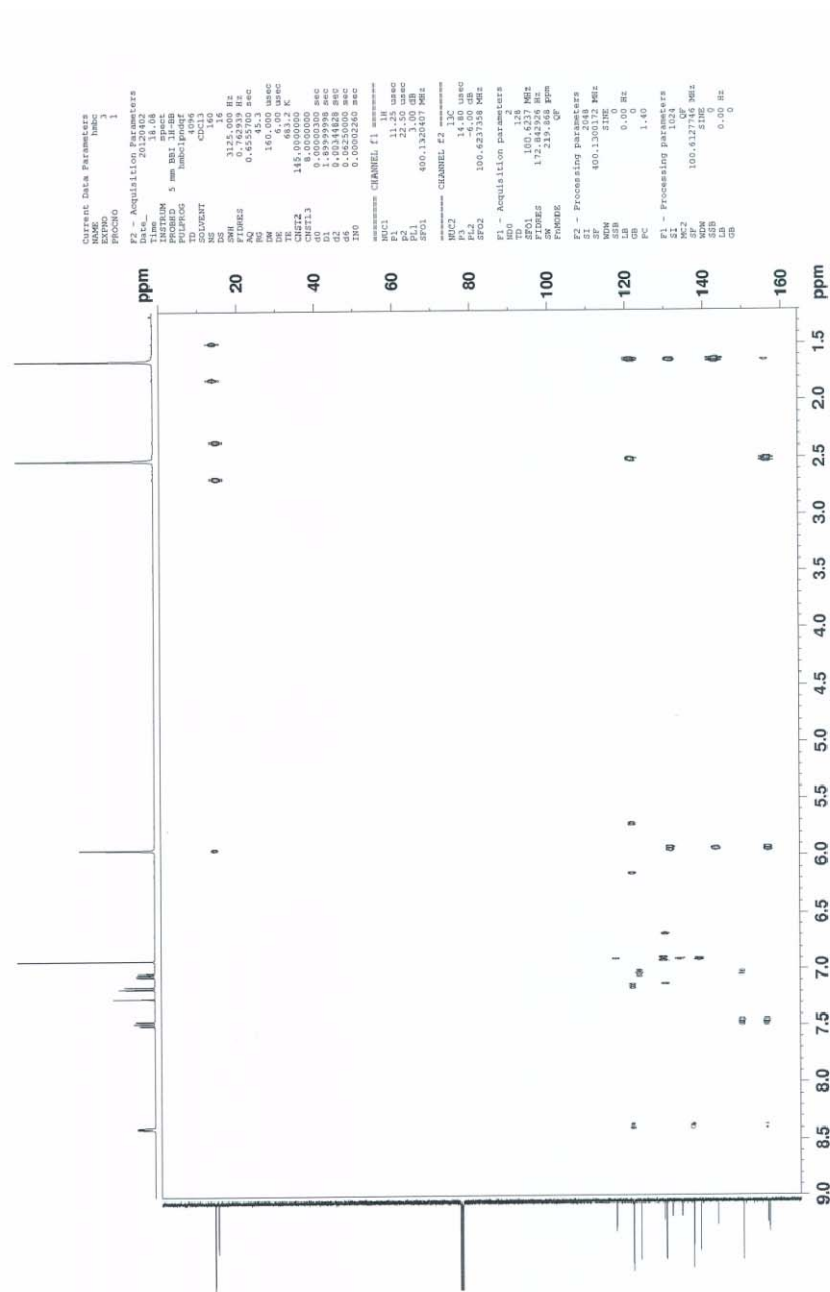


Figure S4.5: HMBC ( $^1\text{H}$ - $^{13}\text{C}$ ) NMR spectrum of compound 4.

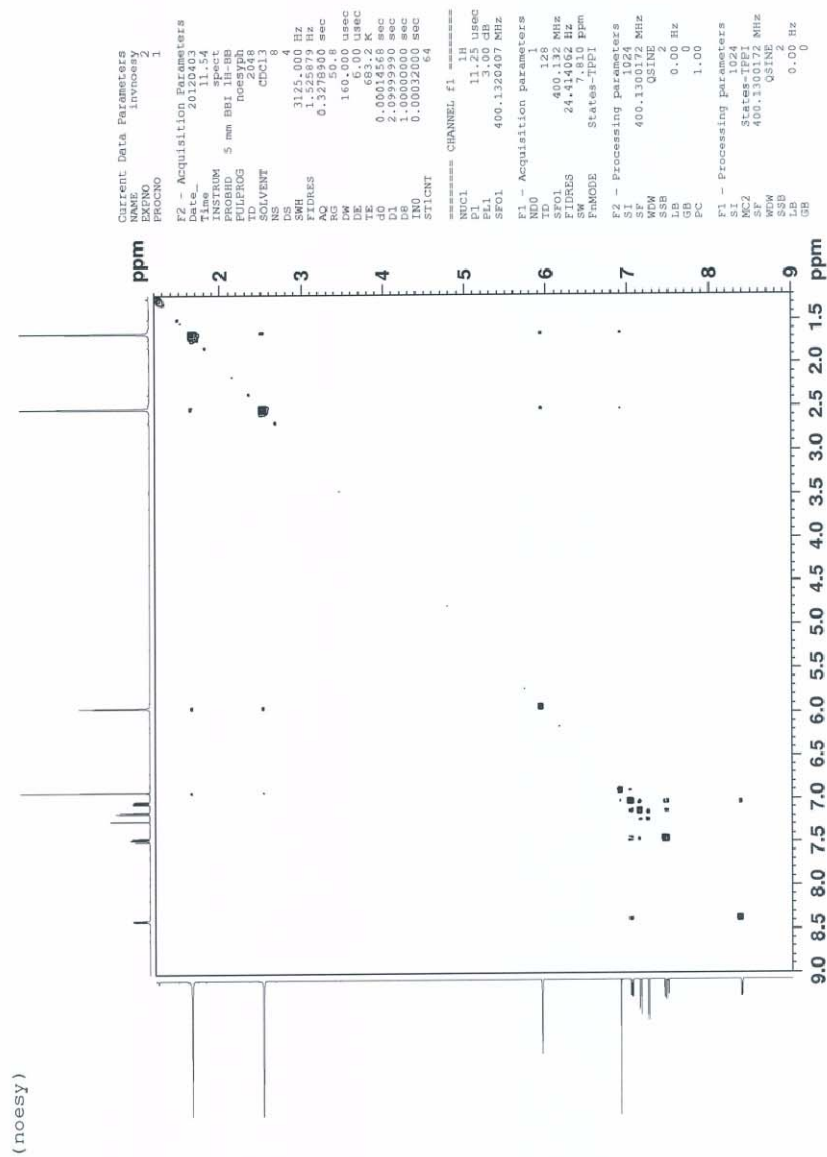
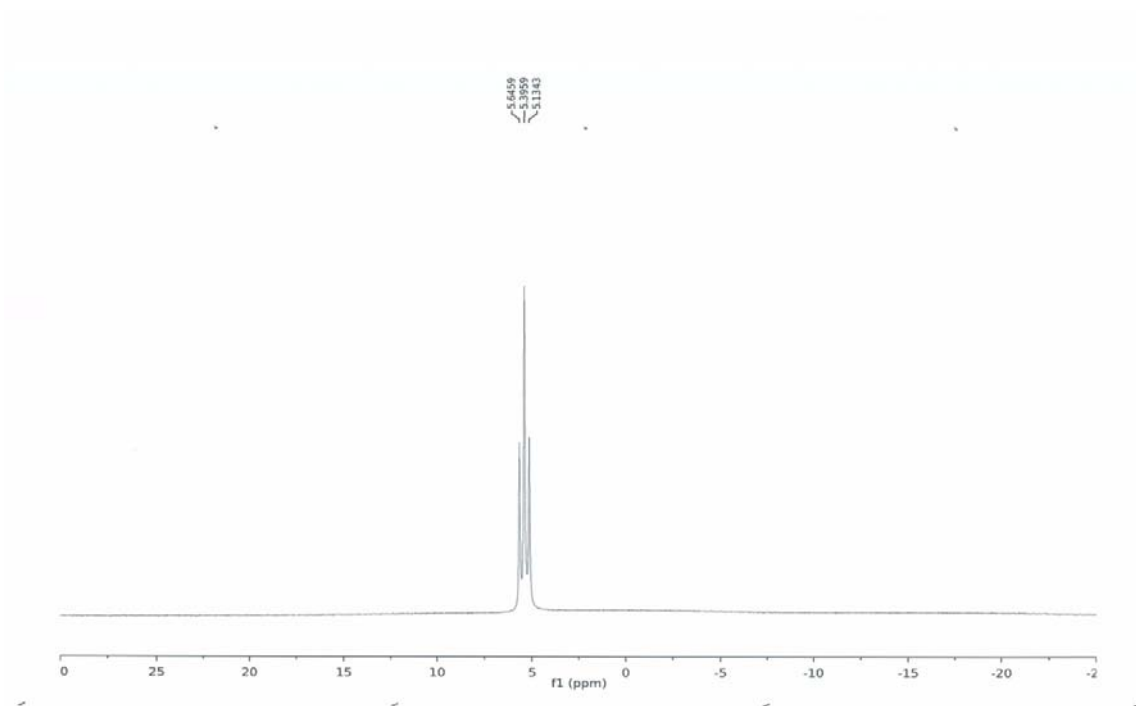


Figure S4.6: NOESY spectrum of compound 4.



**Figure S4.7:**  $^{11}\text{B}$  NMR spectrum of compound 4.

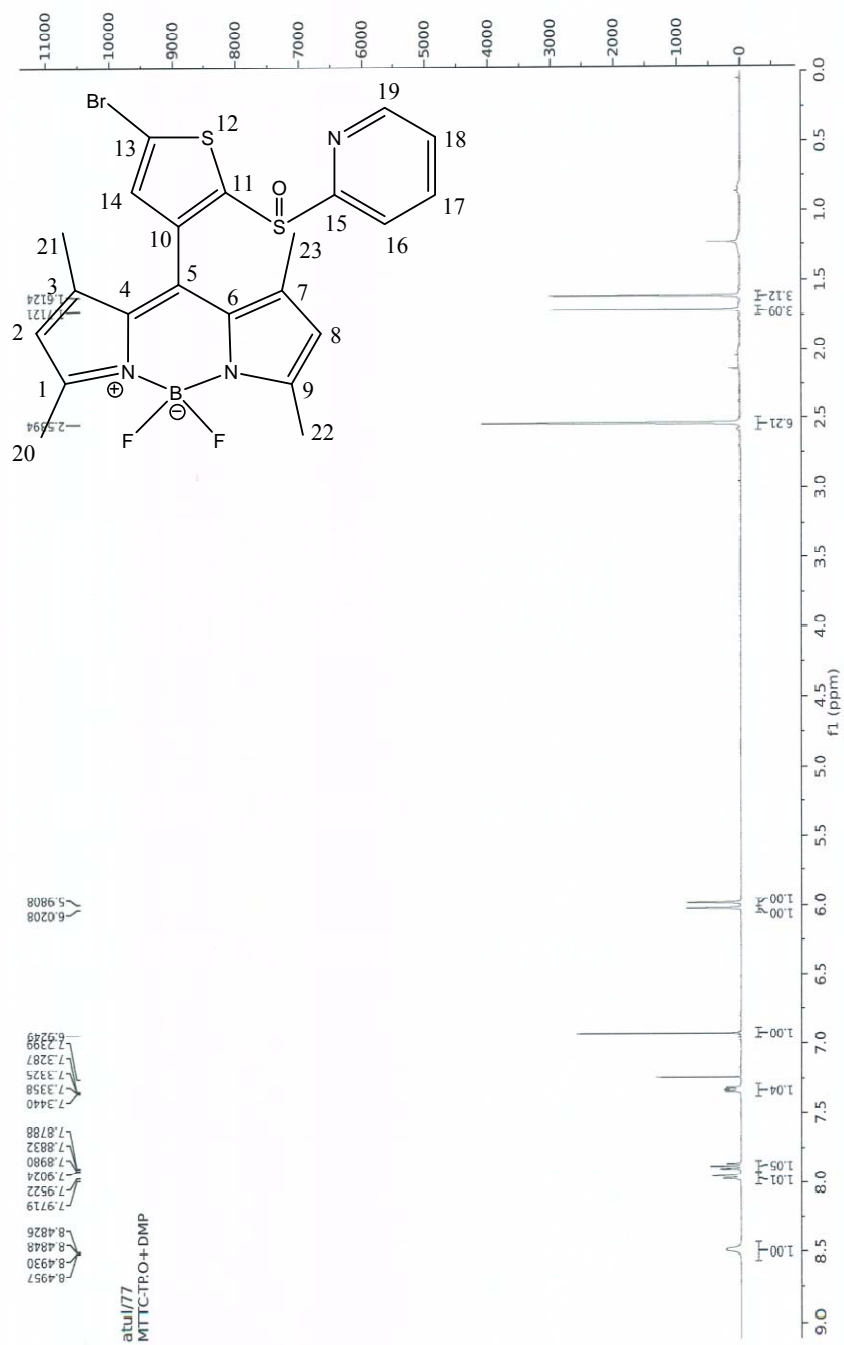


Figure S5.1:  $^1\text{H}$  NMR spectrum of compound 5.

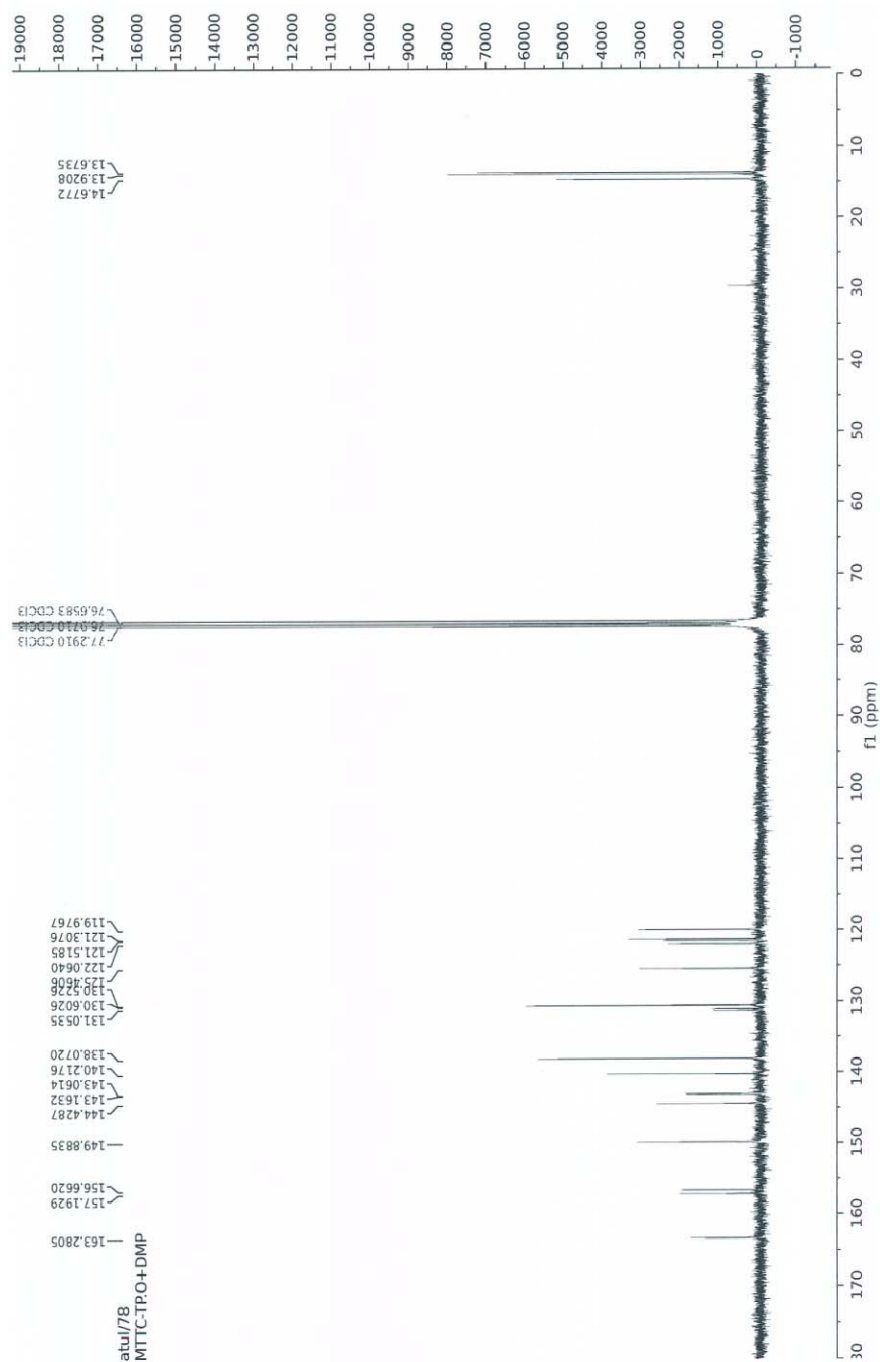
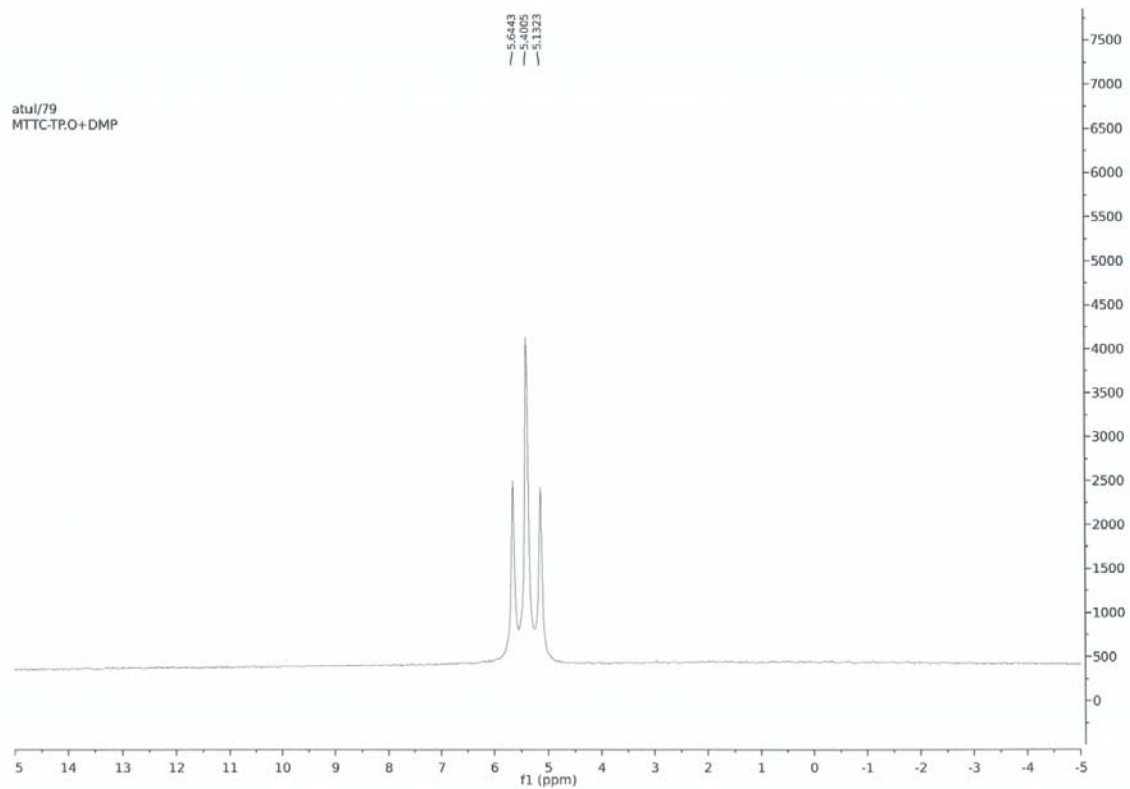


Figure S5.2:  $^{13}\text{C}$  NMR spectrum of compound 5.



**Figure S5.3:**  $^{11}\text{B}$  NMR spectrum of compound **5**.



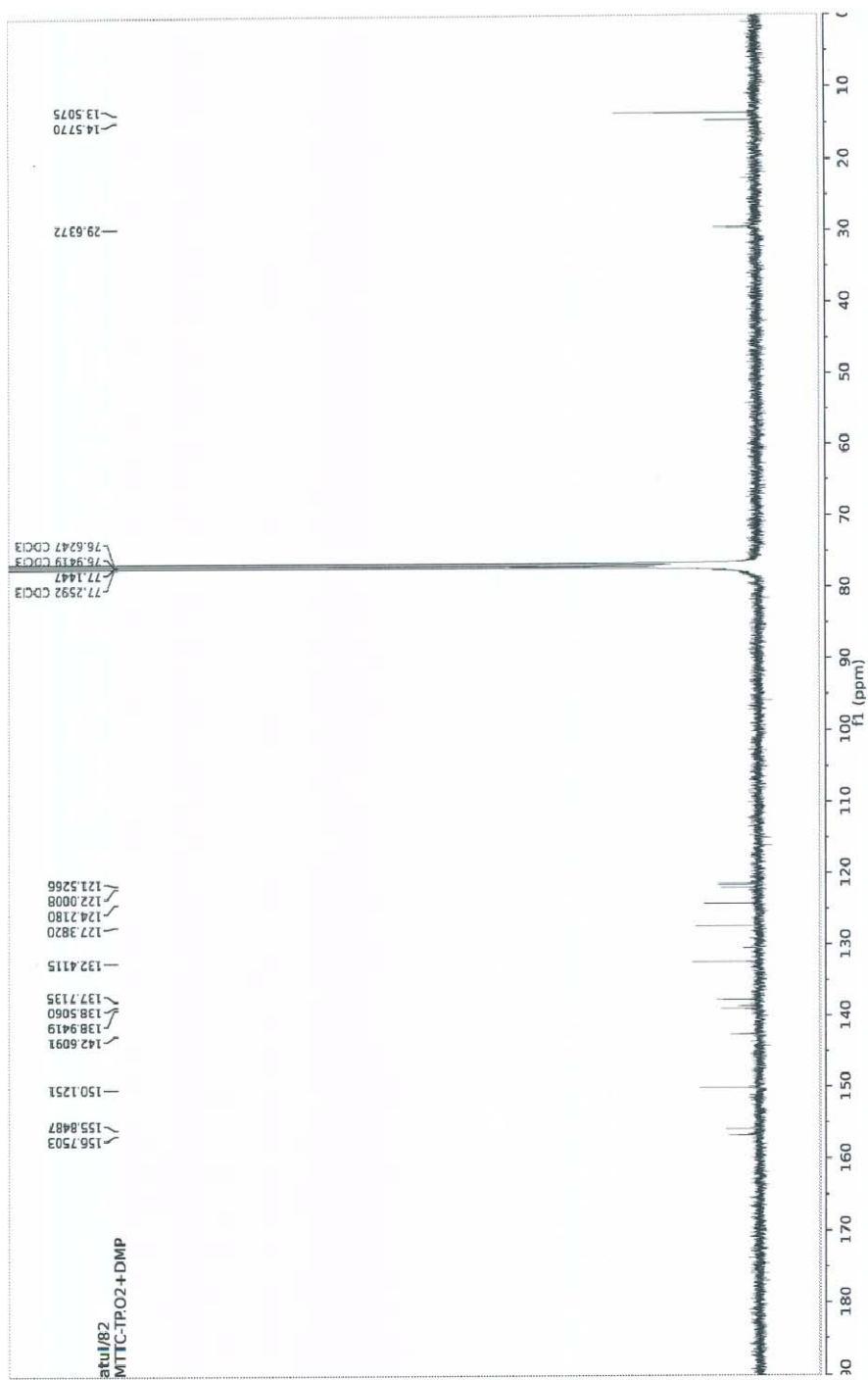
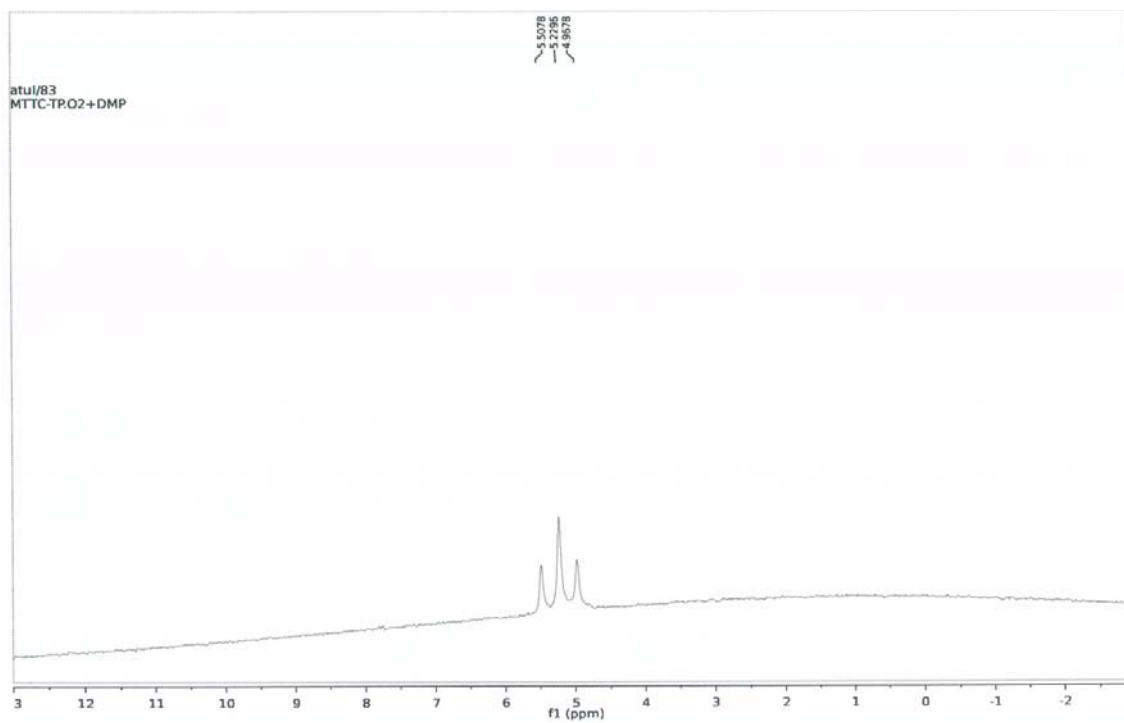
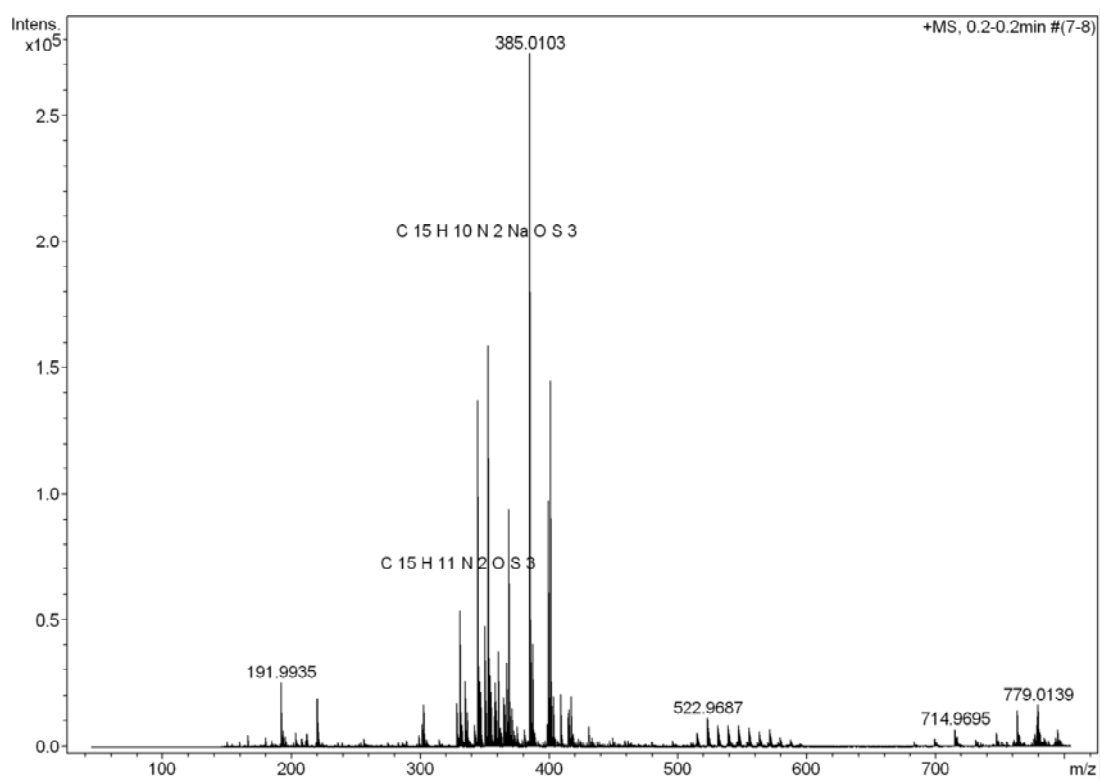


Figure S6.2:  $^{13}\text{C}$  NMR spectrum of compound 6.



**Figure S6.3:**  $^{11}\text{B}$  NMR spectrum of compound **6**.



**Figure S7:** Mass spectrum of compound 1.

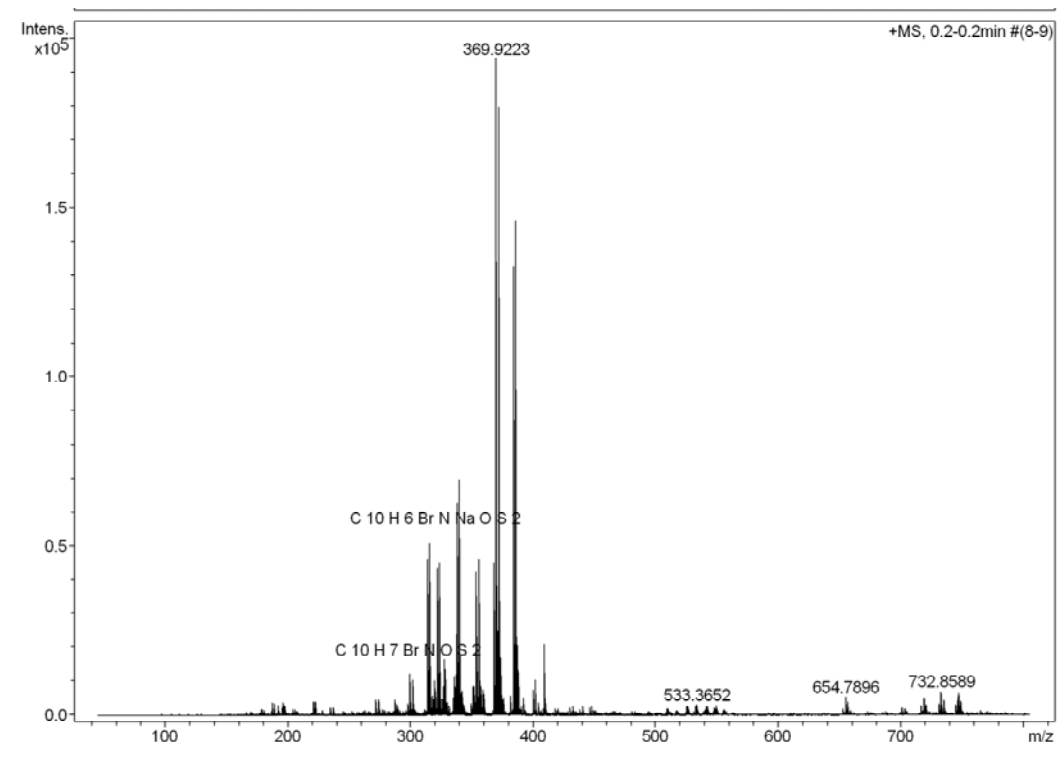


**Figure S8:** Mass spectrum of compound 2.

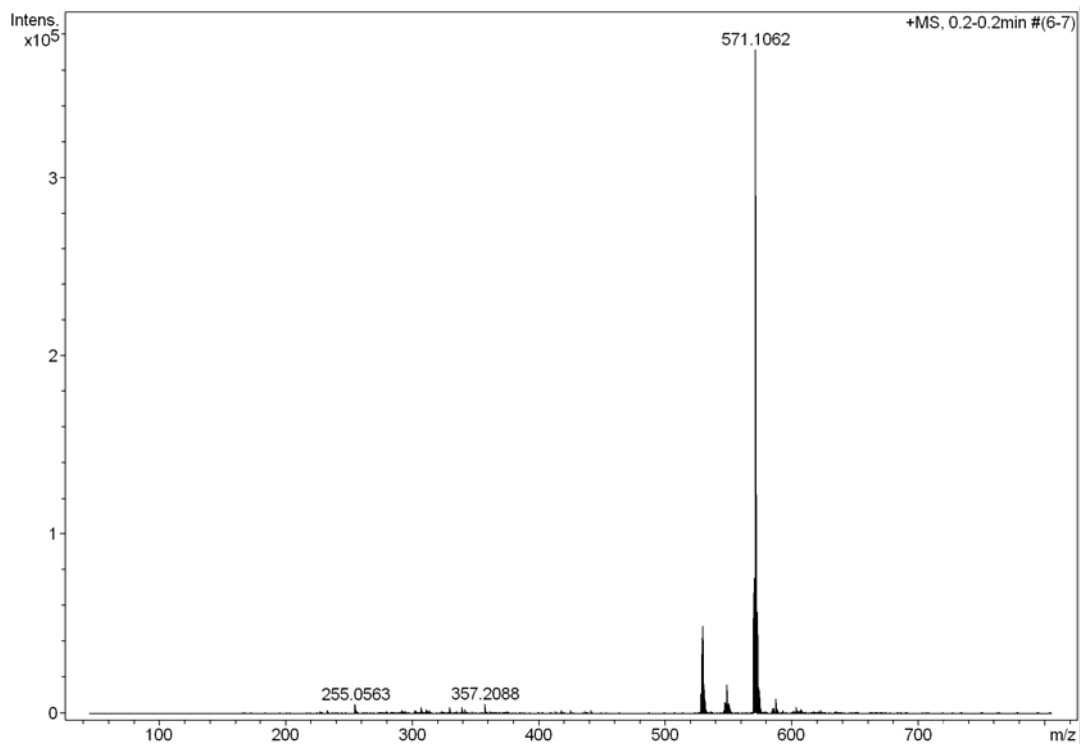


**Figure S9:** Mass spectrum of **3**.

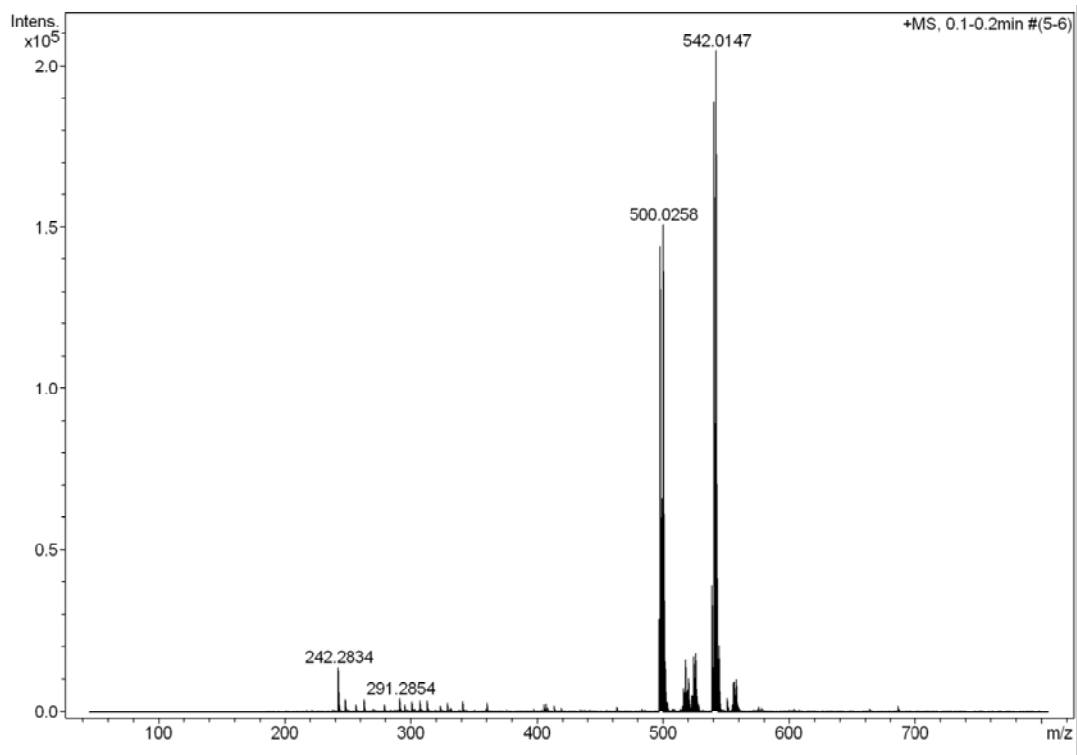


**Figure S10:** Mass spectrum of compound **4**.

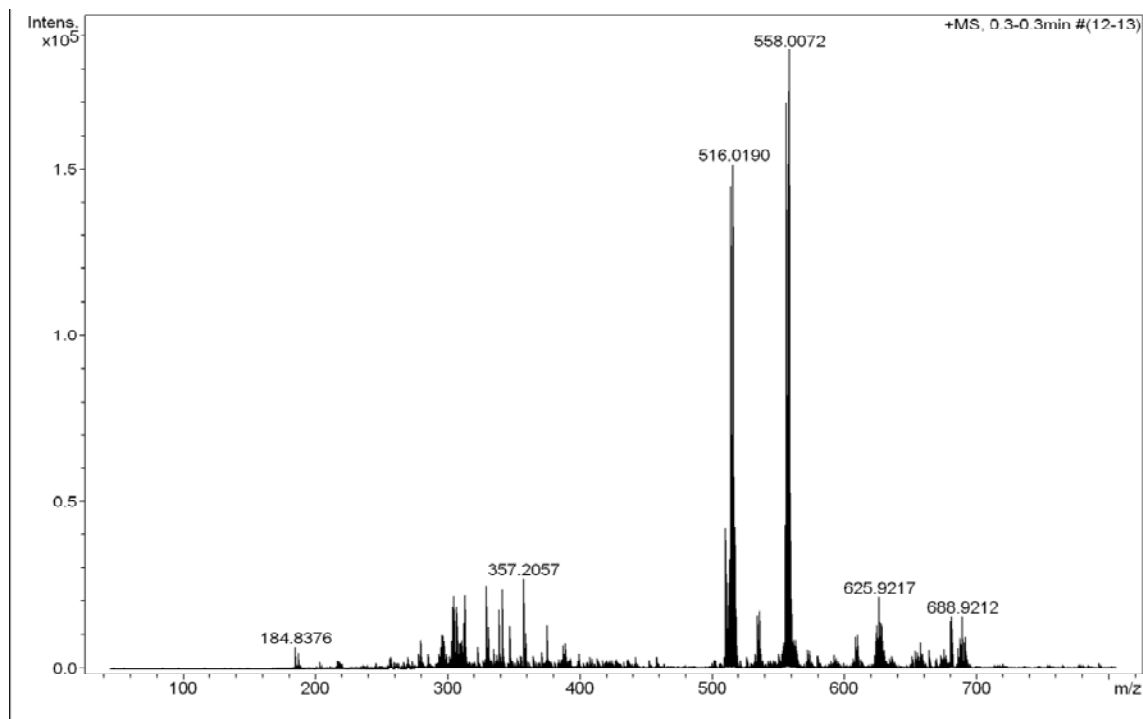


Figure S11: Mass spectrum of compound 5.

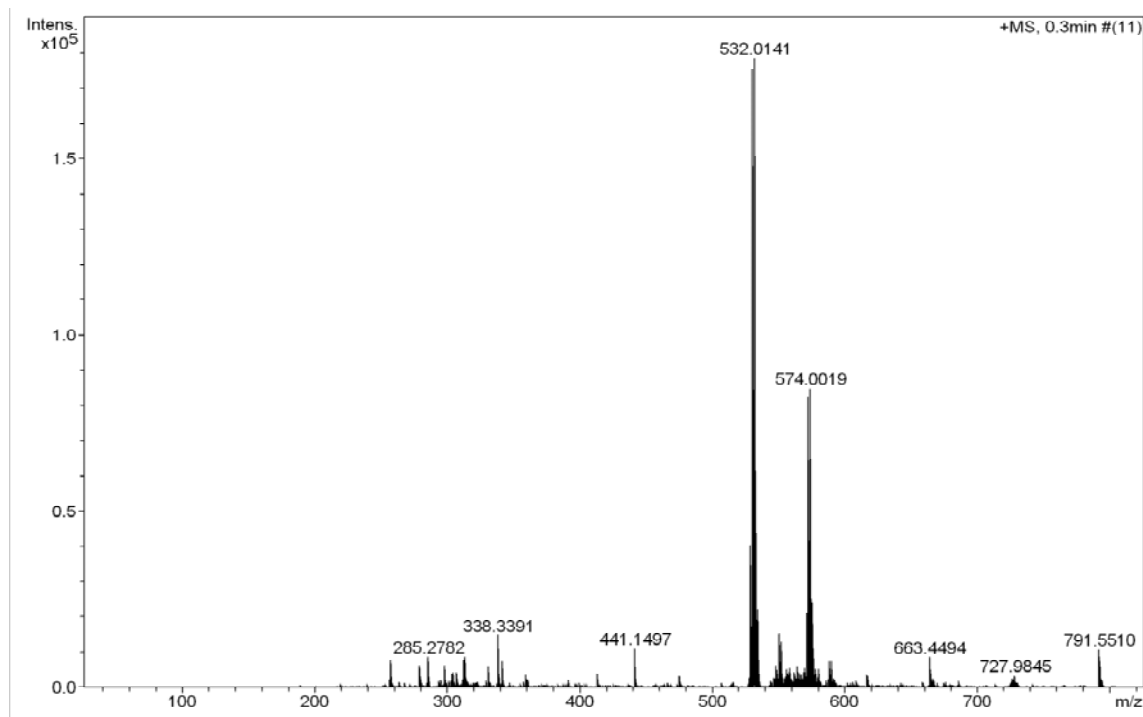
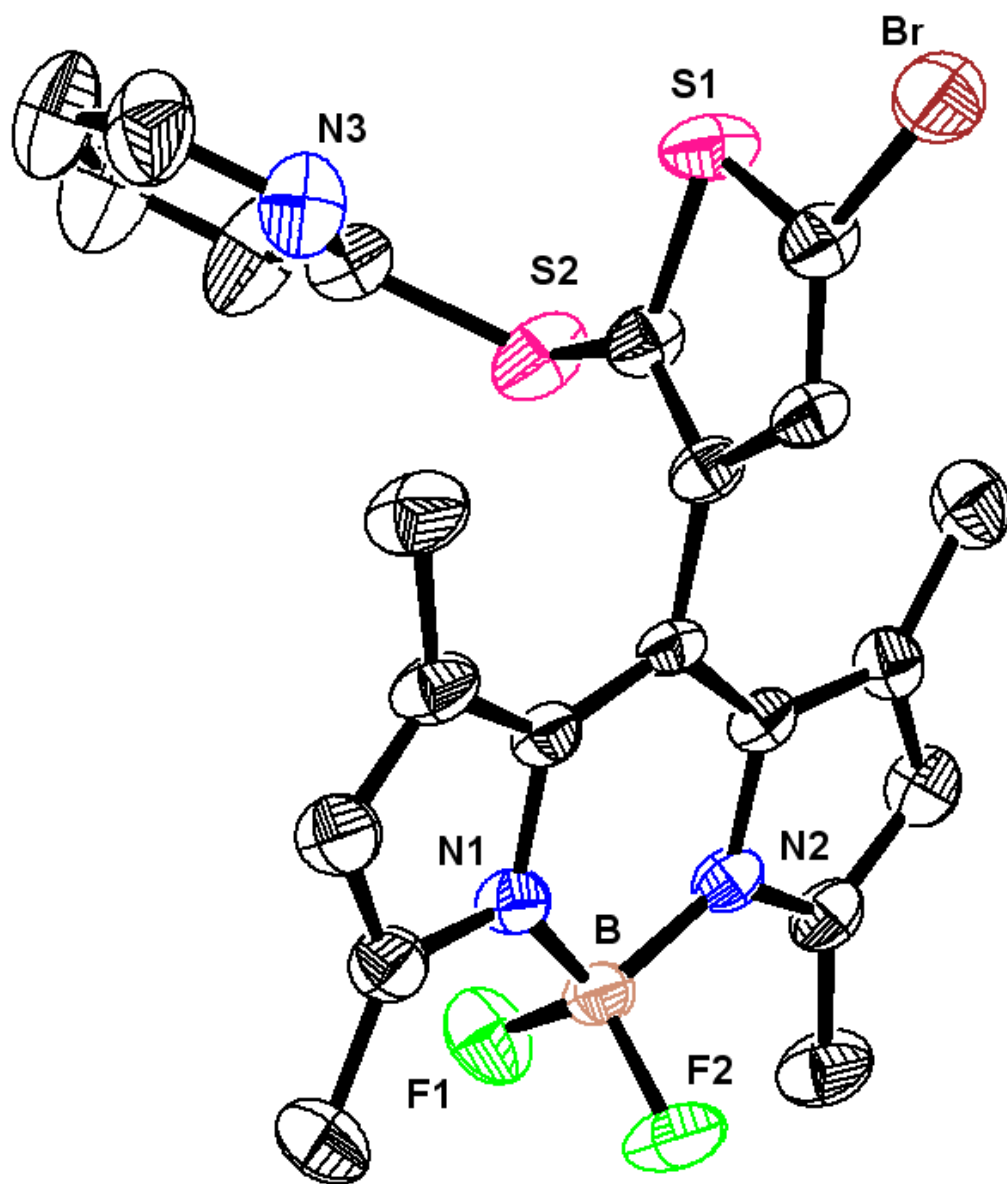


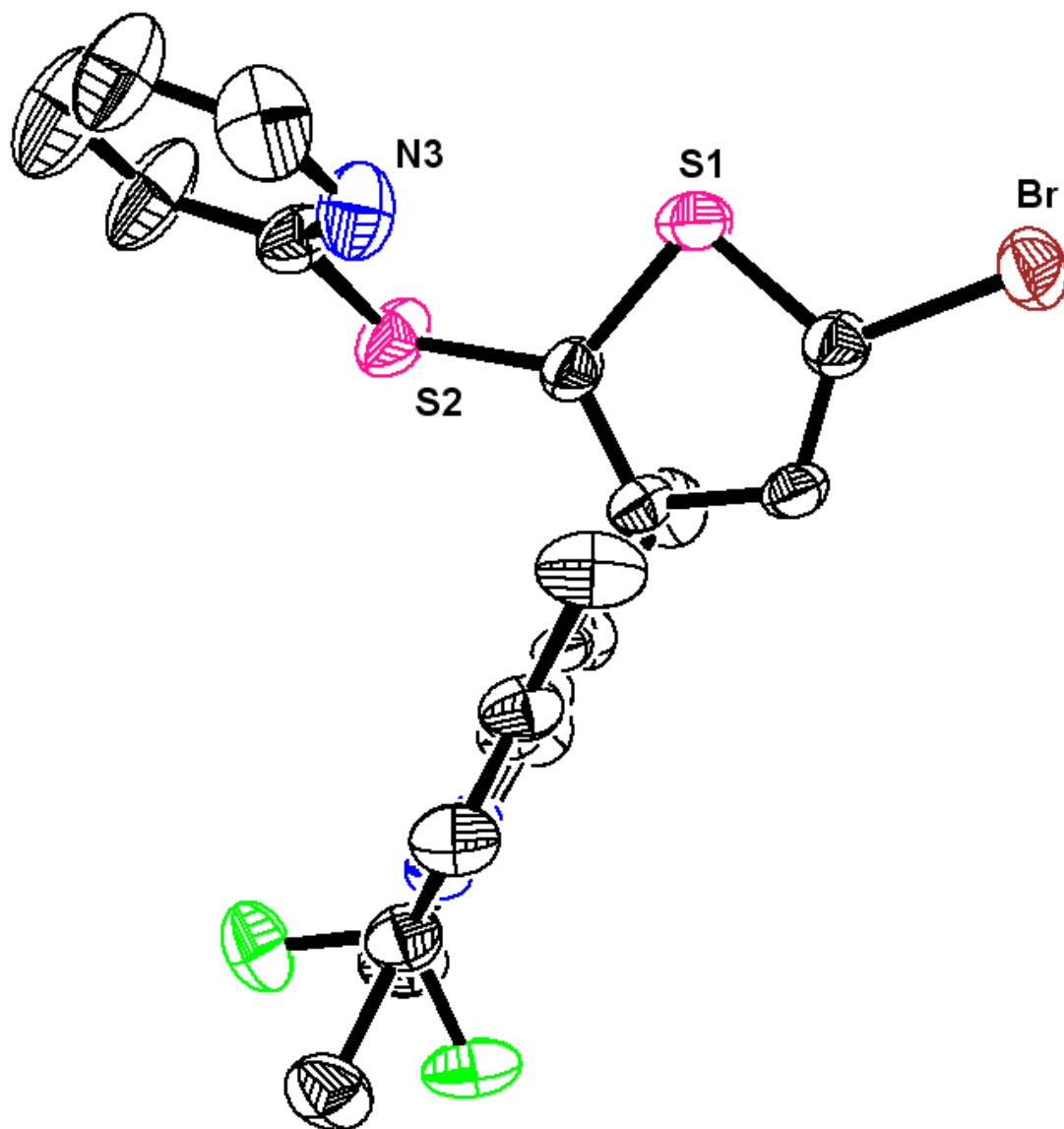
Figure S12: Mass spectrum of compound 6.

**Table S1:** Crystallographic data for compounds **4**.

Compound Number	<b>4</b>
empirical formula	C <sub>22</sub> H <sub>19</sub> BBrF <sub>2</sub> N <sub>3</sub> S <sub>2</sub>
fw	518.24
temperature (K)	296(2)
wavelength (Å)	0.71073
crystal system	Monoclinic
space group	P2(1)/n
a (Å)	7.5410(14)
b (Å)	11.291(2)
c (Å)	27.486(5)
α (deg)	90.00
β (deg)	95.942(8)
γ (deg)	90.00
V (Å <sup>3</sup> )	2327.7(7)
Z	4
density (Mg/m <sup>3</sup> )	1.479
abs coeff (mm <sup>-1</sup> )	1.976
F(000)	1048
crystal size	0.35×0.2× 0.15
θ range for data collection	1.49–30.38
reflns colld	38634
indep reflns	6972
R ( <i>int</i> )	0.1663
absorpt correction	Semi-empirical
max and min transmn	0.941 and 0.930
data/restraint/parameters	6972/0 /284
GOF on <i>F</i> <sup>2</sup>	1.013
final R indices	R1 = 0.0671
[ <i>I</i> > 2σ( <i>I</i> )]	wR2 = 0.1157
R indices	R1 = 0.2729
(all data) <sup>a</sup>	wR2 = 0.1691

Figures 13a and b: Different views of the crystal structure of 4.





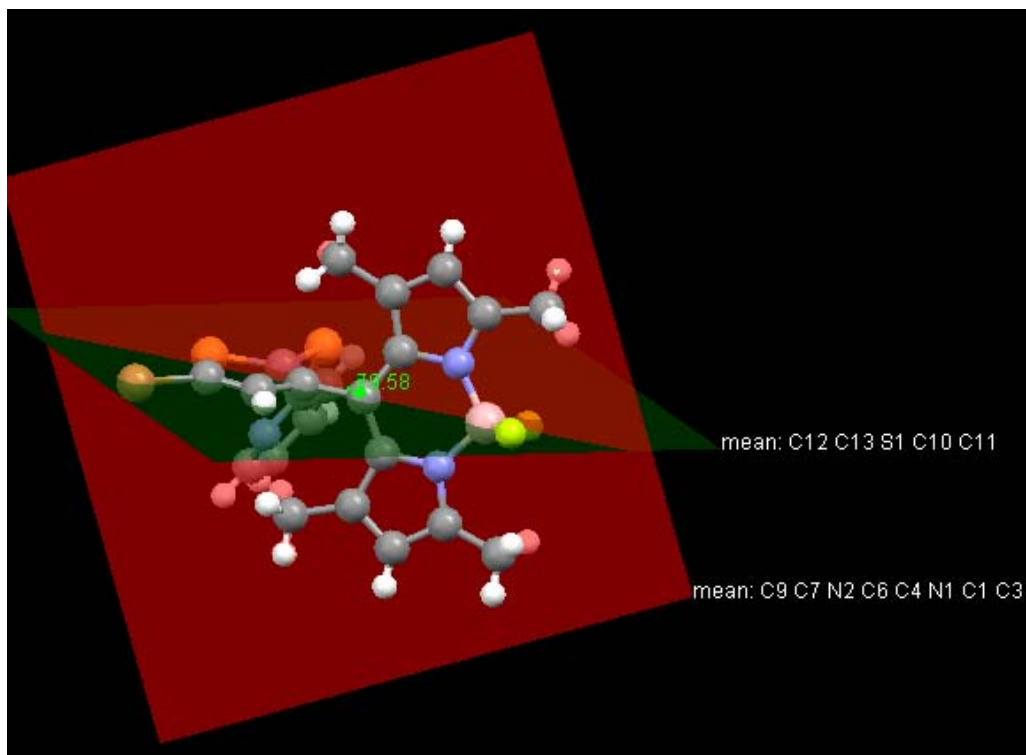


**Figure 14a:** Dihedral angle between the plane of thienyl ring (C12C13S1C10C11) and BODIPY core (C9C7N2C6C4N1C1C3) (79.58°).

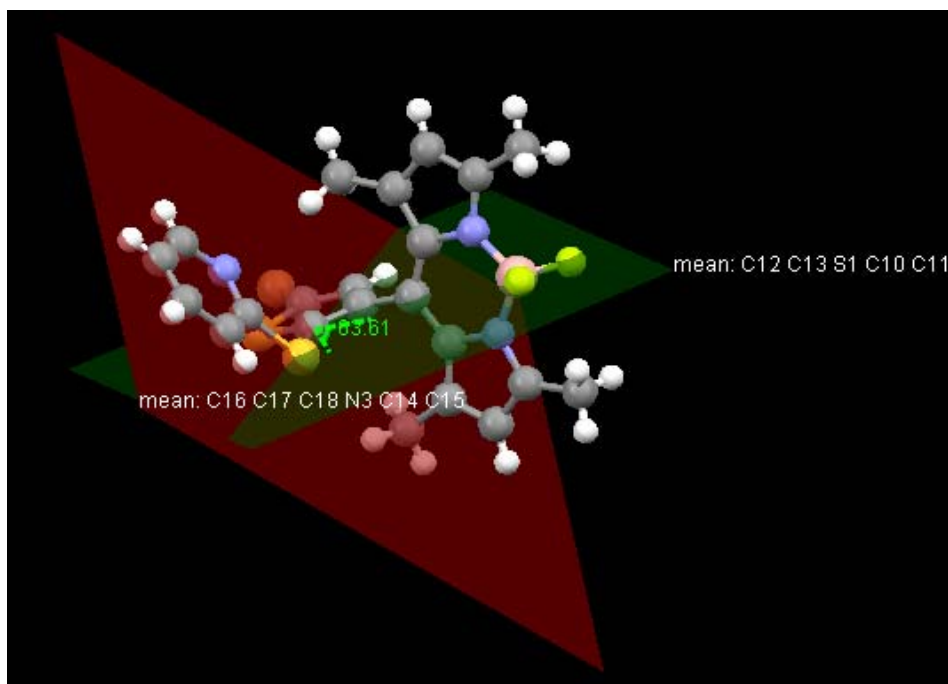


**Figure 14b:** Dihedral angle between the plane of thienyl ring (C12C13S1C10C11) and pyridyl ring (C16C17C18N3C14C15) (63.61°).

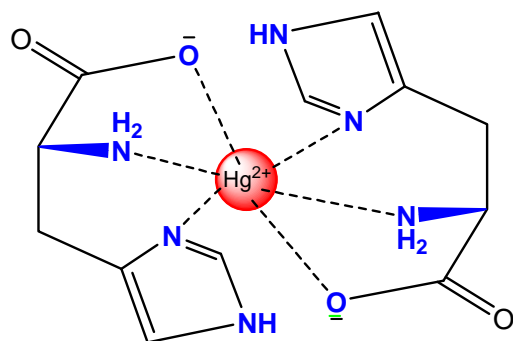


**Figure S15a: Schematic representation of His with  $\text{Hg}^{2+}$  ion.**

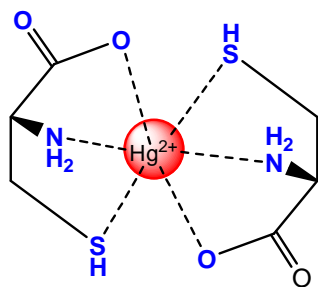


**Figure S15b: Schematic representation of Cys with  $\text{Hg}^{2+}$  ion.**

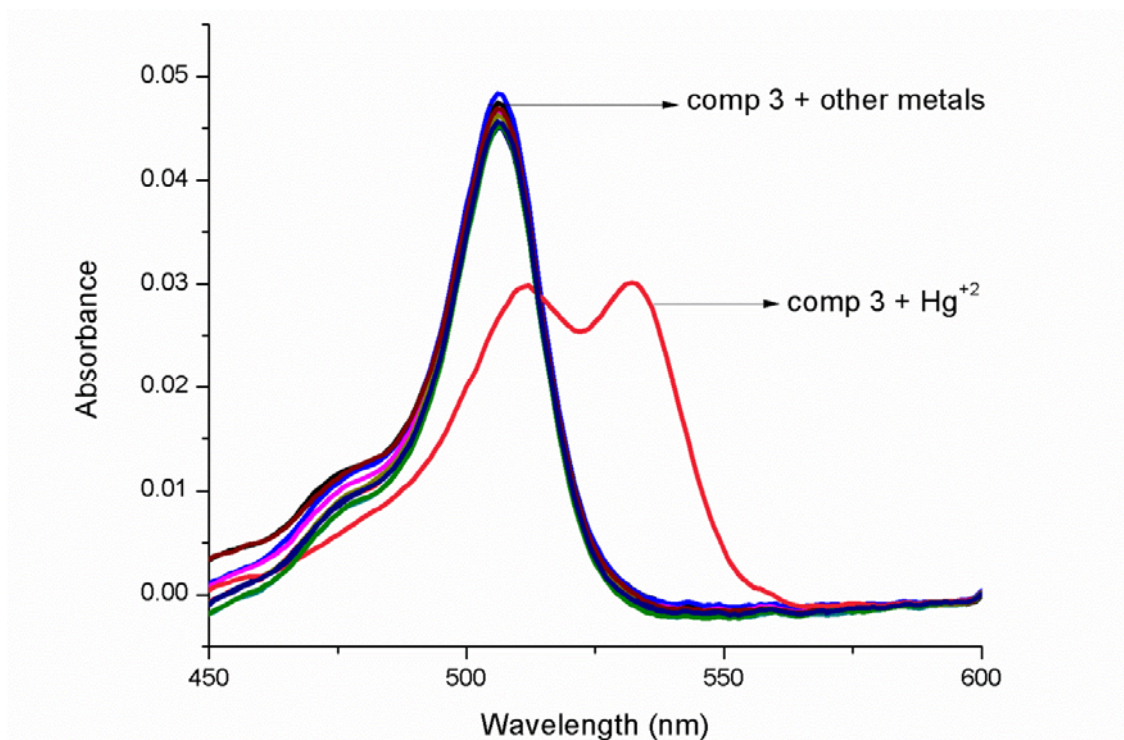


**Figure 16.** Absorption spectra of compound **3** ( $1.0 \times 10^{-6}$  M, 3.0 mL) with ( $1.0 \times 10^{-2}$  M, 50  $\mu$ L) of  $\text{Ca}^{2+}$ ,  $\text{Cd}^{2+}$ ,  $\text{Co}^{2+}$ ,  $\text{Cu}^{2+}$ ,  $\text{Fe}^{2+}$ ,  $\text{Hg}^{2+}$ ,  $\text{Mg}^{2+}$ ,  $\text{Mn}^{2+}$ ,  $\text{Pb}^{2+}$ , and  $\text{Zn}^{2+}$ .

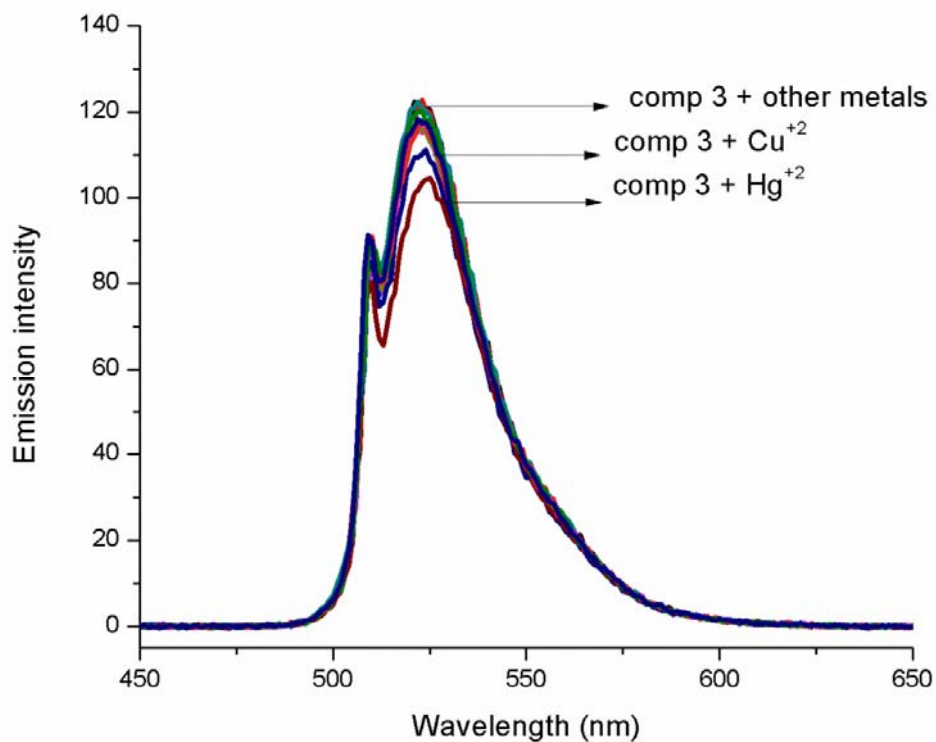


**Figure 17.** Emission spectra of compound **3** ( $1.0 \times 10^{-6}$  M, 3.0 mL) with ( $1.0 \times 10^{-2}$  M, 50  $\mu$ L) of  $\text{Ca}^{2+}$ ,  $\text{Cd}^{2+}$ ,  $\text{Co}^{2+}$ ,  $\text{Cu}^{2+}$ ,  $\text{Fe}^{2+}$ ,  $\text{Hg}^{2+}$ ,  $\text{Mg}^{2+}$ ,  $\text{Mn}^{2+}$ ,  $\text{Pb}^{2+}$ , and  $\text{Zn}^{2+}$ .

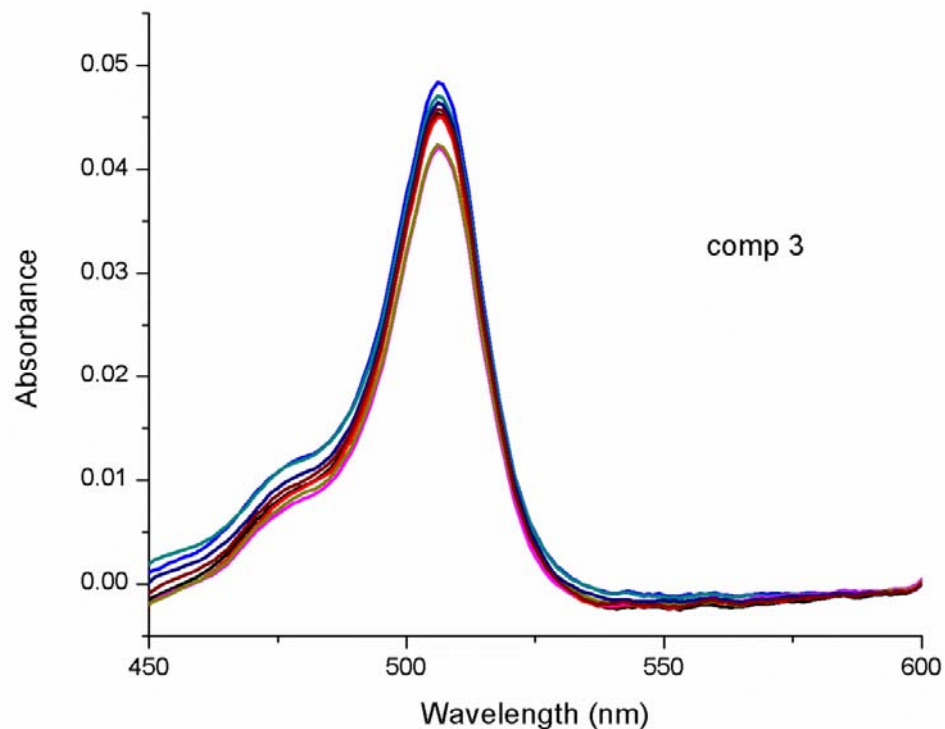


**Figure 18.** Absorbance spectra of compound **3** ( $1.0 \times 10^{-6}$  M, 3.0 mL) with ( $1.0 \times 10^{-2}$  M, 50  $\mu$ L) of *m*-CPBA,  $\text{KO}_2$ ,  $\text{H}_2\text{O}_2$ , NaOCl, *t*-BuOOH,  $\cdot\text{OH}$ ,  $\cdot\text{O}t\text{-Bu}$ .

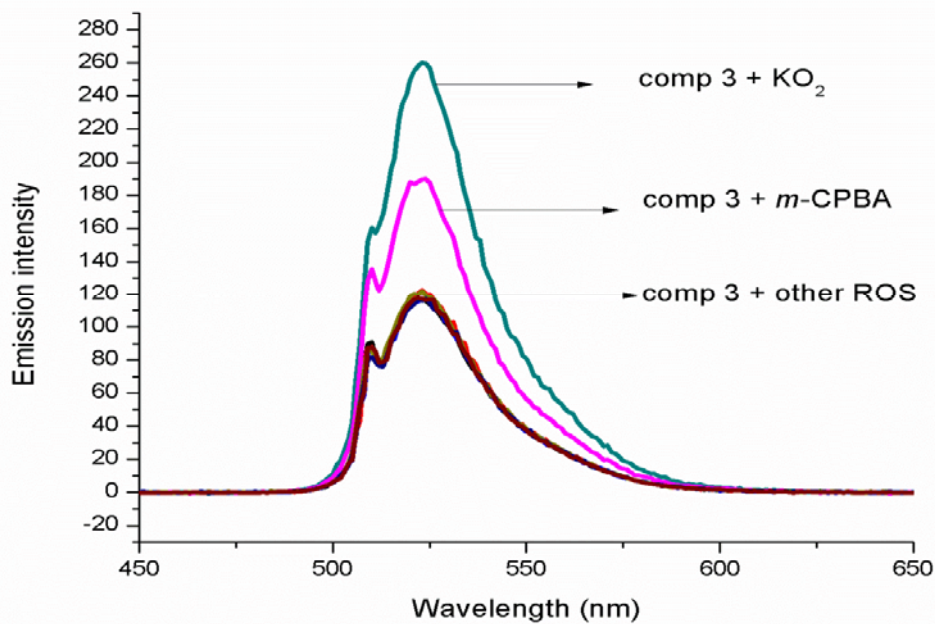


**Figure 19.** Emission spectra of compound **3** ( $1.0 \times 10^{-6}$  M, 3 mL) with ( $1.0 \times 10^{-2}$  M, 50  $\mu$ L) of *m*-CPBA,  $\text{KO}_2$ ,  $\text{H}_2\text{O}_2$ , NaOCl, *t*-BuOOH,  $\cdot\text{OH}$ ,  $\cdot\text{O}t\text{-Bu}$ .

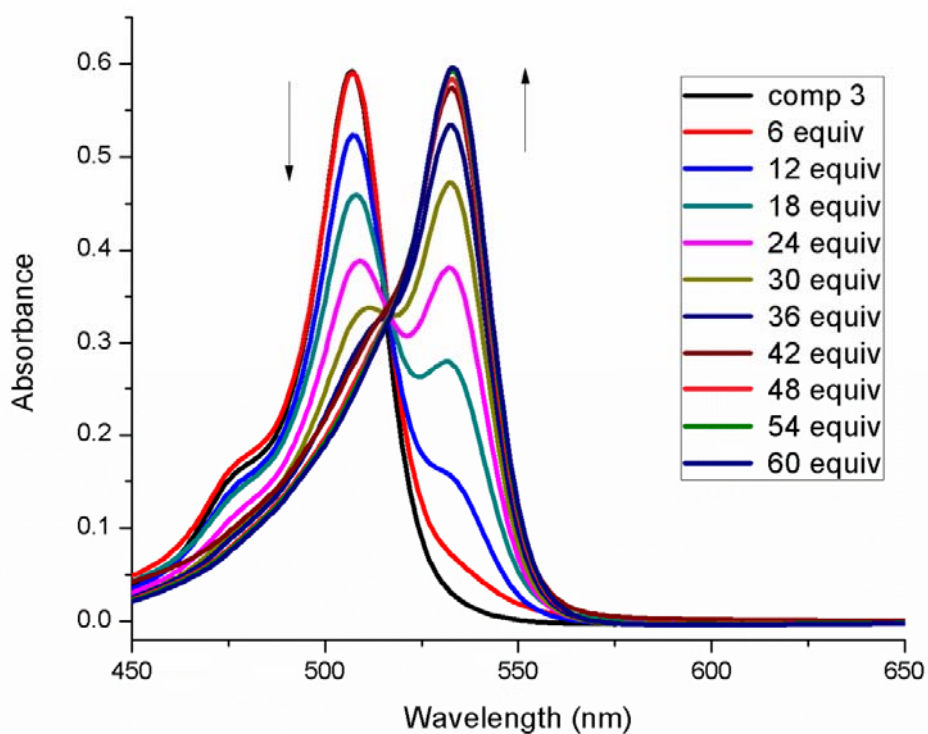


**Figure 20.** Absorbance spectra of compound **3** ( $1.0 \times 10^{-5}$  M, 3 mL) with the increasing concentration of  $\text{Hg}^{2+}$  in acetonitrile/water (70/30).

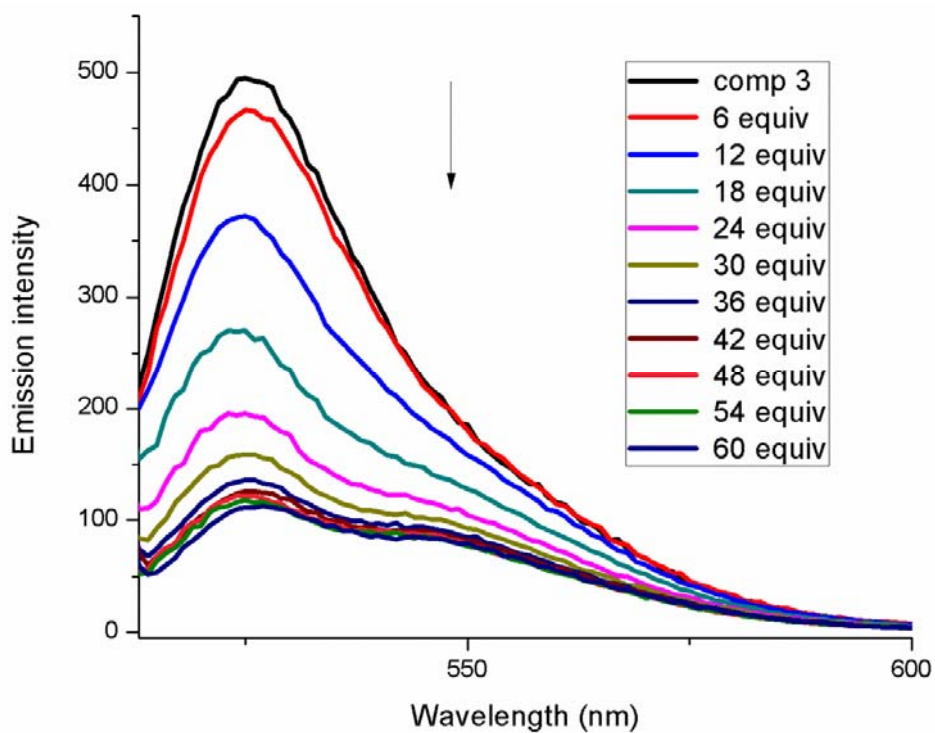


**Figure 21.** Emission spectra of compound **3** ( $1.0 \times 10^{-5}$  M, 3 mL) with the increasing concentration of  $\text{Hg}^{2+}$  in acetonitrile/water.

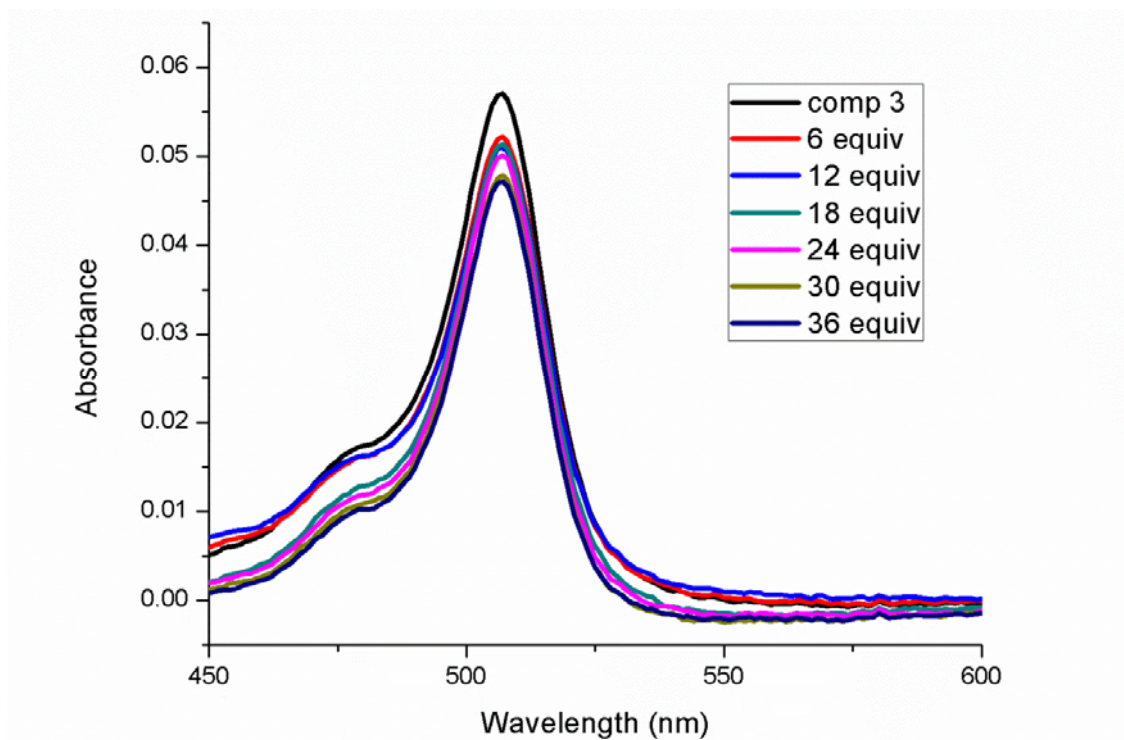


**Figure 22.** Absorbance spectra of compound **3** ( $1.0 \times 10^{-6}$  M, 3 mL) with the increasing concentration of KO<sub>2</sub> in acetonitrile/water (70/30).

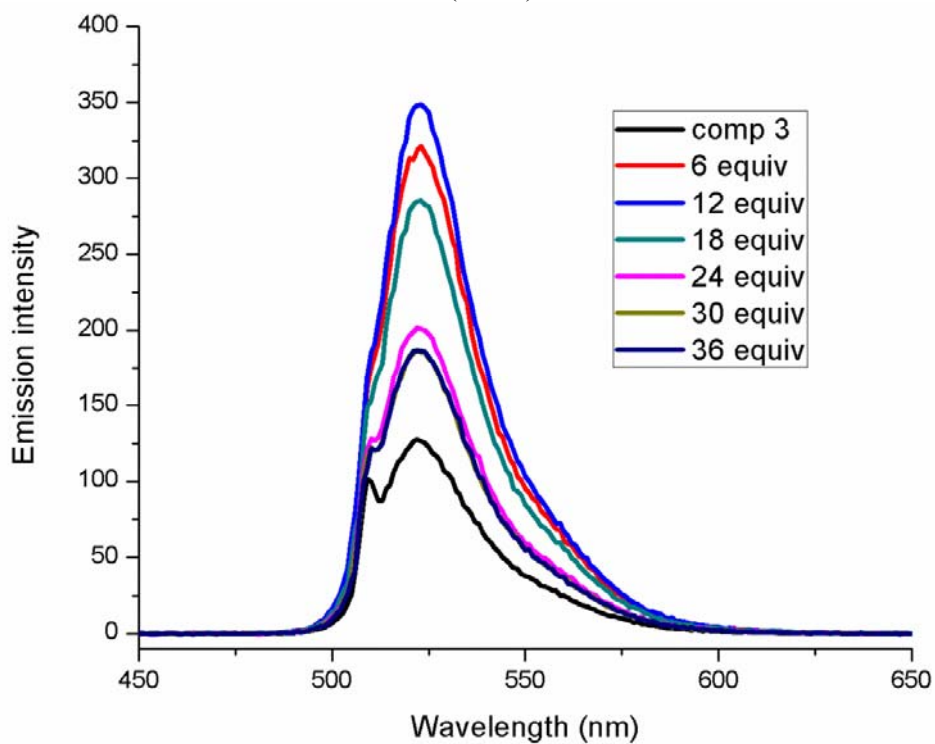


**Figure 23.** Emission spectra of compound **3** ( $1.0 \times 10^{-6}$  M, 3 mL) with the increasing concentration of KO<sub>2</sub> in acetonitrile/water (70/30).

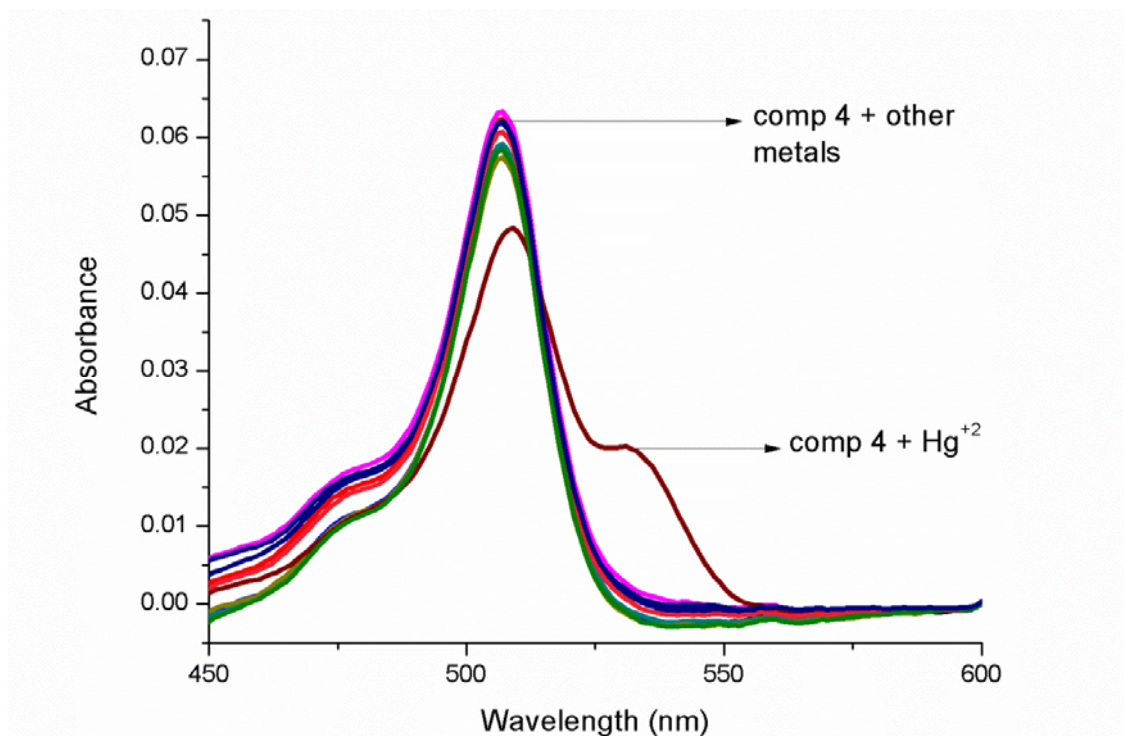


**Figure 24.** Absorption spectra of compound **4** ( $1.0 \times 10^{-6}$  M, 3.0 mL) with ( $1.0 \times 10^{-2}$  M, 50  $\mu$ L) of  $\text{Ca}^{2+}$ ,  $\text{Cd}^{2+}$ ,  $\text{Co}^{2+}$ ,  $\text{Cu}^{2+}$ ,  $\text{Fe}^{2+}$ ,  $\text{Hg}^{2+}$ ,  $\text{Mg}^{2+}$ ,  $\text{Mn}^{2+}$ ,  $\text{Pb}^{2+}$ , and  $\text{Zn}^{2+}$ .

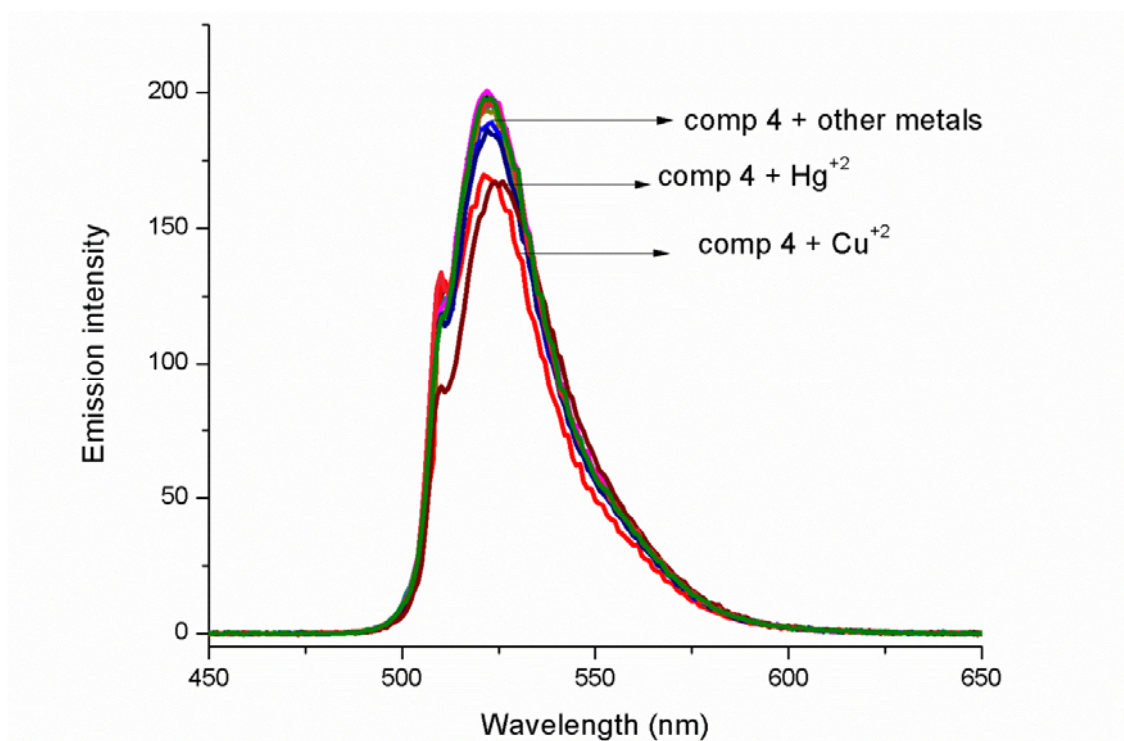


**Figure 25.** Emission spectra of compound **4** ( $1.0 \times 10^{-6}$  M, 3.0 mL) with ( $1.0 \times 10^{-2}$  M, 50  $\mu$ L) of  $\text{Ca}^{2+}$ ,  $\text{Cd}^{2+}$ ,  $\text{Co}^{2+}$ ,  $\text{Cu}^{2+}$ ,  $\text{Fe}^{2+}$ ,  $\text{Hg}^{2+}$ ,  $\text{Mg}^{2+}$ ,  $\text{Mn}^{2+}$ ,  $\text{Pb}^{2+}$ , and  $\text{Zn}^{2+}$ .

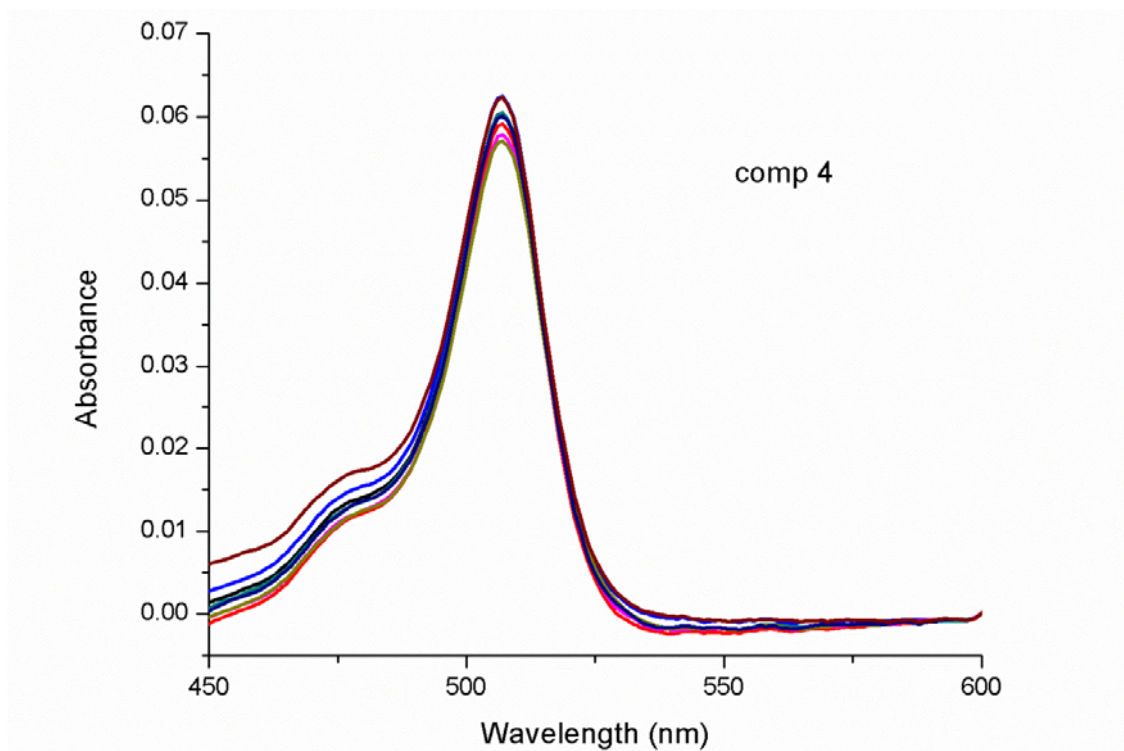


**Figure 26.** Absorbance spectra of compound **4** ( $1.0 \times 10^{-6}$  M, 3.0 mL ) with ( $1.0 \times 10^{-2}$  M, 50  $\mu$ L,) of *m*-CPBA, KO<sub>2</sub>, H<sub>2</sub>O<sub>2</sub>, NaOCl, *t*-BuOOH,  $\cdot$ OH,  $\cdot$ O*t*-Bu.

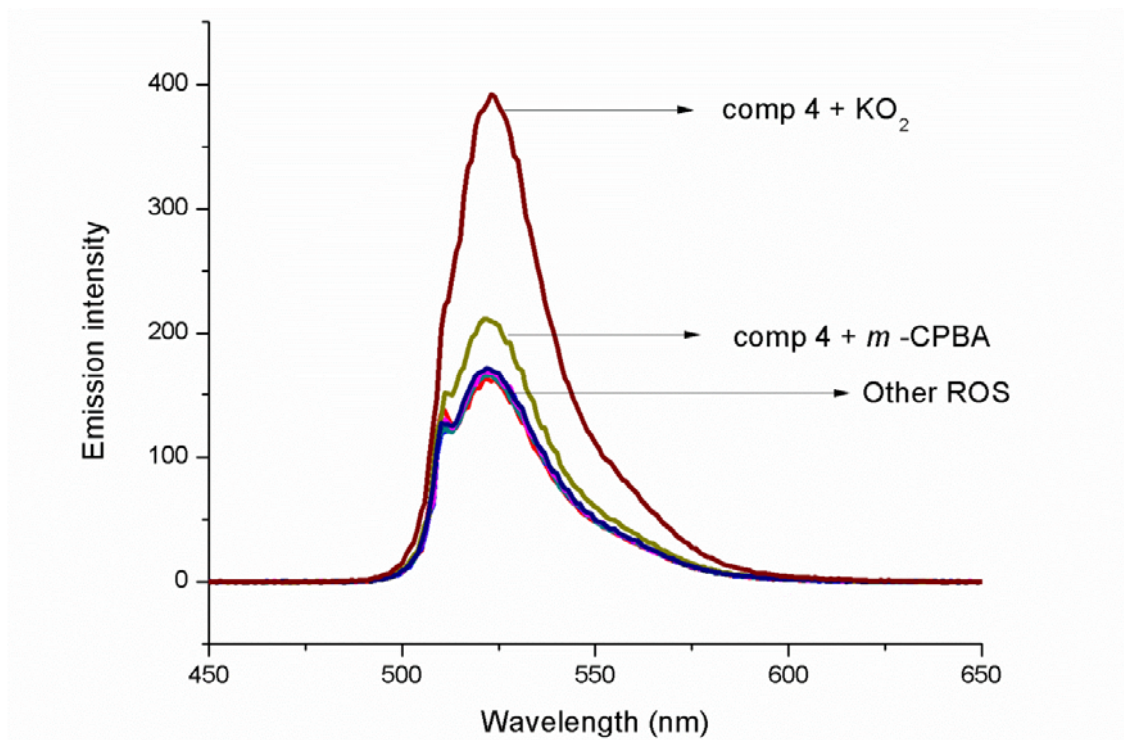


**Figure 27.** Emission spectra of compound **4** ( $1.0 \times 10^{-6}$  M, 3.0 mL ) with ( $1.0 \times 10^{-2}$  M, 50  $\mu$ L,) of *m*-CPBA, KO<sub>2</sub>, H<sub>2</sub>O<sub>2</sub>, NaOCl, *t*-BuOOH,  $\cdot$ OH,  $\cdot$ O*t*-Bu.

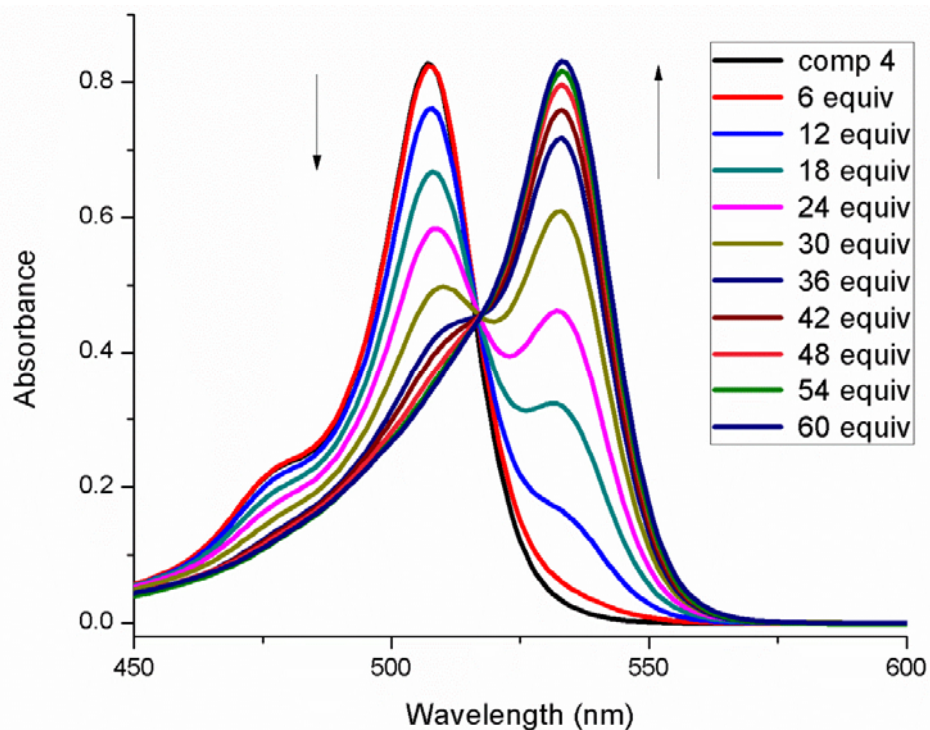


**Figure 28.** Absorbance spectra of compound **4** ( $1.0 \times 10^{-5}$  M, 3 mL) with the increasing concentration of  $\text{Hg}^{2+}$  in acetonitrile/water (70/30).

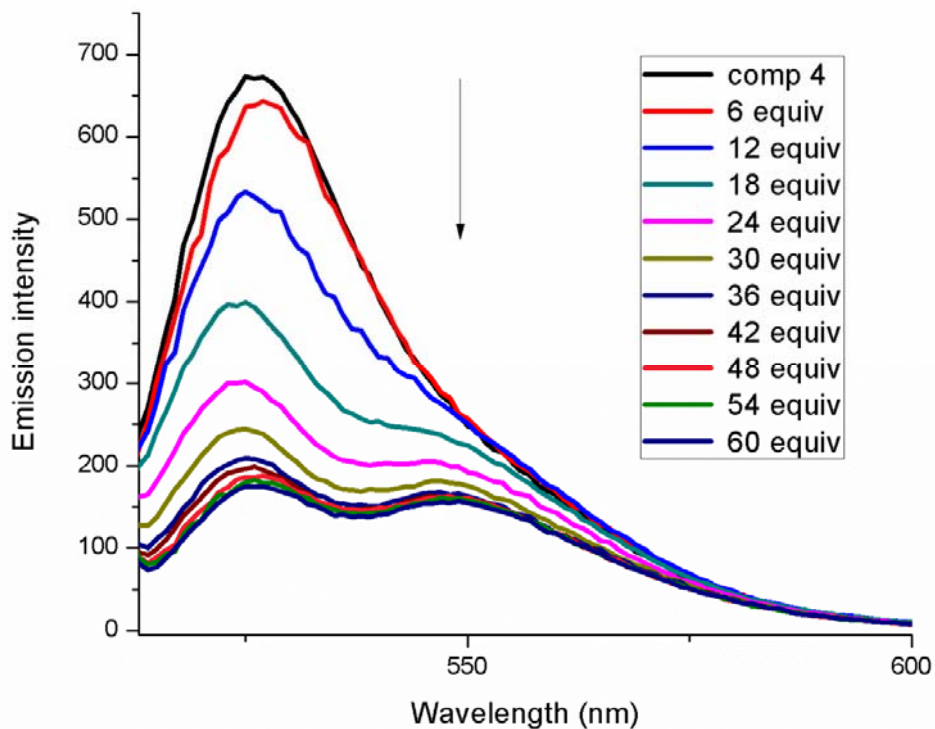


**Figure 29.** Emission spectra of compound **4** ( $1.0 \times 10^{-5}$  M, 3 mL) with the increasing concentration of  $\text{Hg}^{2+}$  in acetonitrile/water (70/30).

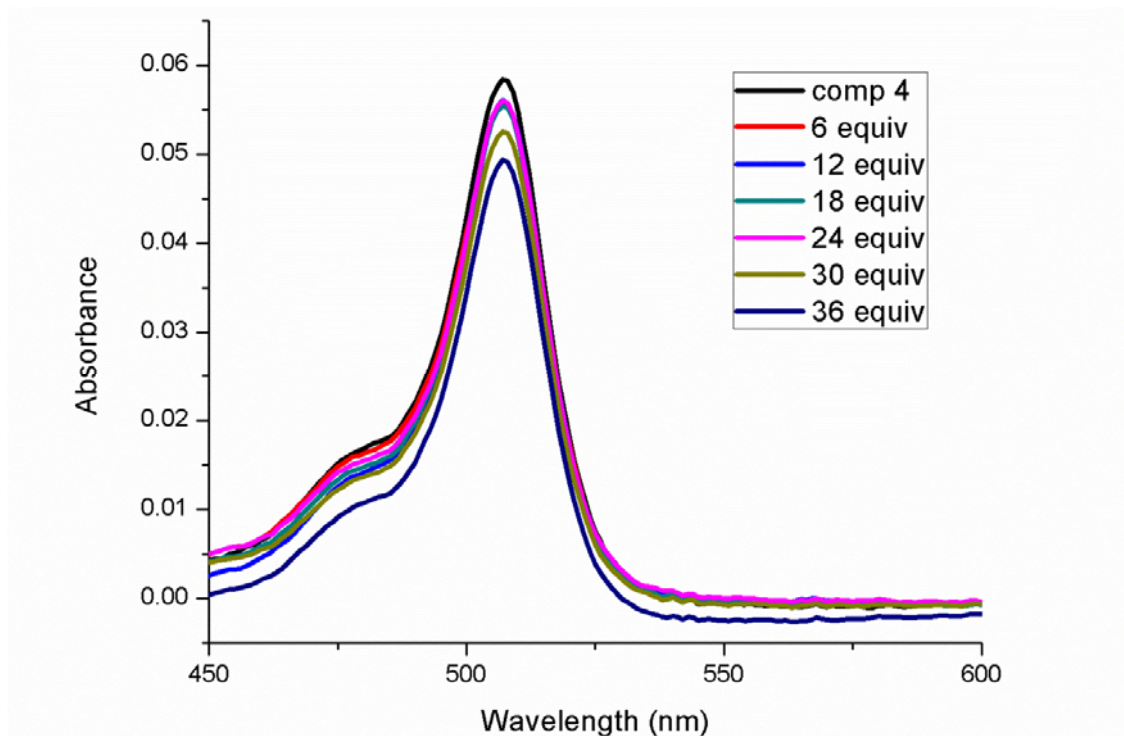


**Figure 30.** Absorbance spectra of compound **4** ( $1.0 \times 10^{-6}$  M, 3 mL) with the increasing concentration of KO<sub>2</sub> in acetonitrile/water (70/30).

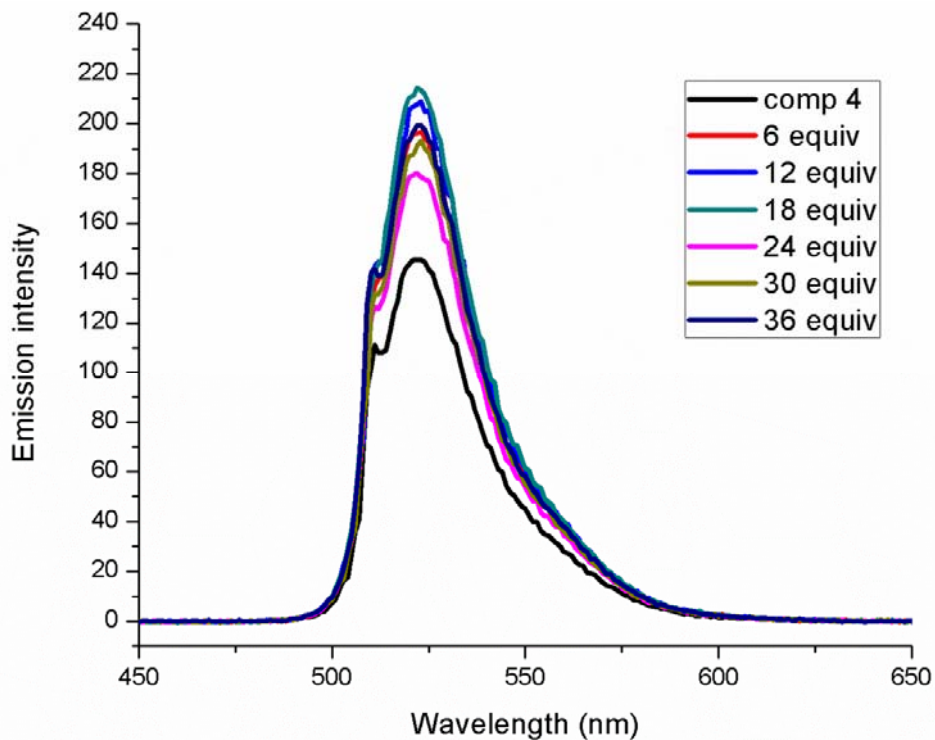


**Figure 31.** Emission spectra of compound **4** ( $1.0 \times 10^{-6}$  M, 3 mL) with the increasing concentration of KO<sub>2</sub> in acetonitrile/water (70/30).

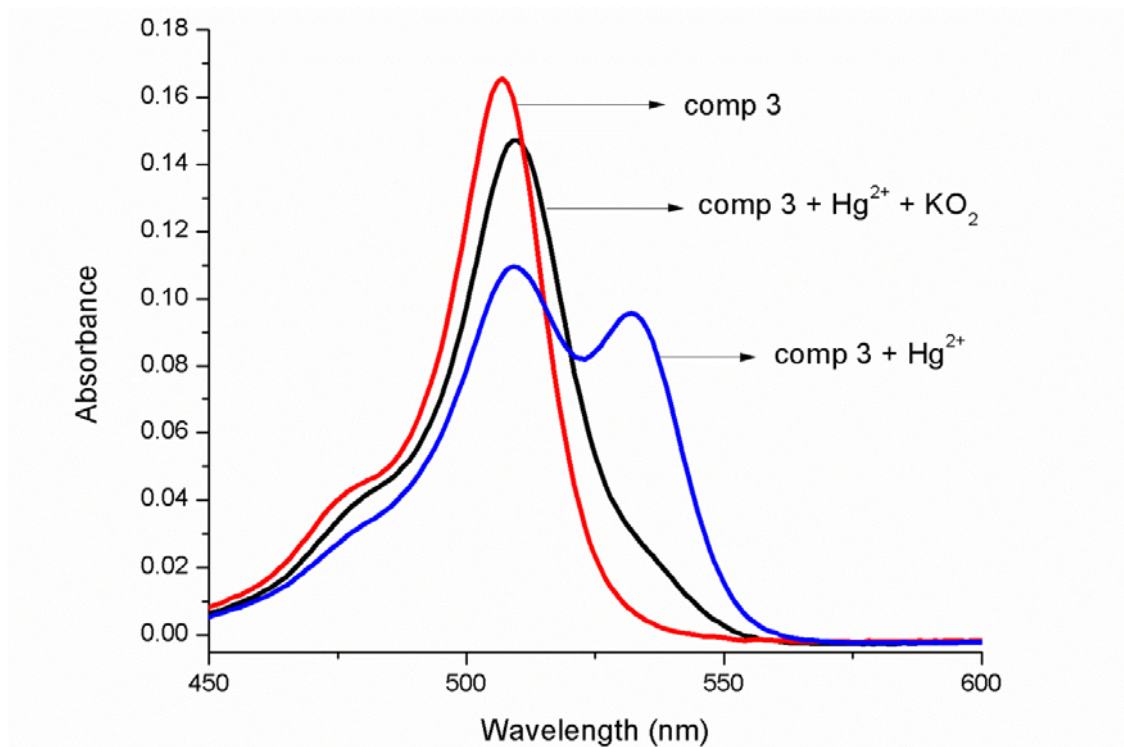


**Figure 32.** Absorbance spectra of compound **3** ( $1.0 \times 10^{-6}$  M, 3 mL) with Hg<sup>2+</sup> (18 equiv.) and KO<sub>2</sub> (18 equiv.) in acetonitrile/water (70/30).

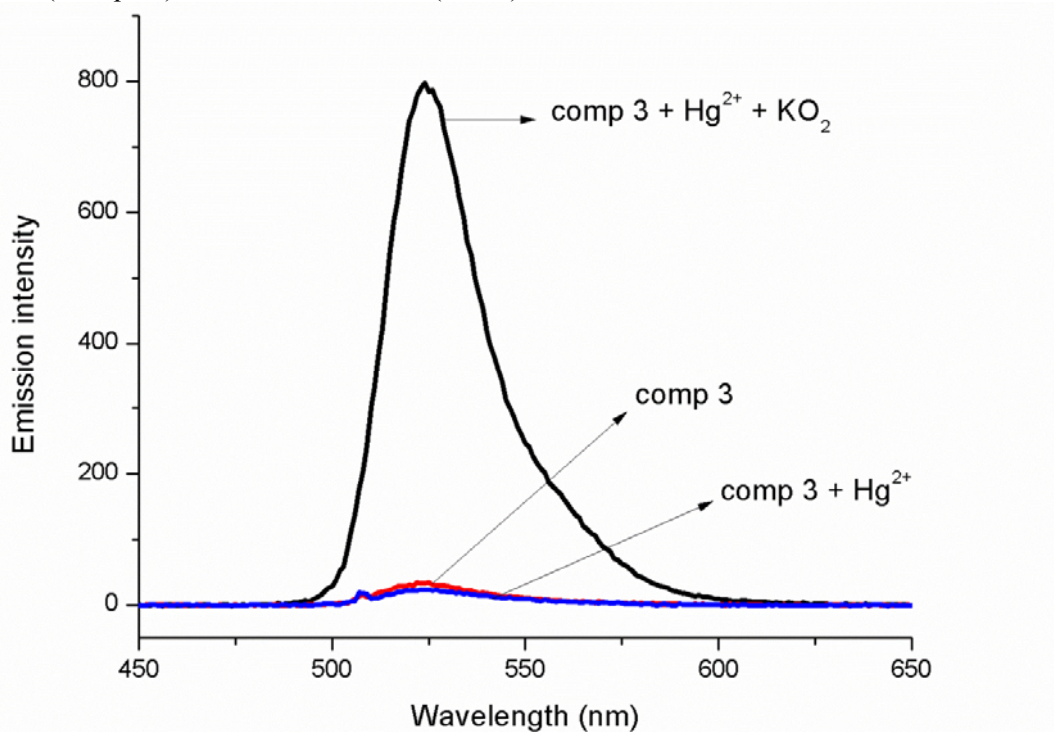


**Figure 33.** Emission spectra of compound **3** ( $1.0 \times 10^{-6}$  M, 3 mL) with Hg<sup>2+</sup> (18 equiv.) and KO<sub>2</sub> (18 equiv.) in acetonitrile/water (70/30).

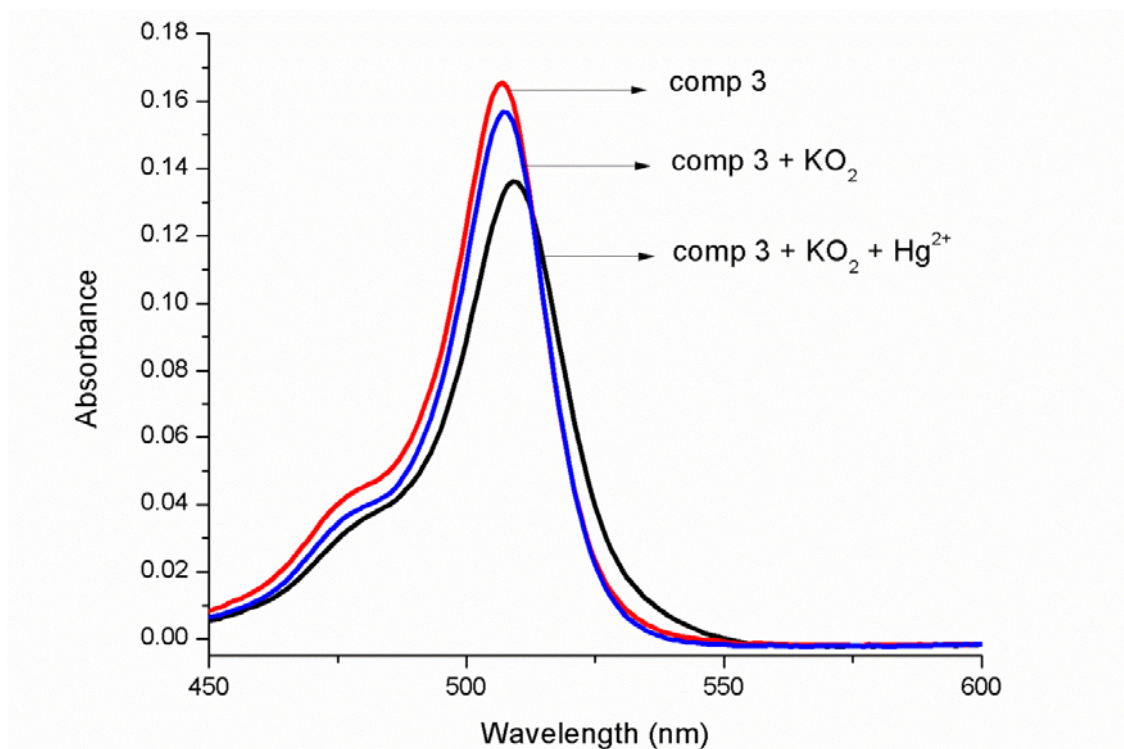


**Figure 34.** Absorbance spectra of compound **3** ( $1.0 \times 10^{-6}$  M, 3 mL) with KO<sub>2</sub> (18 equiv.) and Hg<sup>2+</sup> (18 equiv.) in acetonitrile/water (70/30).

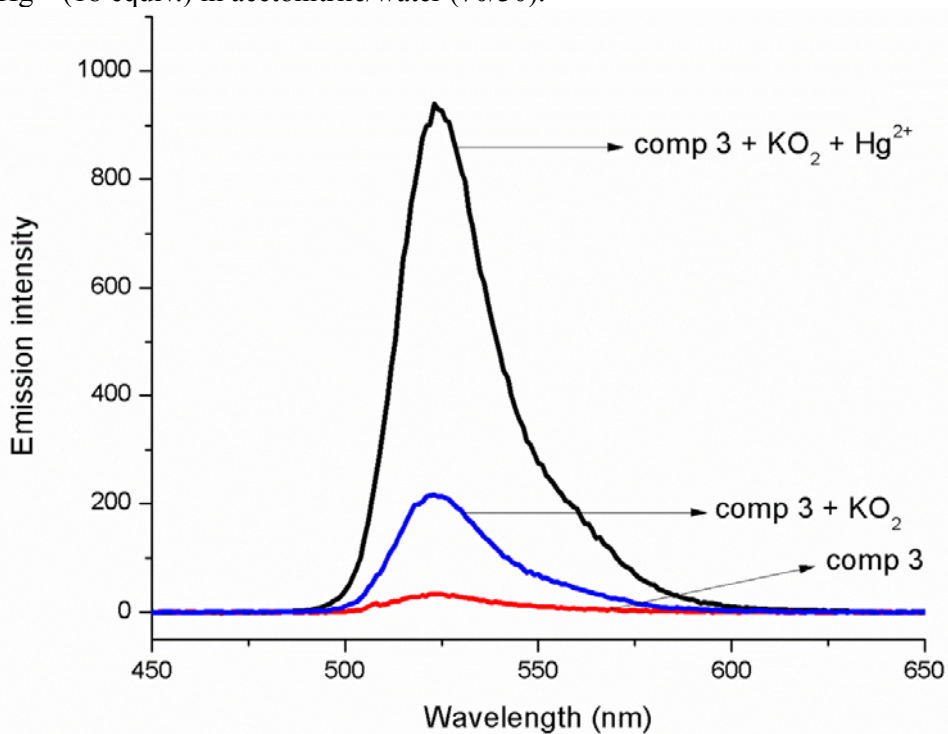


**Figure 35.** Emission spectra of compound **3** ( $1.0 \times 10^{-6}$  M, 3 mL) with KO<sub>2</sub> (18 equiv.) and Hg<sup>2+</sup> (18 equiv.) in acetonitrile/water (70/30).

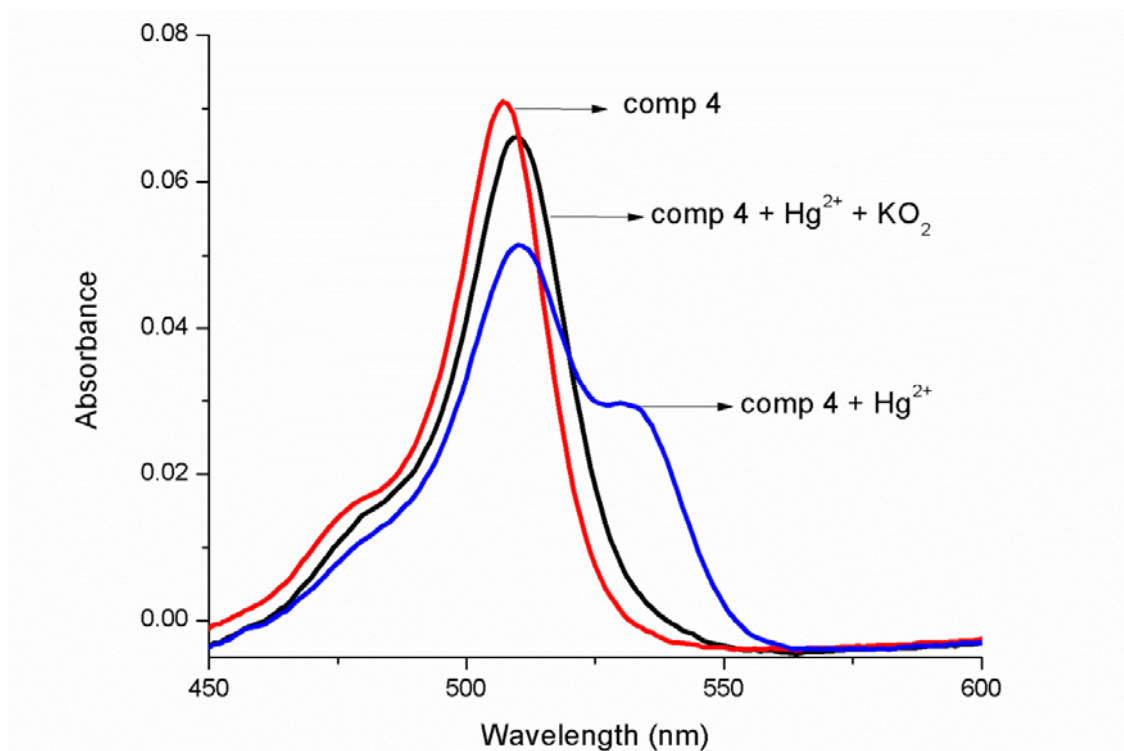


**Figure 36.** Absorbance spectra of compound **4** ( $1.0 \times 10^{-6}$  M, 3 mL) with Hg<sup>2+</sup> (18 equiv.) and KO<sub>2</sub> (18 equiv.) in acetonitrile/water (70/30).

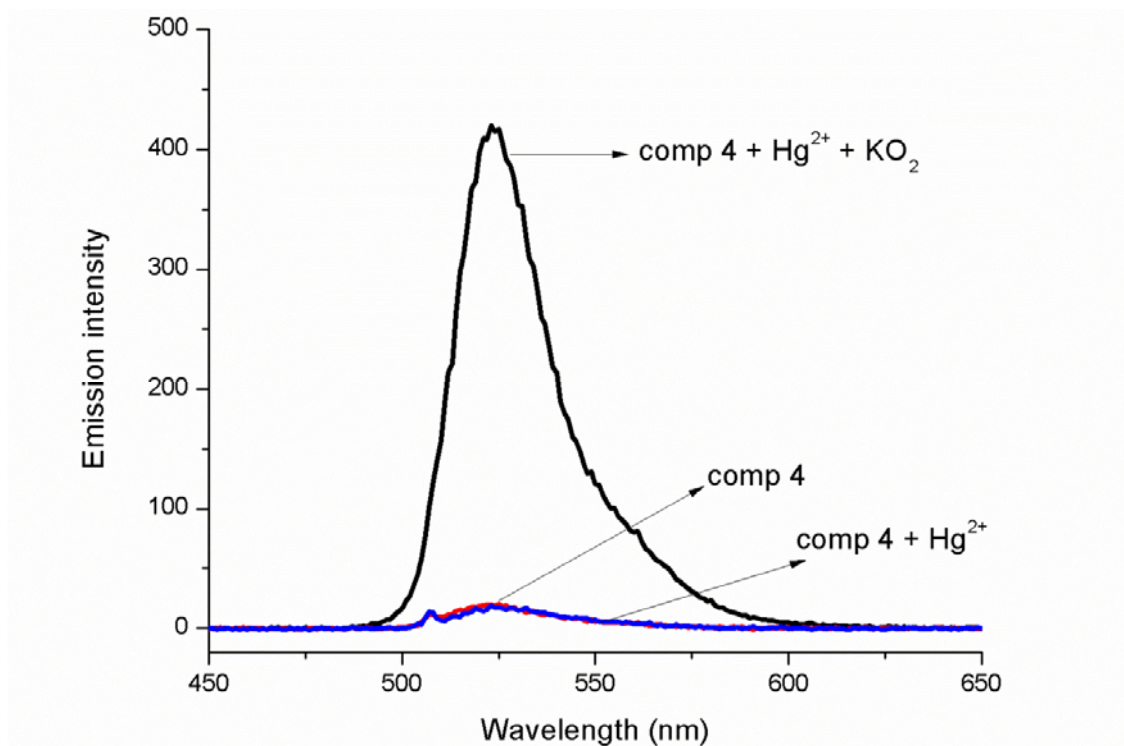


**Figure 37.** Emission spectra of compound **4** ( $1.0 \times 10^{-6}$  M, 3 mL) with Hg<sup>2+</sup> (18 equiv.) and KO<sub>2</sub> (18 equiv.) in acetonitrile/water (70/30).

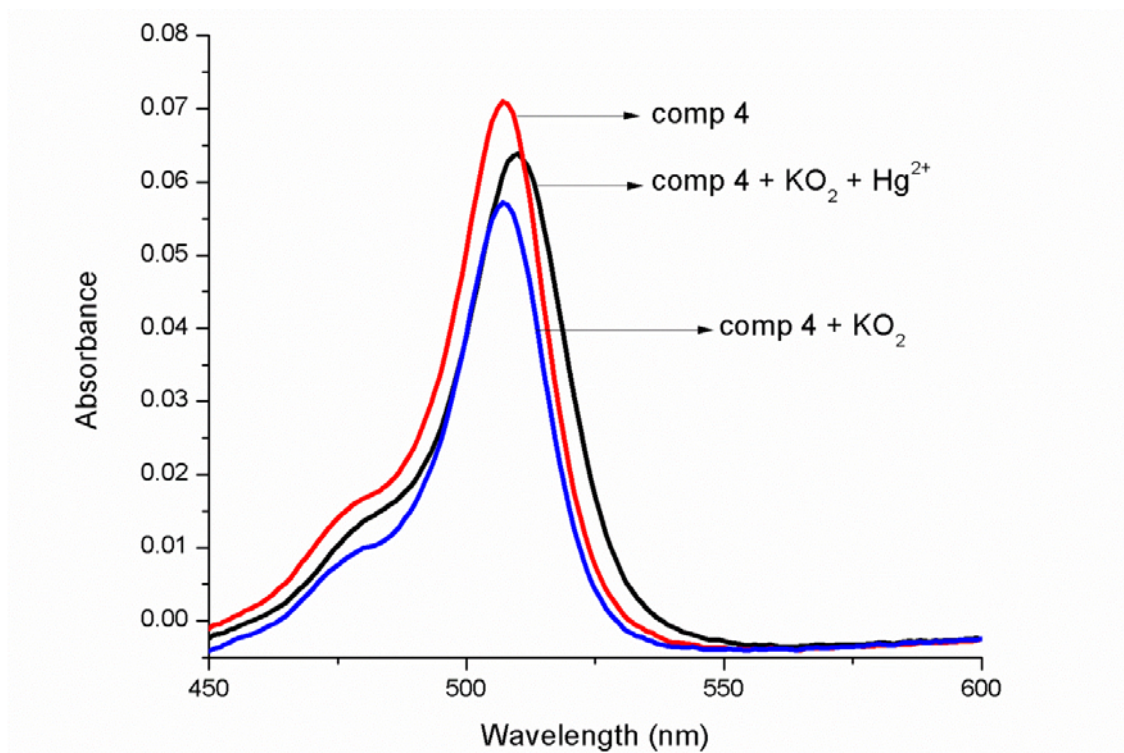


**Figure 38.** Absorbance spectra of compound **4** ( $1.0 \times 10^{-6}$  M, 3 mL) with KO<sub>2</sub> (18 equiv.) and Hg<sup>2+</sup> (18 equiv.) in acetonitrile/water (70/30).

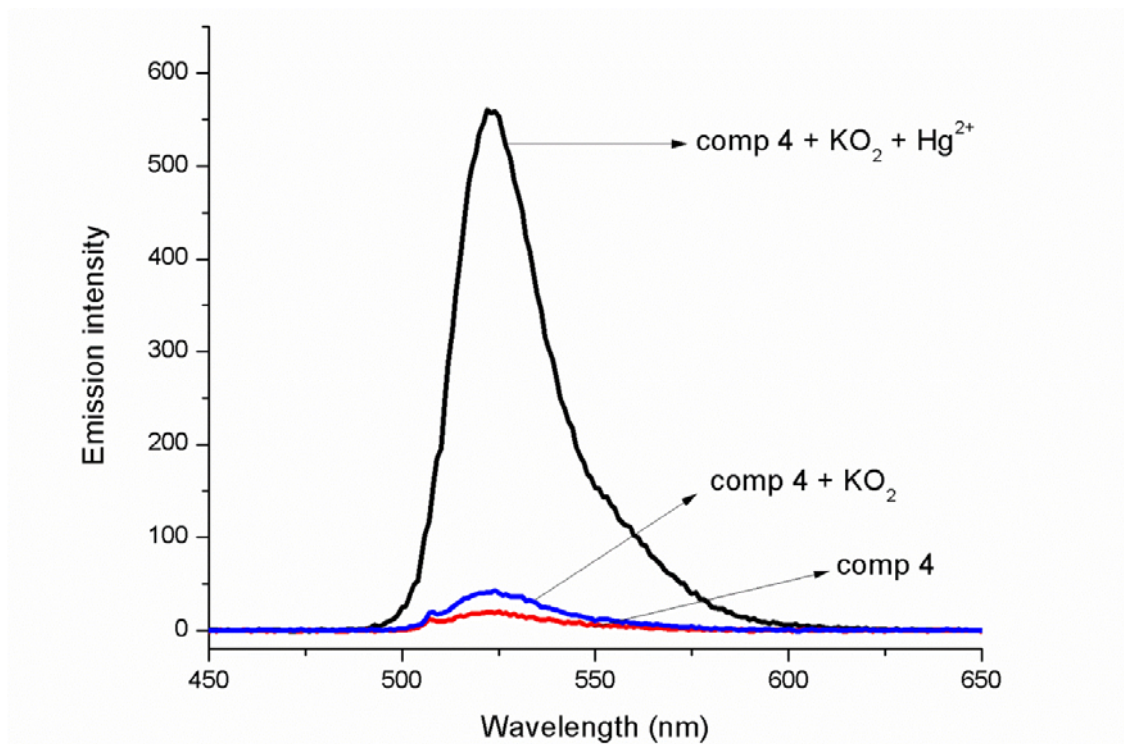


**Figure 39.** Emission spectra of compound **4** ( $1.0 \times 10^{-6}$  M, 3 mL) with KO<sub>2</sub> (18 equiv.) and Hg<sup>2+</sup> (18 equiv.) in acetonitrile/water (70/30).

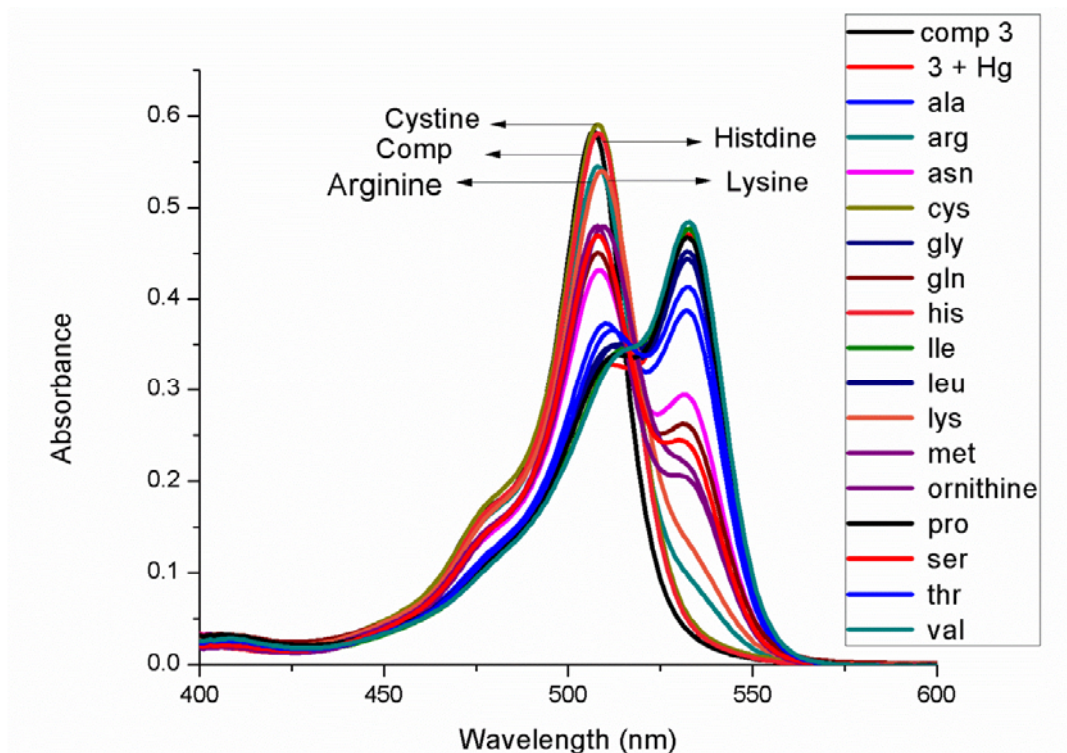


**Figure 40.** Absorbance spectra of compound **3** ( $1.0 \times 10^{-5}$  M, 3 mL) with AAs ( $1.0 \times 10^{-1}$  M, 10  $\mu$ L) in acetonitrile/water (70/30).

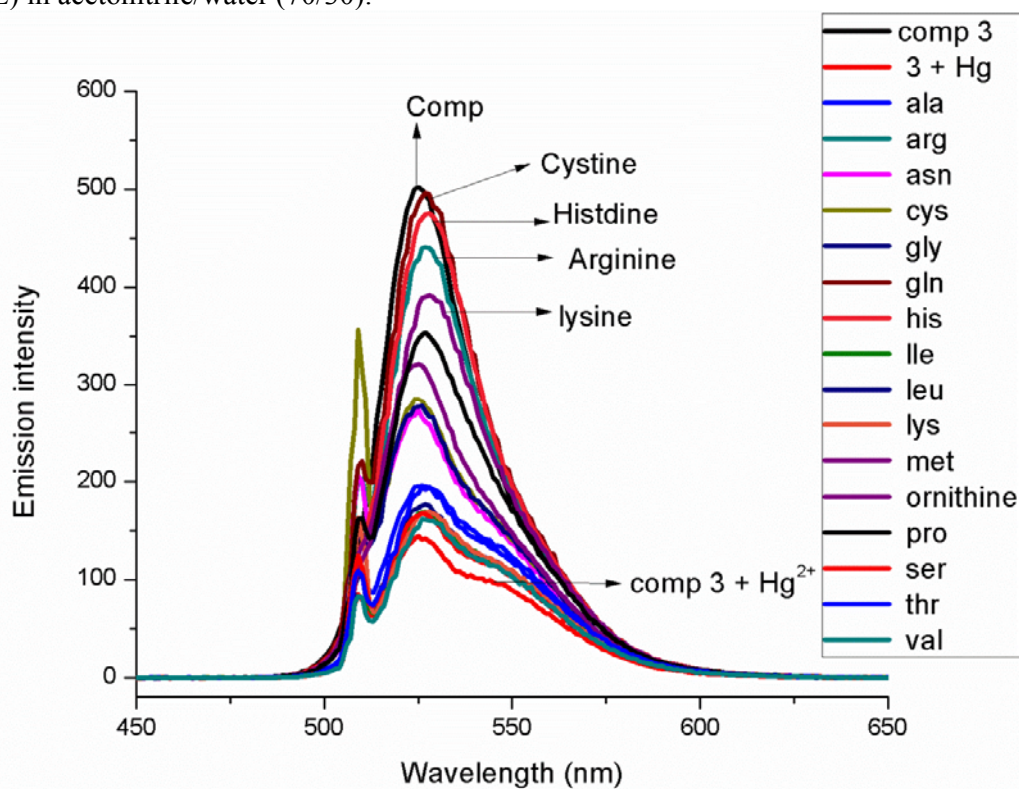


**Figure 41.** Emission spectra of compound **3** ( $1.0 \times 10^{-5}$  M, 3 mL) with AAs ( $1.0 \times 10^{-1}$  M, 10  $\mu$ L) in acetonitrile/water (70/30).

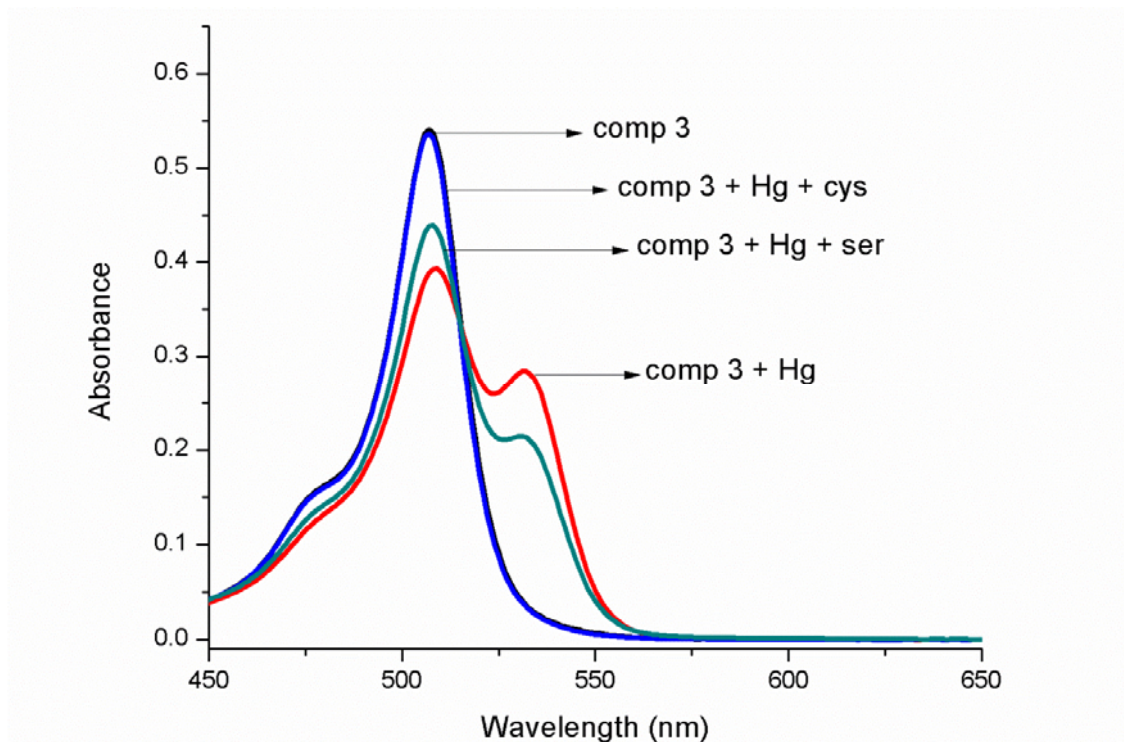


**Figure 42.** Absorbance spectra of compound **3** ( $1.0 \times 10^{-5}$  M, 3 mL) with Cys and Ser ( $1.0 \times 10^{-1}$  M, 10  $\mu$ L) in acetonitrile/water (70/30).

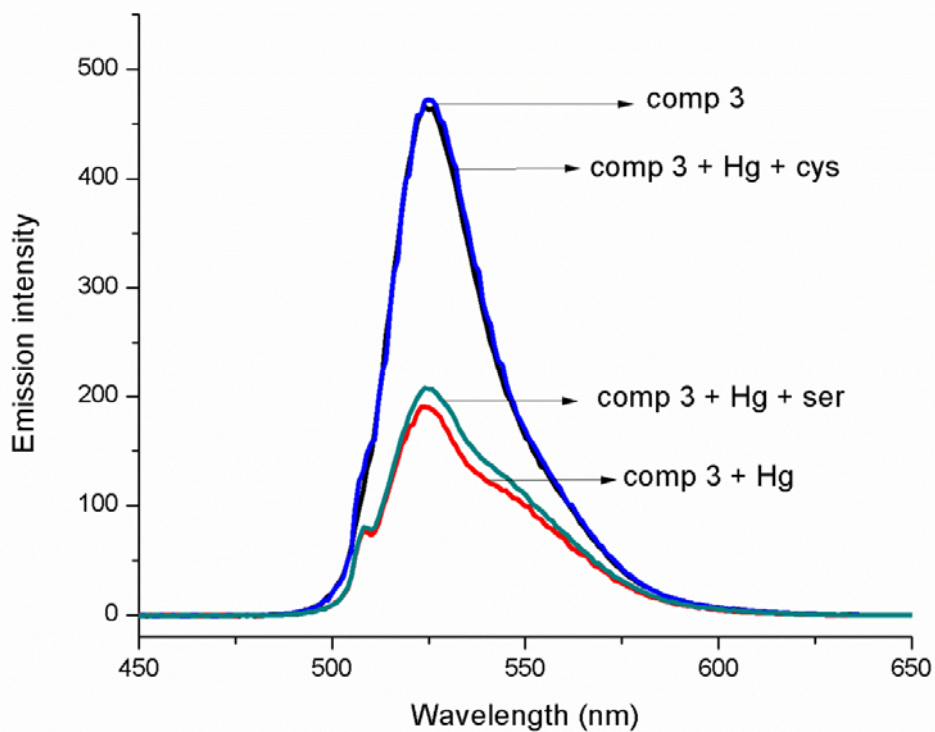


**Figure 43.** Emission spectra of compound **3** ( $1.0 \times 10^{-5}$  M, 3 mL) with Cyst and Ser ( $1.0 \times 10^{-1}$  M, 10  $\mu$ L) in acetonitrile/water (70/30).

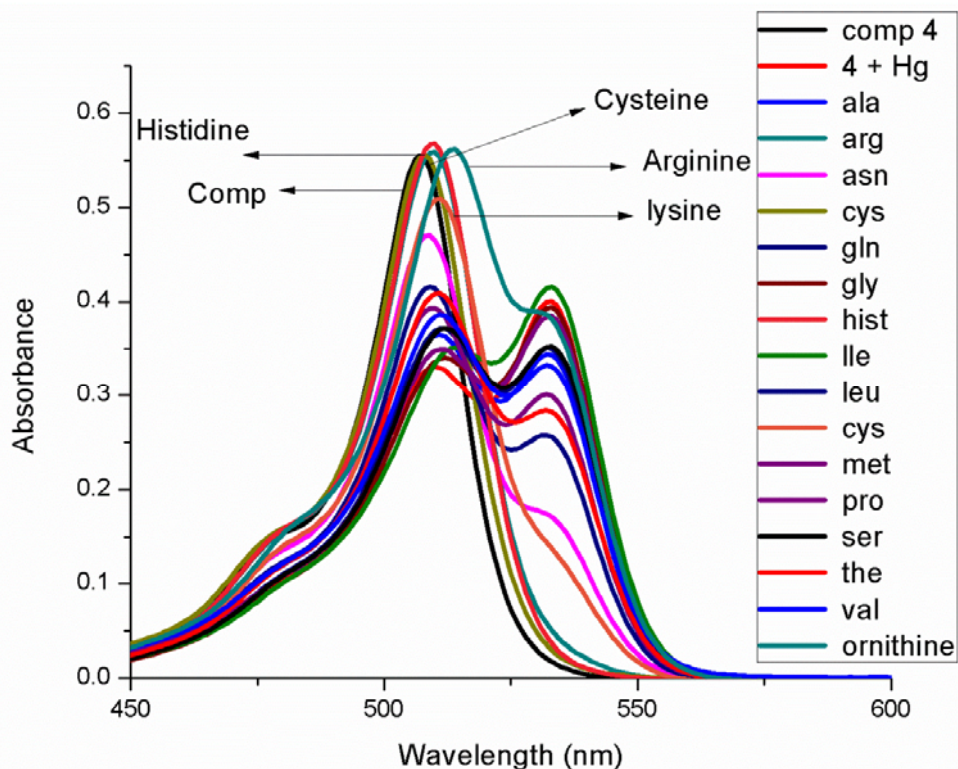


**Figure 44.** Absorbance spectra of compound **4** ( $1.0 \times 10^{-5}$  M, 3 mL) with AAs ( $1.0 \times 10^{-1}$  M, 10  $\mu$ L) in acetonitrile/water (70/30).

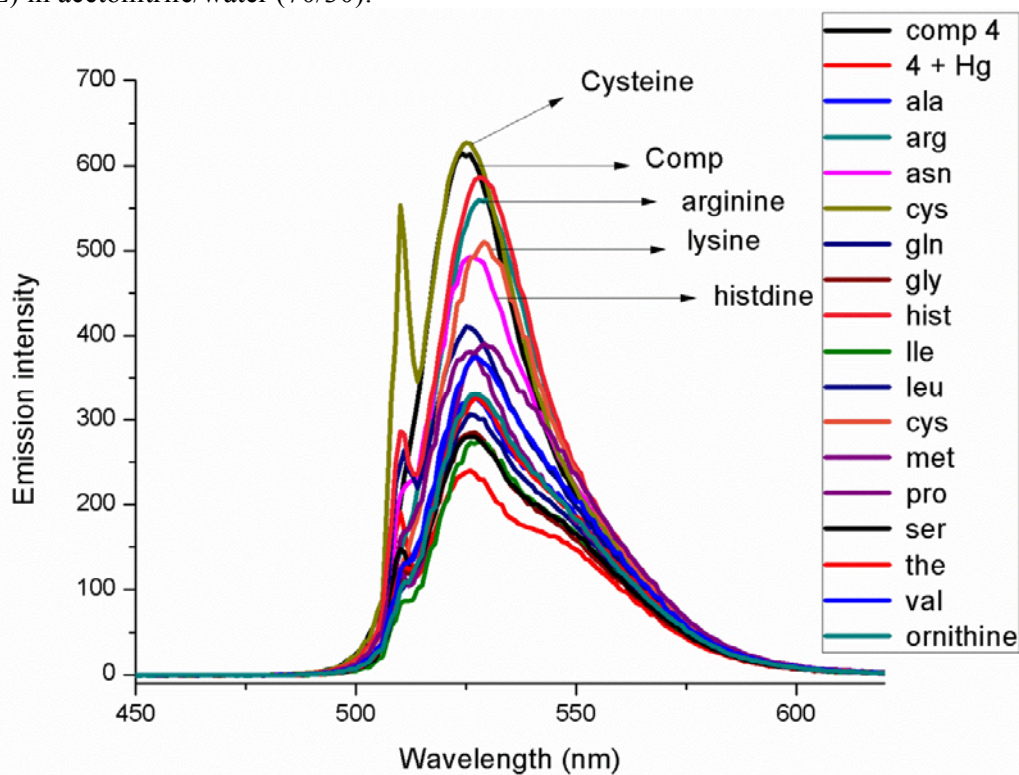


**Figure 45.** Emission spectra of compound **4** ( $1.0 \times 10^{-5}$  M, 3 mL) with AAs ( $1.0 \times 10^{-1}$  M, 10  $\mu$ L) in acetonitrile/water (70/30).

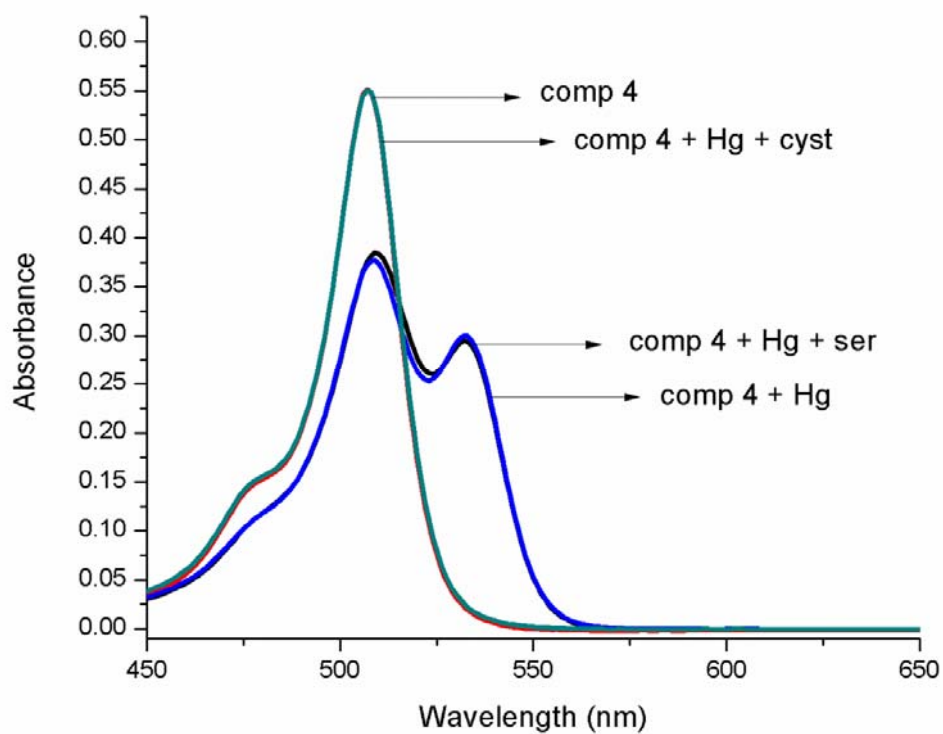


**Figure 46.** Absorbance spectra of compound **4** ( $1.0 \times 10^{-5}$  M, 3 mL) with Cyst and Ser ( $1.0 \times 10^{-1}$  M, 10  $\mu$ L) in acetonitrile/water (70/30).

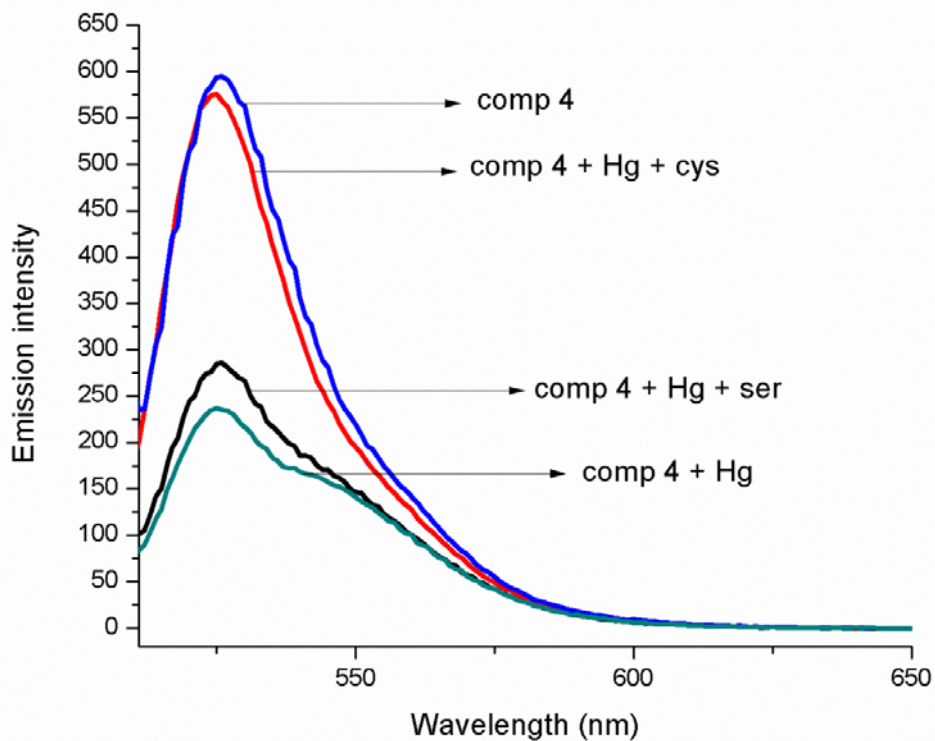


**Figure 47.** Absorbance spectra of compound **4** ( $1.0 \times 10^{-5}$  M, 3 mL) with Cyst and Ser ( $1.0 \times 10^{-1}$  M, 10  $\mu$ L) in acetonitrile/water (70/30).

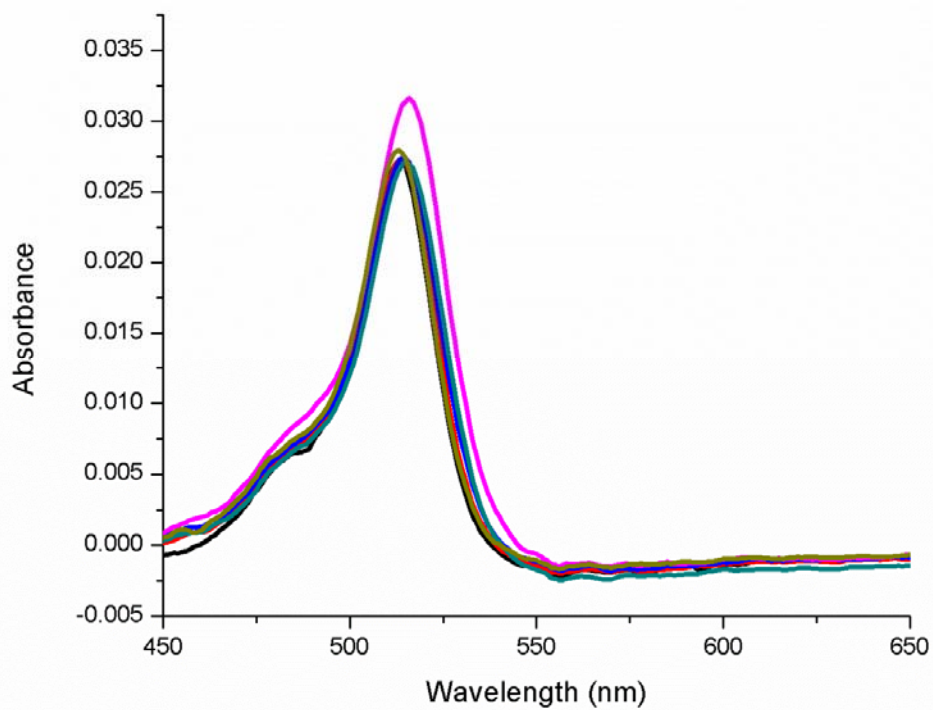


**Figure 48.** Absorbance spectra of compound **5** ( $1.0 \times 10^{-5}$  M, 3 mL) with the increasing concentration of Hg<sup>2+</sup> (50–300 equiv.) in acetonitrile/water (70/30).

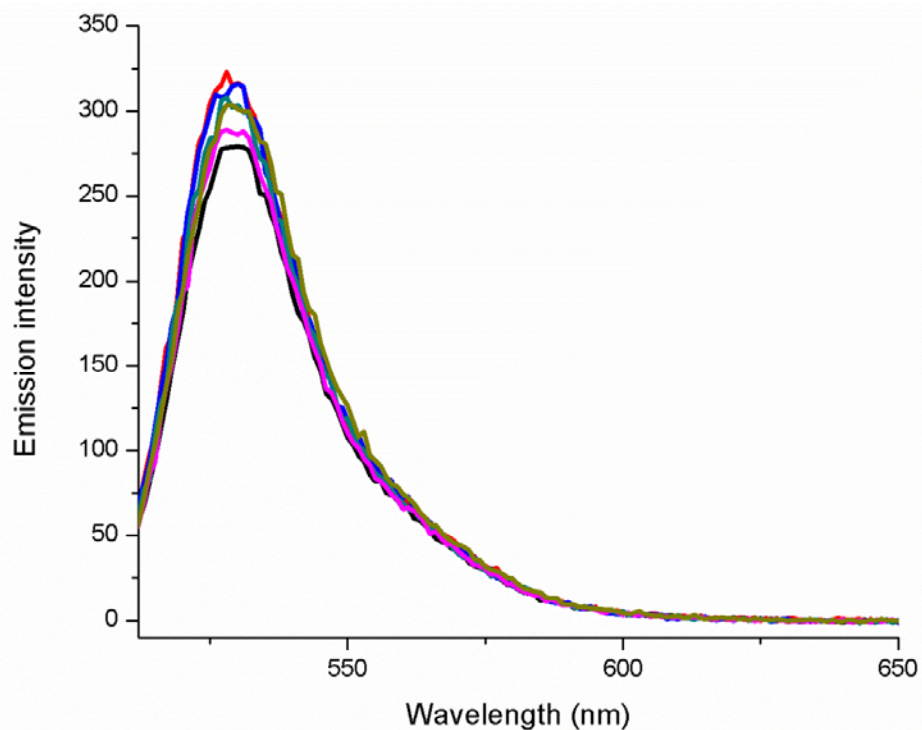


**Figure 49.** Emission spectra of compound **5** ( $1.0 \times 10^{-5}$  M, 3 mL) with the increasing concentration of Hg<sup>2+</sup> (50–300 equiv.) in acetonitrile/water (70/30).

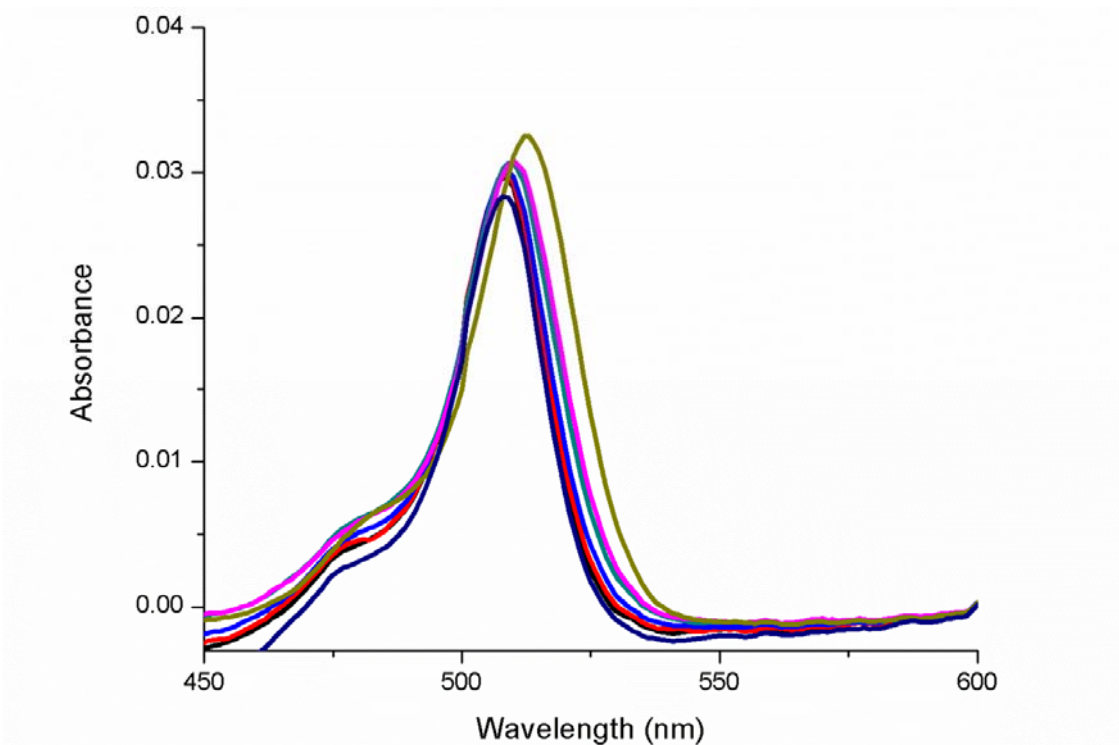


**Figure 50.** Absorbance spectra of compound **6** ( $1.0 \times 10^{-5}$  M, 3 mL) with increasing concentration of Hg<sup>2+</sup> (50–300 equiv.) in acetonitrile/water (70/30).

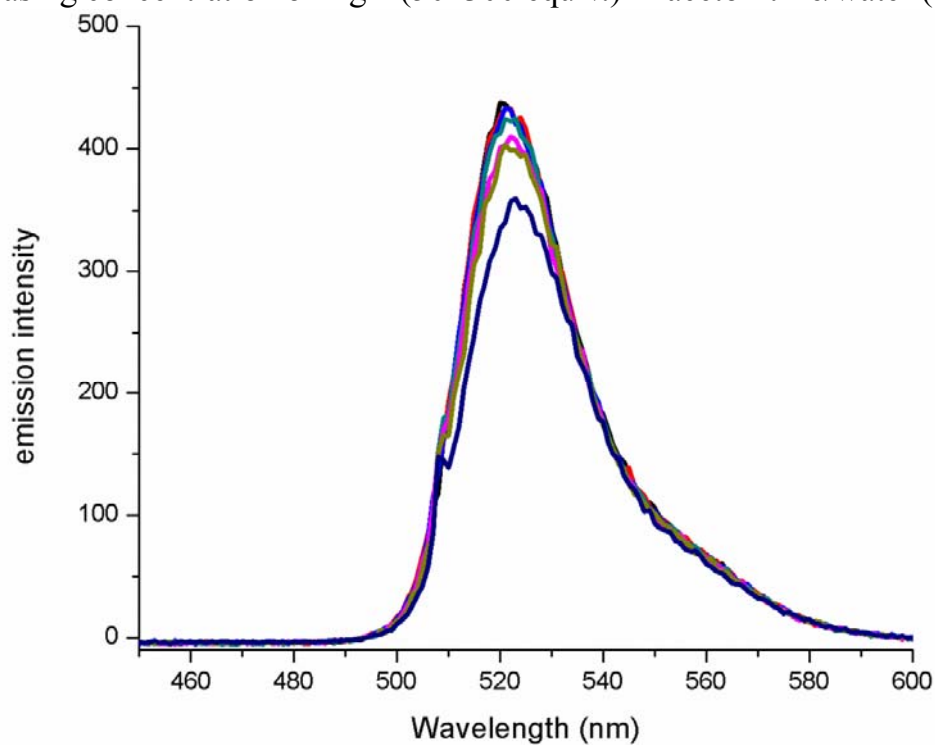


**Figure 51.** Emission spectra of compound **6** ( $1 \times 10^{-5}$  M, 3 mL) with increasing concentration of Hg<sup>2+</sup> (50–300 equiv.) in acetonitrile/water (70/30).

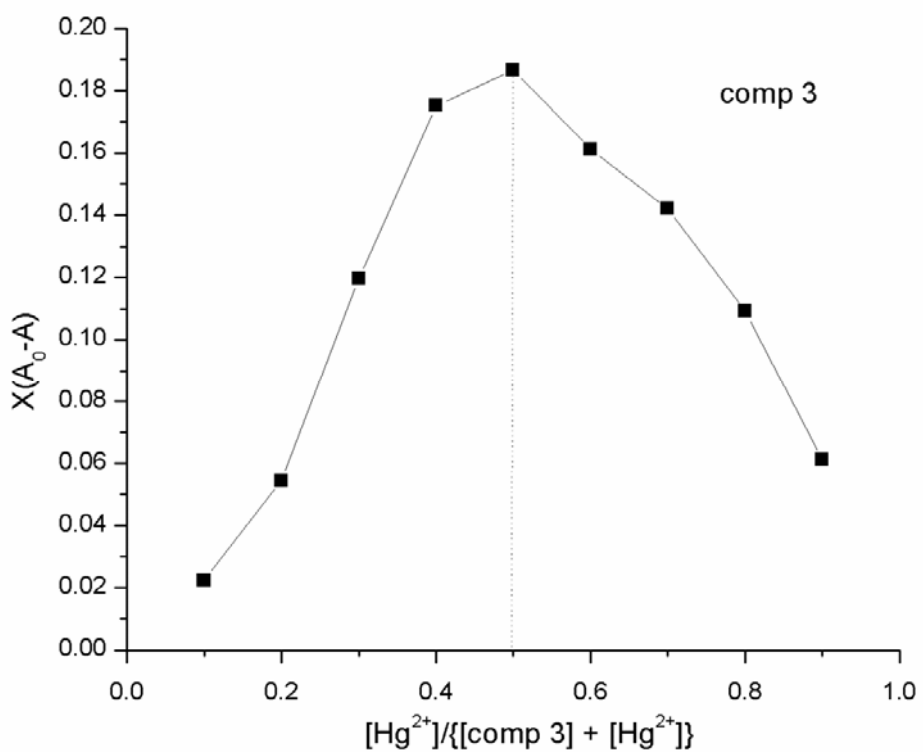


**Figure 52.** Job's plot for compound **3** with mercuric concentration from UV-visible absorption data.

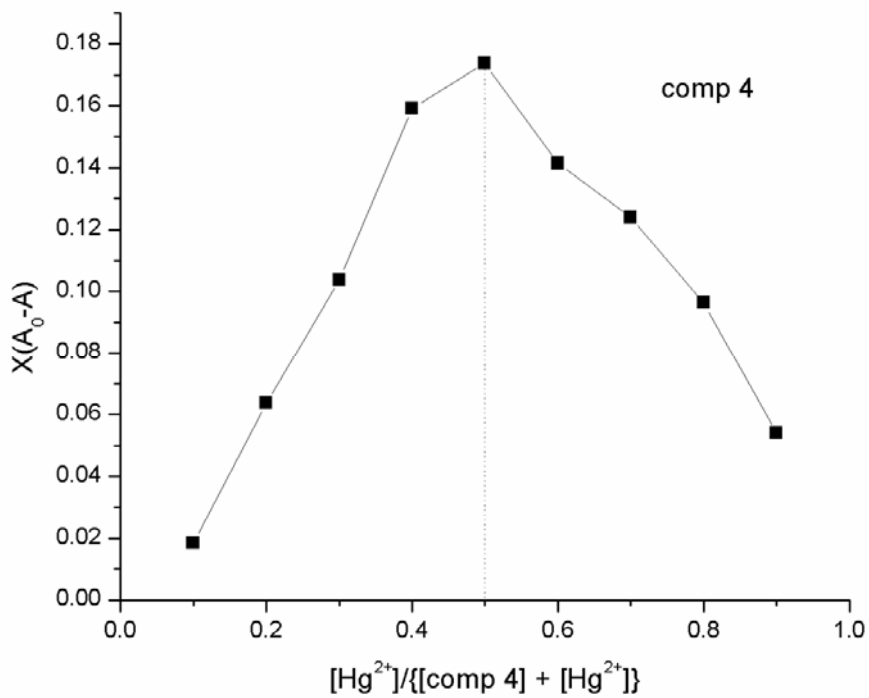


**Figure 53.** Job's plot for compound **4** with mercuric concentration from UV-visible absorption data.

**Table S2.** Photophysical data for compounds **3-6**.

<b>Compound</b>	<b>Absorbance (nm)</b>	<b>Emission (nm)</b>	<b>Stoke's Shift (nm)</b>	<b>Absorption coefficient</b>	<b>Q. Y.</b>	<b>Std. dev.</b>
<b>3</b>	506	522	605.8	64480	0.019	0.0002
<b>4</b>	507	521	530.0	66390	0.026	0.002
<b>5</b>	507	520	493.1	41580	0.87	0.008
<b>6</b>	512	527	555.9	28090	0.77	0.005

### **Artificial neural networks to improve overall sensor performance**

We trained an artificial neural network (ANN) to “learn” to identify mercury concentration. By using the ANN in concert with our tailored sensor arrays we obtained improvement

### **Results and discussion**

Artificial neural network (ANN) algorithms are employed for a range of applications where the objective is to detect a pattern in a large quantity of imperfect data.<sup>3–11</sup> For instance, ANNs have been deployed in combination with “electronic noses” to identify nitrohydrocarbons in air,<sup>12</sup> O<sub>2</sub> detection in blood,<sup>13</sup> lung cancer patients from their breath,<sup>14</sup> and assess food quality.<sup>15</sup>

In the present work, we have trained an ANN to “learn” to identify mercury concentrations in the present systems. Our ANN system consists of a multilayer perceptron (MLP)<sup>3,4</sup> network trained with backward error propagation (BEP) for feature extraction.

The MLP network is a supervised training method, in which the neural network is trained to learn the given set of inputs – the mercury sensor values, and produce an output for the related specific target values – the mercury concentration. The network memory is kept in adjustable variables called “weights”. In the network, the weights set the influence that each sensor value of the input pattern has on the network output. As shown below in Fig. 54, the MLP network training by BEP has the following phases: *(i)* input training pattern or vector feed forward; *(ii)* calculation and back propagation of the resulting error; and then *(iii)* the learning phase in which the network connections are updated.

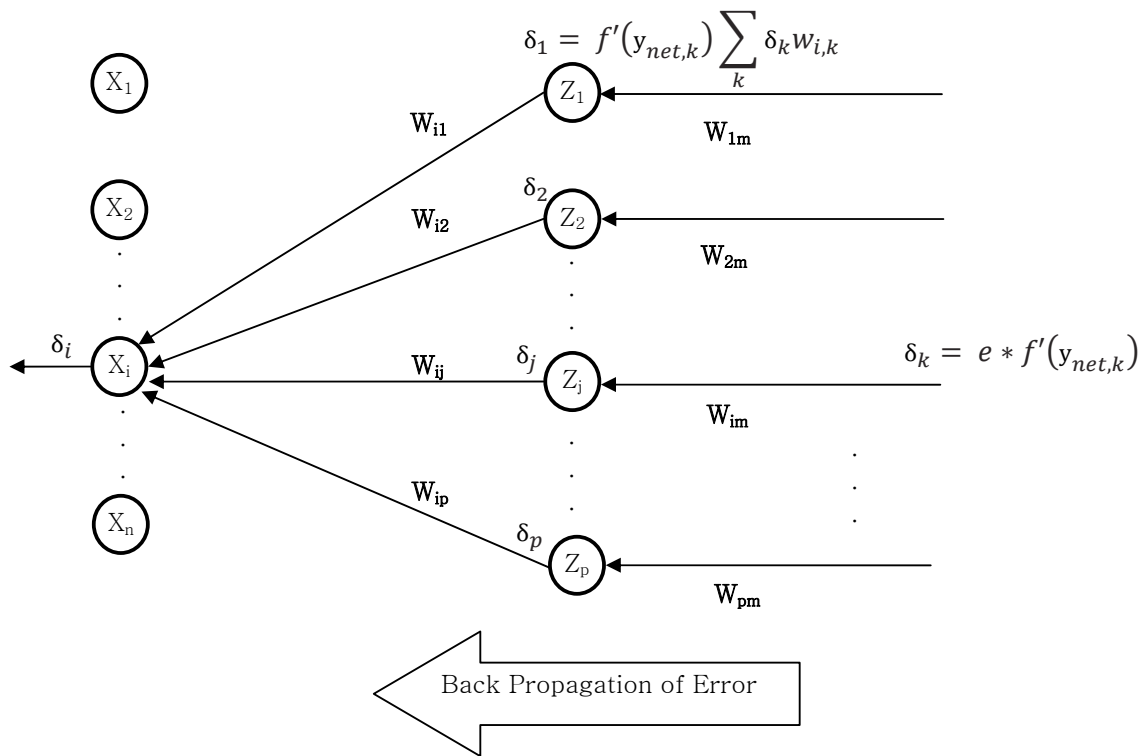
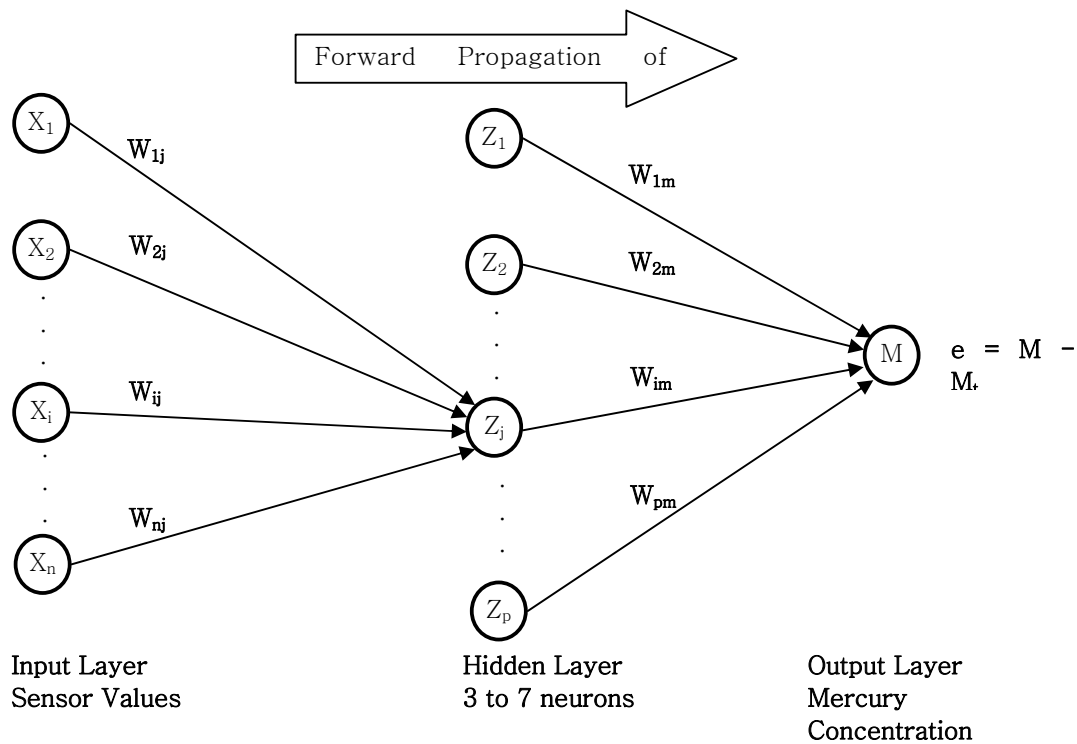


**Fig. S54.** Illustration of the forward (top) and backward (bottom) propagation for training the MLP.

The feed forward phase is the calculation of the outputs of each *perceptron* unit, or neuron, in each MLP layer. The output of each neuron,  $y_j$ , is the sum of the product of the weights,  $w_{i,j}$ , and the inputs  $x_i$  as follows:

$$y_j = f \left[ \sum_{i=1}^n w_{i,j} x_i \right] = f(y_{net,j})$$

In phase two, the calculated output from the MLP final layer is compared to the desired MLP output to determine the existing error compared to the true mercury value; we employ this error to adjust the weights in the learning phase. The BEP is obtained by using the error from the deeper layer (closer to the output) to compute the weight update term in the shallower layers (closer to the input). Thus, the error is propagated back through the network. The adjustment of the weights follows a gradient descent approach where the goal is to achieve a minimum total error. Each weight in the network is updated based on the backward propagated error signal,  $d_j$ , the previous value of the weight,  $w_{i,j}(old)$ , and a learning rate term,  $a$ .

$$w_{i,j}(new) = w_{i,j}(old) + ad_j$$

Training continues until the average error drops below a preset value, or for a total of N training runs; in our case 10,000 and 100,000 training runs were evaluated. After training, the network not only learns to respond correctly to the trained input patterns but also can correctly respond to an input that is similar but not identical to those used in training.

**Table S3:** Probe compound 3 – State after 10000 training runs.

Hidden layer neurons		3		4		5		6		7	
Mercury	Evaluated	Error	Evaluated	Error	Evaluated	Error	Evaluated	Error	Evaluated	Error	
0	0.329	0.329	0.2444	0.2444	0.1487	0.1487	0.0447	0.0447	0.7858	0.7858	
10	9.9887	-0.0113	9.9917	-0.0083	9.9827	-0.0173	9.5052	-0.4948	10.054	0.054	
20	20.0906	0.0906	20.0741	0.0741	20.0255	0.0255	19.9606	-0.0394	20.2953	0.2953	
30	29.9902	-0.0098	29.9973	-0.0027	29.9913	-0.0087	29.9419	-0.0581	30.0084	0.0084	
40	40.0066	0.0066	40.0131	0.0131	39.9987	-0.0013	40.0146	0.0146	39.9884	-0.0116	
50	49.9723	-0.0277	49.9985	-0.0015	49.9896	-0.0104	50.0217	0.0217	49.9126	-0.0874	
Average error		0.079167		0.05735		0.035317		0.112217		0.207083	

**Table S4:** Probe compound 4– State after 10000 training runs

Probe 2 - State after 10000 training runs											
Hidden layer neurons		3		4		5		6		7	
Mercury	Evaluated	Error	Evaluated	Error	Evaluated	Error	Evaluated	Error	Evaluated	Error	
0	-0.0166	-0.0166	0.0289	0.0289	0.0004	0.0004	0.0377	0.0377	0.0891	0.0891	
10	9.8791	-0.1209	9.9431	-0.0569	9.9232	-0.0768	9.9772	-0.0228	9.9542	-0.0458	
20	20.0163	0.0163	20.0157	0.0157	20.0057	0.0057	20.0262	0.0262	20.0485	0.0485	
30	29.9911	-0.0089	29.9981	-0.0019	29.9966	-0.0034	30.0051	0.0051	30.0064	0.0064	
40	40.0004	0.0004	39.9999	-0.0001	40.0021	0.0021	39.9972	-0.0028	39.9968	-0.0032	
50	50.0025	0.0025	50.0046	0.0046	50.003	0.003	49.9988	-0.0012	49.9992	-0.0008	
Average error		0.0276		0.018017		0.015233		0.015967		0.0323	

**Table S5:** Probes Compounds 3 + 4 – State after **100000** training runs

Hidden layer neurons		3		4		5		6		7	
Mercury	Evaluated	Error									
0	0.0921	0.0921	0.0028	0.0028	-0.0369	-0.0369	0.0131	0.0131	0	0	
10	9.951	-0.049	9.9479	-0.0521	9.9146	-0.0854	9.9228	-0.0772	9.9796	-0.0204	
20	20.0343	0.0343	19.9941	-0.0059	19.9852	-0.0148	19.9938	-0.0062	19.997	-0.003	
30	30.0225	0.0225	30.0069	0.0069	30.0015	0.0015	30.0061	0.0061	29.9999	-0.0001	
40	39.982	-0.018	39.9989	-0.0011	40	0	39.9967	-0.0033	40	0	
50	49.9961	-0.0039	49.9986	-0.0014	49.9957	-0.0043	49.998	-0.002	49.9999	-0.0001	
0	0.0921	0.0921	0.0028	0.0028	-0.0369	-0.0369	0.0131	0.0131	0	0	
10	10.1132	0.1132	10.0345	0.0345	10.0215	0.0215	10.0583	0.0583	10.0095	0.0095	
20	20.0256	0.0256	20.0042	0.0042	19.9962	-0.0038	20.0092	0.0092	20.0004	0.0004	
30	30.0014	0.0014	29.9934	-0.0066	29.9931	-0.0069	29.9996	-0.0004	29.9993	-0.0007	
40	40.0019	0.0019	40.0016	0.0016	39.9971	-0.0029	39.9988	-0.0012	40.0005	0.0005	
50	49.9982	-0.0018	50.001	0.001	50.0046	0.0046	50.0053	0.005	50.0004	0.0004	
Average error		0.037983		0.010075		0.018292		0.016258		0.002925	

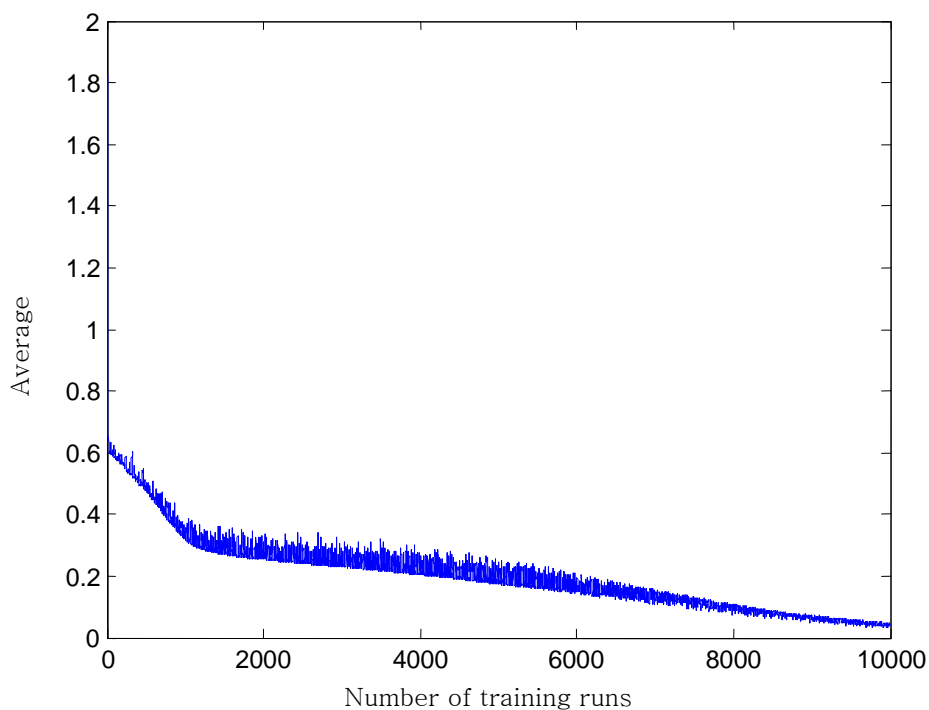


**Figure S55:** Probe 1 – Evaluated error decrease versus number of training runs.

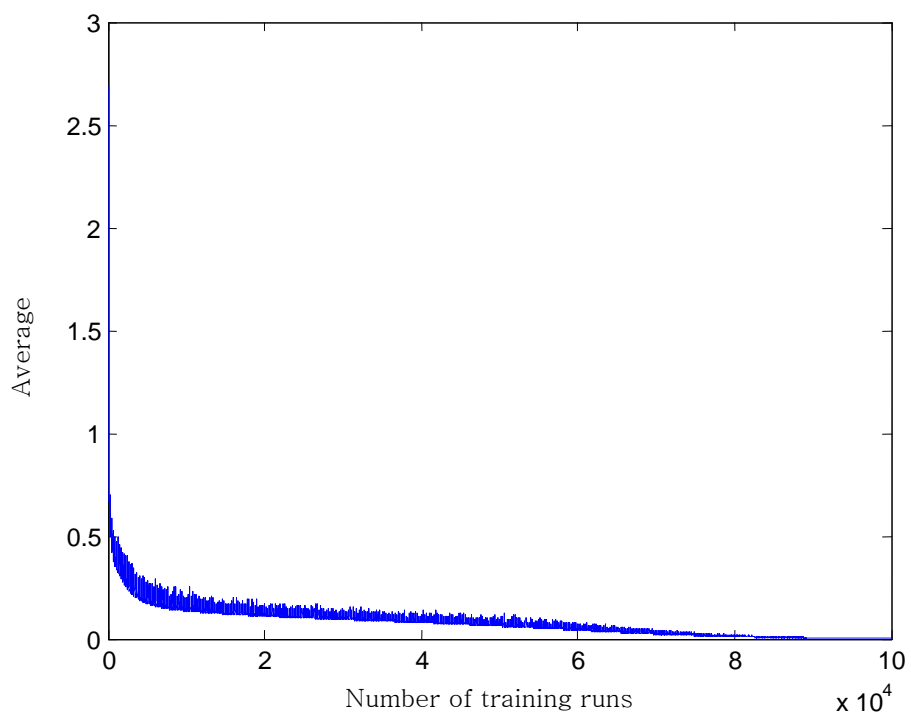


**Figure S56:** Probe 1 + 2 – Evaluated error decrease versus number of training runs.

## REFERENCES

1. (a) C. Brückner, V. Karunaratne, S. J. Rettig, D. Dolphin, *Can. J. Chem.* 1996, **74**, 2182. (b) R. W. Wagner, J. S. Lindsey, *Pure Appl. Chem.* 1996, **68**, 1373. (c) C. H. Lee, J. S. Lindsey, *Tetrahedron* 1994, **50**, 11427.
2. J. N. Demas, In *Optical Radiation Measurements*; K. D. Mielenz, Ed.; Academic Press: New York, **1982**; Vol. 3 (Measurement of Photoluminescence), 195–248.
3. A. K. Verma, J. Singh, R. Chaudhary, *Tetrahedron Letters* 2007, **48**, 7199.
4. E. J. Cho, Z. Tao, Y. Tang, E. C. Tehan, F. V. Bright, W. L. Hicks, J. A. Gardella and R. Hard, *Appl. Spectrosc.*, 2002, **56**, 1385–1389.
5. C. Bishop, *Neural Networks for Pattern Recognition*, Oxford University Press, Oxford, 1995.
6. S. Haykin, *Neural Networks – A Comprehensive Foundation*, 2nd edn, Prentice–Hall, Englewood Cliffs, 1998.
7. B. Widrow, R. G. Winter and R. A. Baxter, *IEEE Trans. Acoust., Speech, Signal Process.*, 1988, **36**, 1109–1118.
8. S. Y. King and J. N. Hwang, *IEEE Trans. Robot. Autom.*, 1989, **5**, 641–657.
9. J. Alirezaie, M. E. Jernigan and C. Nahmias, *IEEE Trans. Nucl. Sci.*, 1997, **44**, 194–198.
10. M. Davenport and A. H. Titus, *IEEE Trans. Neural Net.*, 2004, **15**, 145–158.
11. J. Zupan, *Data Handl. Sci. Technol.*, 2003, **23**, 199–229.
12. J. Yinon, *Anal. Chem.*, 2003, **75**, 99A–105A.
13. P. Boilot, E. L. Hines, M. A. Gongora and R. S. Folland, *Sens. Actuators, B*, 2003, **88**, 80.

14. Y. Tang, Z. Tao, R. M. Bukowski, E. C. Tehan, S. Karri, A. H. Titusb and F. V. Bright, Tailored xerogel-based sensor arrays and artificial neural networks yield improved O<sub>2</sub> detection accuracy and precision, *Analyst*, 2006, 131, 1129–1136
15. A. V. Kalach, *Sensors*, 2005, 5, 97–102. A. K. Deisingh, D. C. Stone and M. Thompson, Applications of electronic noses and tongues in food analysis, *Int. J. Food Sci. Technol.*, 2004, 39(6), 587–604.